Pre-normative REsearch for Safe use of Liquid Hydrogen (PRESLHY)

Fuel Cells and Hydrogen Joint Undertaking (FCH JU)

Grant Agreement Number 779613

Deliverable Number:	D5.7
Title:	Summary of experiment series E5.5 (Congestion) results
Authors:	Kieran Lyons
Submitted Date:	02/2021
Due Date:	10/2020
Report Classification:	Confidential

Deliverable	
Contractual delivery date	10/2020
Actual delivery date	02/2021
Deliverable Number	D5.7
Deliverable Name	Summary of experiment series E5.5 (Congestion) results
Internal document ID	EA/20/6
Nature	Report

Approvals			
	Name	Organisation	Date
Author	K Lyons	HSE	22/02/21
Issue	E de Lewandowicz	HSE	26/02/21
Customer	T Jordan	KIT	

Disclaimer

Acknowledgments

This project has received funding from the Fuel Cells and Hydrogen 2 Joint Undertaking under the European Union's Horizon 2020 research and innovation programme under grant agreement No 779613. The HSE work programme acknowledges funding from its sponsors Shell, Lloyd's Register Foundation and Equinor and instrumentation provided by NREL and Dräger.

FUEL CELLS AND HYDROGEN
JOINT UNDERTAKING

Publishable summary

Work package five of the PRESLHY project focusses on the combustion phenomena of liquid hydrogen (LH_2). The experimental programme was designed to provide insight into a number of credible and poorly understood LH_2 combustion scenarios. One such scenario is the effect of congestion or confinement on an ignited hydrogen cloud stemming from a release of LH_2, potentially leading to deflagration to detonation transition (DDT).

This report summarises the large-scale experiments carried out at the HSE Science and Research Centre in Buxton investigating the effect of differing levels of congestion and confinement on the combustion properties of a hydrogen cloud developing from a release of LH2.

Various combustion parameters were measured, including; the overpressure, heat flux, and noise. Monitoring of ambient and release conditions were also made to allow for a thorough analysis of the results. A total of 23 ignited trials were completed and involved releasing LH2 using the same initial conditions as in the rainout experiments of work package 3, meaning that the dispersion patterns should remain similar.

The congestion and confinement was created by a configurable steel structure placed directly in the path of the release. Two congestion levels, confinement and pool experiments were planned, however due to the safe noise level being reached, only the congestion experiments were completed. To compensate for this, multiple repeats and experiments with a wide variety of source conditions were conducted.

From the results, it is clear that higher levels of volumetric congestion increases the measured overpressures in releases with the same initial conditions. The results also show that an increasing hydrogen inventory, either through an increased release pressure or larger nozzle, can result in a larger event upon ignition. However, the mixing of the jet also plays a part; some releases through the largest release orifice diameter showed lower overpressures potentially due to the hydrogen cloud being too rich.

It was observed that the ambient conditions, in particular the wind speed and direction, were a significant factor in the outcome of each ignition. This was particularly prominent in trials 21 to 23.

Key words

Liquid hydrogen, dispersion, ignition, congestion, explosion

Abbreviations

barg	Shorthand for gauge pressure in bar
DDT	Deflagration to Detonation Transition
GH2	Gaseous Hydrogen
LFL	Lower Flammable Limit
LH2	Liquefied Hydrogen

Table of Contents

1 Introduction

1.1 Background

The aim of the PRESLHY project is to address knowledge gaps with some high-risk liquid hydrogen (LH_2) accident scenarios to enable the safe implementation of the widespread use of LH_2. This report outlines the 'congestion' experiments undertaken at the HSE Science and Research Centre, Buxton, UK, which form part of Work Package 5 of the PRESLHY project.

1.2 Objectives

The objective of this experimental campaign was to determine the effect of differing levels of congestion upon the ignition behaviour of a cryogenic hydrogen plume. To this end, 23 ignited trials were carried out at the HSE Science and Research Centre whereby cryogenic hydrogen was released into a steel congestion frame. As well as two levels of congestion, the initial conditions of the release were altered with similar conditions to the other experiments carried out as part of this project, within Work Packages 3 and 4.

1.3 Previous ignited LH_2 experiments

Previous work studying the behaviour of ignited LH_2 clouds has been conducted at HSE [1]. The scenario investigated was an accidental spill during a transfer operation into open space and parameters such as the heat flux, flame speed, and overpressures were measured.

A total of 14 tests were undertaken, including three scoping trials and four non-ignitions. The releases were from a LH_2 tanker through a vacuum insulated hose with a 25.4 mm nominal bore.

Three regimes were identified from this scenario: the initial deflagration of the cloud with flame speeds of up to 50 m/s; a secondary condensed phase explosion (on one occasion) and finally a jet fire.

Safety distances for radiative heat transfer were calculated from the results. A separation distance of 11.1 m to 11.5 m was required to avoid pain from the radiative heat in all of the regimes.

The secondary explosion observed on one occasion caused significant overpressures. These were not directly measured but the TNT equivalence was estimated to be a less than 2.7 kg. This resulted in an estimated overpressure of less than 730 mbar at 7 m distance. The uncongested deflagrations in other trials did not result in measurable overpressures.

These previous studies provide a useful comparison point whereby the effects of congestion can be quantified. The conditions resulting in the secondary explosion were not replicated in this series, but have been studied further as a part of the PRESLHY project in Work Package 4, deliverable 4.8 [2].

2 Method

This section contains a brief description of the test facility, data acquisition and experiment procedure. The details needed to fully interpret the results are found in Appendix A in the form of figures and tables. The dimensions of the equipment, locations of instrumentation and the format of the output data are also included.

2.1 Test facility

The experiments were conducted using the LH_2 release facility, which was located on a 32 m diameter concrete pad at the Frith Valley site at the HSE Science and Research Centre in Buxton, UK. An image including a sketch of the experimental layout is shown in figure 1.

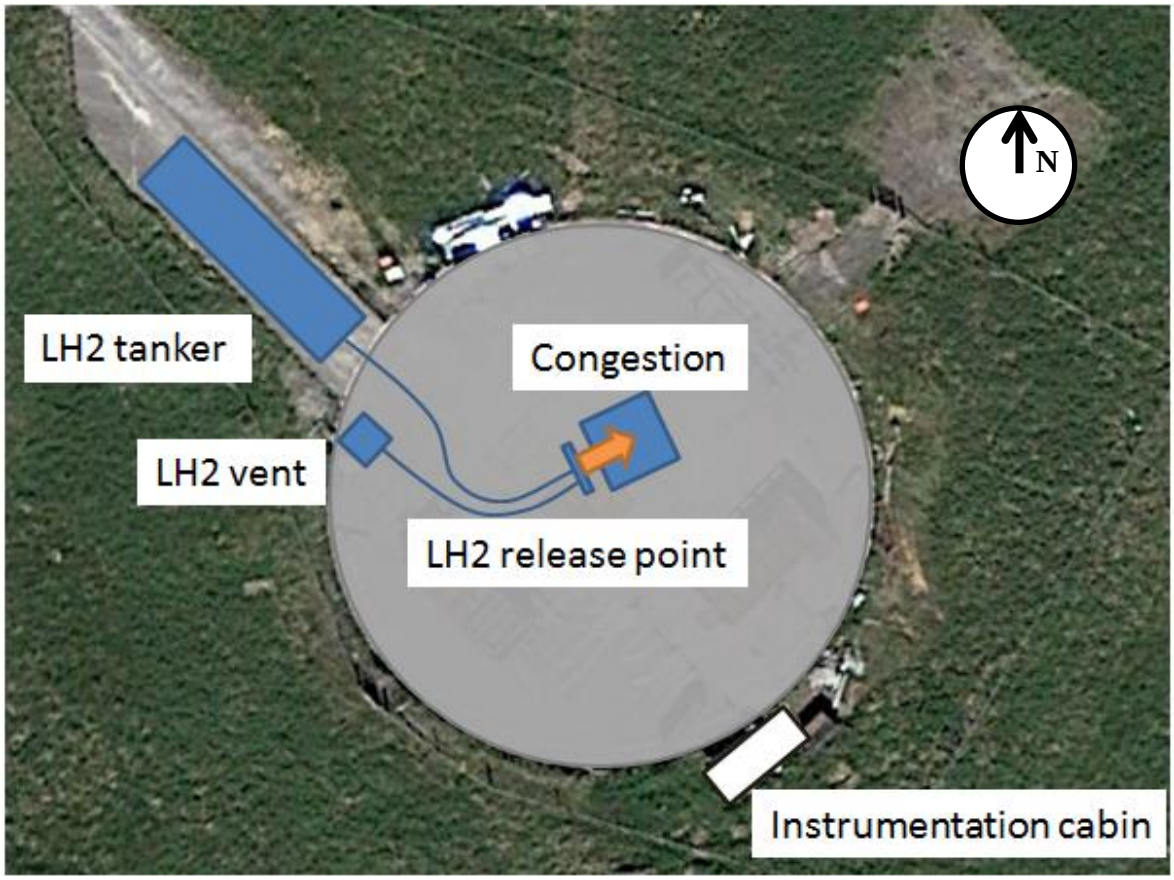

Fig. 1: Diagram of WP5 layout.

2.1.1 *Tanker, vent stack & release station*

The tanker, vent stack and release station was the same as used in previous experiments carried out in Work Package 3. This consisted of insulated steel pipework, remotely operated valves and instrumentation. The instrumentation enabled measurements of the pipework temperature and pressure at various points, and the mass flow rate. The electrically isolated pipework used in work packages 3 and 4 was also still in place to create consistent outflow behaviour across the work packages. Deliverable 3.6 [3] contains a more thorough description of the equipment used. The release height was approximately 0.8 m for these experiments.

The LH_2 was supplied by Air Liquide in a vacuum insulated tanker, with a content of up to 2.5 tonnes. A 12 barg safety relief valve and a higher pressure bursting disk protected

the tanker against over pressurisation. The tanker was connected directly to the release pipework, 3 m vent stack and valve control system. The tanker is displayed in figure 2.

Fig. 2: Photo of the tanker connected to the vent stack.

2.1.2 *Congestion*

The congestion rig is a steel frame consisting of 18, 1 m^3 sections configured as a 3 m square base with a height of 2 m. Congestion is added in the form of ladder-like structures, referred to as congestion frames. Each of these is made up of made up of 26 +/- 1 mm (nominal 1") cylindrical bars spaced 125 mm apart between two 5 mm x 50 mm bars. These have varying lengths dependant on the position in the rig.

In the top half, the congestion frames were inserted horizontally and spanned the entire length of the congestion rig (3 m). Three congestion frames were used in each layer, and four layers were used.

The bottom half had a more complex congestion pattern with the congestion grids installed vertically. Photographs and sketches of this is shown in figures 3 to 6. The arrow in figure 3 indicates the LH_2 release, the sparks show the potential ignition points and the circles are instrument locations (small, red are collocated thermocouples and sampling tubes and the large green are pressure transducers).

Scaffold poles (o.d. 48 mm) were inserted vertically to achieve a higher level of congestion. They were placed in a pattern with 11 in each 1 m^2 area of the grid and protruded from the congestion frame. Figures 4 and 6 show the congestion frame with low and high levels of congestion respectively. Appendix A contains a sketch of the scaffold placement.

The congestion resulted in a volumetric blockage ratio of approximate 1.52% for the low level, and 4.2 % for the high.

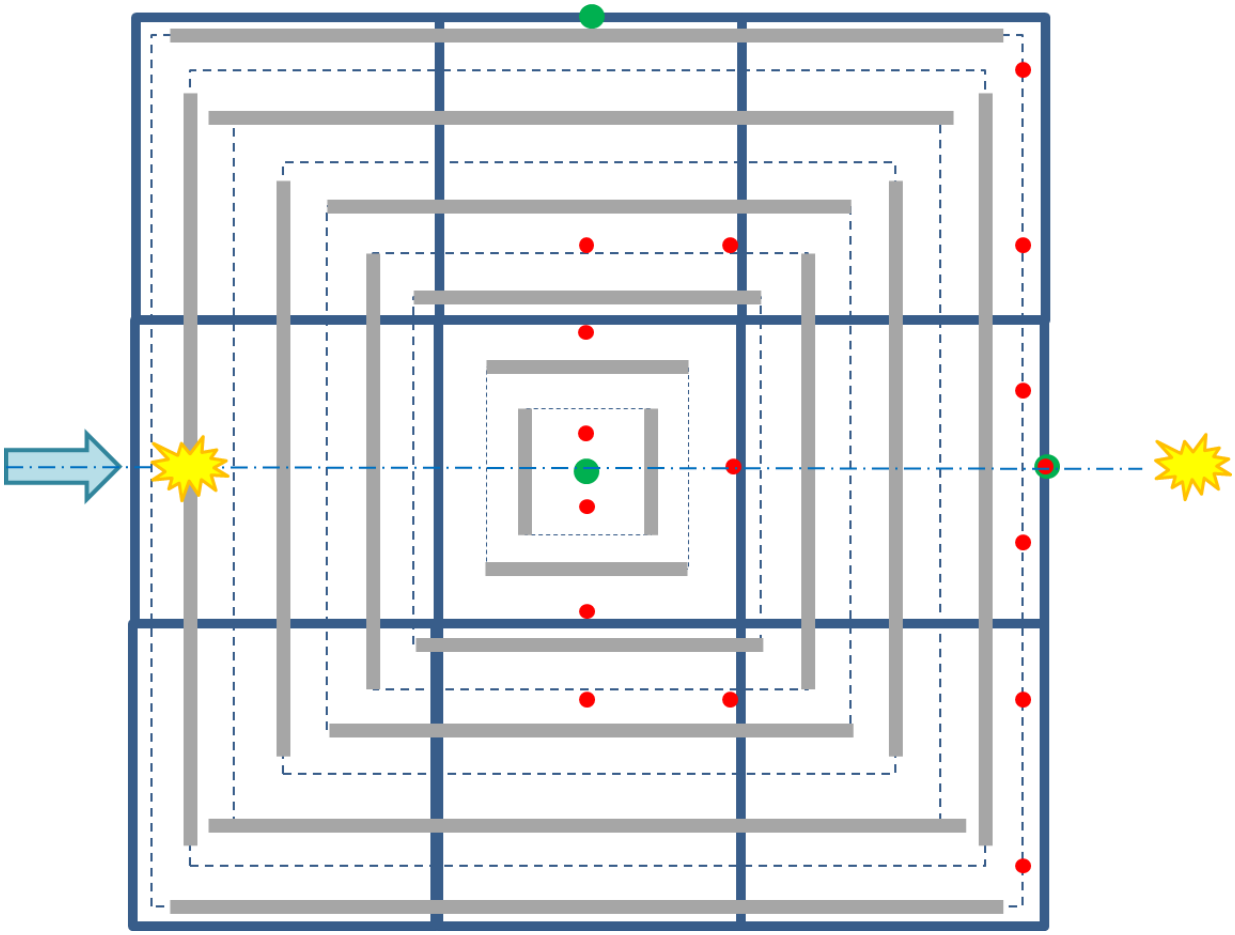

Fig. 3: A sketch of the lower congestion frame positions.

Fig.4: Photo of the congestion rig with low level of congestion.

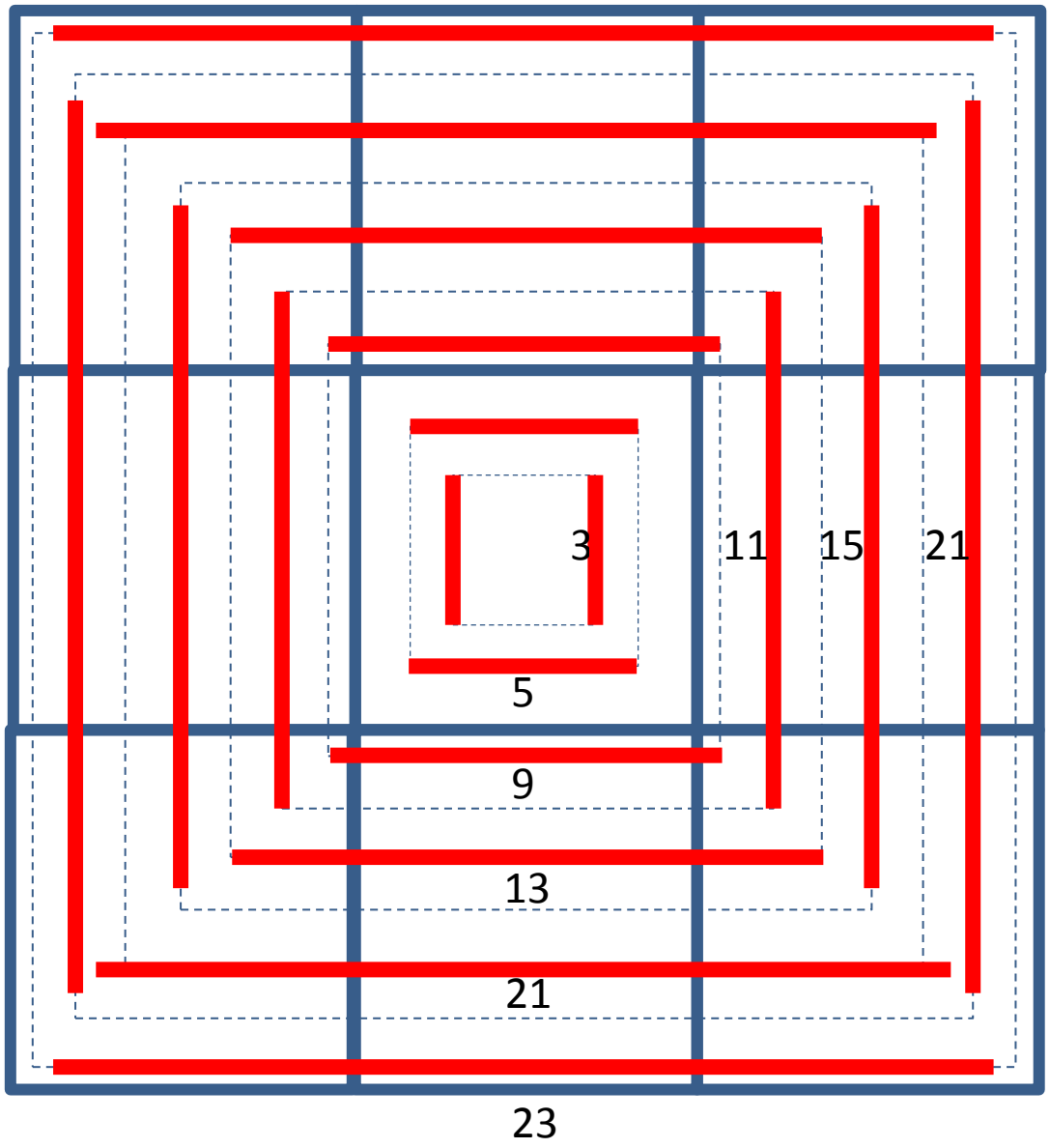

Fig.5: Number of bars in each gate for the congestion rig with low level of congestion.

Area blockage:

Low congestion level:	Bottom half	0.80 m^2/m^3
	Top half	1.00 m^2/m^3
High congestion :	Bottom half	1.33 m^2/m^3
	Top half	1.53 m^2/m^3

Volume blockage:

Low congestion level:	Bottom half	1.54 %
	Top half	1.93 %
High congestion :	Bottom half	4.20 %
	Top half	4.60 %

Fig.6: Photo of the congestion rig with high level of congestion.

2.1.3 *Ignition system*

In order to avoid misfires, pyrotechnic igniters that created a fountain of sparks were used, bringing the probability of ignition close to 1. The ignition system was separate from the other systems and could be configured for either front or rear ignition points.

2.2 Instrumentation & Data Acquisition

The purpose of the instrumentation fell into three broad categories: release and dispersion measurements, explosion measurements, and general measurements including ambient conditions and video footage.

2.2.1 *Blast Logging*

To characterise the blast wave, 8 Kulite HKL-375 (M) series pressure transducers were arranged in and around the congestion rig, centred on the midpoint. Figure 7 shows a diagram of the concrete pad with the pressure transducer locations marked. Each stood approximately 0.5 m off the ground and was oriented 90° from the expected blast wave to register an incident blast pressure. K1 to K4 were held horizontally and K5 to K8 were held vertically.

The pressure transducers were logged through a high-speed logging system that was separate to the primary operation system. The system was capable of a 500 kHz logging rate, but various rates were used throughout the campaign to ensure that the peak pressure was not being missed.

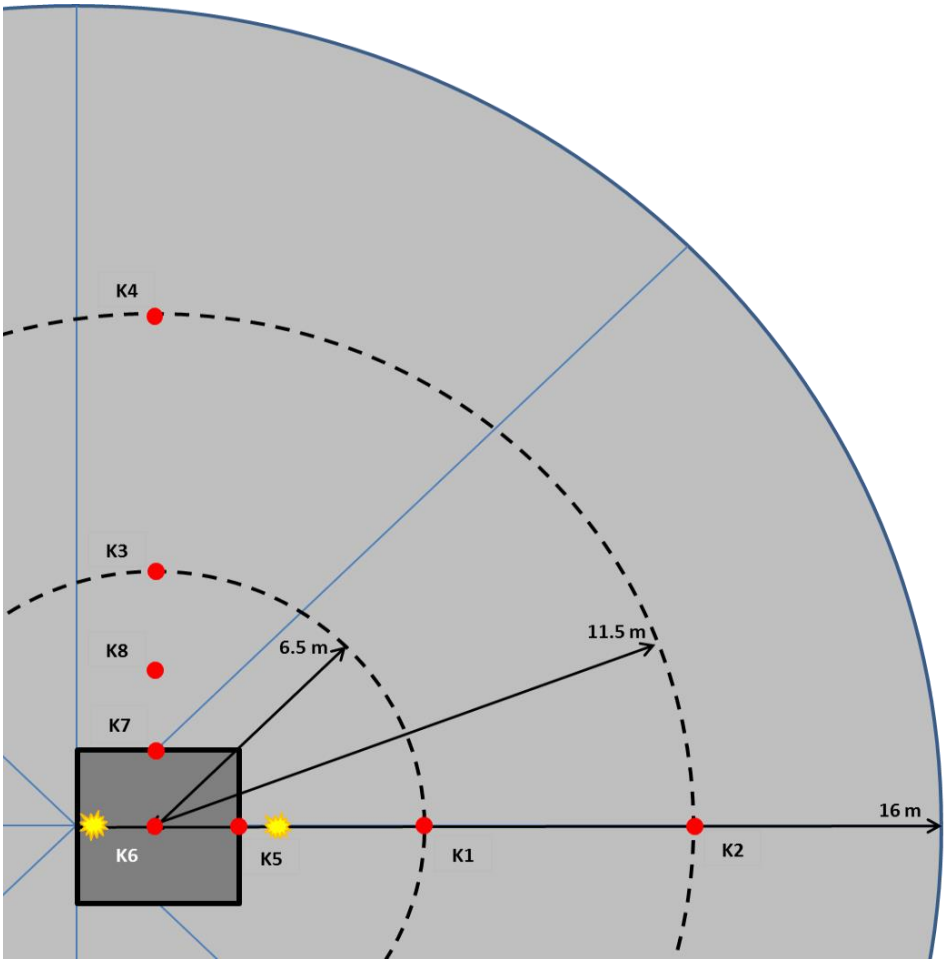

Fig.7: Pressure transducer layout diagram.

2.2.2 *Temperature and Concentration*

The temperature and hydrogen concentration was measured inside the congestion frame at 16 points. Each point held a type T sheathed thermocouple collocated with a stainless steel gas sampling line. These sampling lines ran approximately 30 m and each connected to a Xensor thermal conductivity sensor. The hydrogen concentration system was supplied by NREL (HyWAM) and logged at 4 Hz, whereas the thermocouples were logged through the primary control and logging system at 1 Hz.

2.2.3 *Pipework Measurements*

The instrumentation in the main release pipework consisted of two 10 bar Wika IS-3 pressure transducers, four type T thermocouples and a MicroMotion coriolis mass flow meter with an Elite 5700 transmitter. The mass flow meter was modified by the manufacturer to help facilitate operation at temperatures below 70 K. Each instrument was logged through the primary system, which also controlled the remote release valves, and was logged at 1 Hz.

2.2.4 *Noise Measurements*

Noise measurements were taken at two locations, shown on the map in figure 8. One was just outside the main control building and the other on a hill 215 m away from the centre of the concrete pad. For the majority of the trials the peak noise levels were recorded. Crucially, as exposure to noise was a safety concern, the trials would be halted if the noise levels at the control building reached a pre-set threshold.

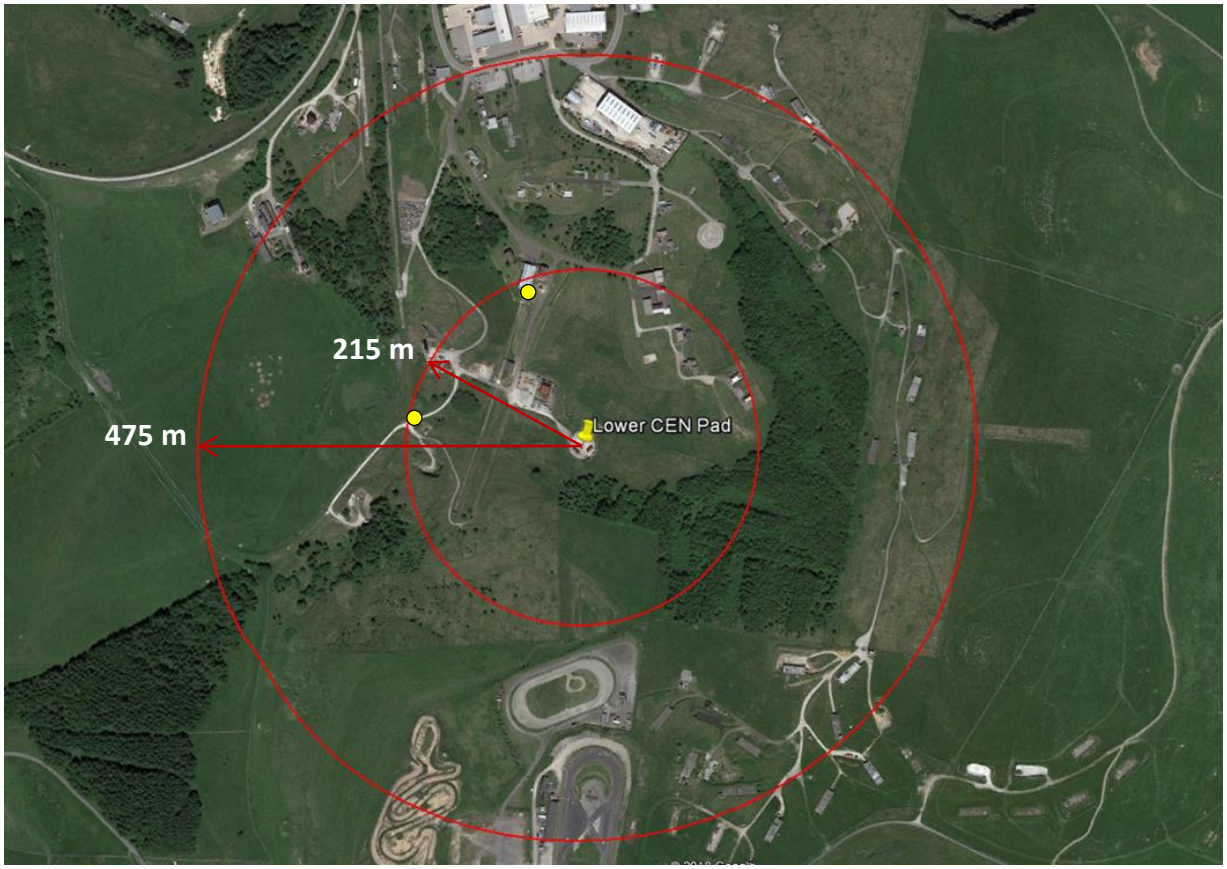

Fig. 8: Map showing noise measurement locations and distance to points of interest.

2.2.5 *Heat Flux*

The heat flux was measured by three Medtherm radiometers positioned at a height of 0.5 m and distances of 2.5, 3.5 and 6.5 m from the centre of the congestion rig. The orientation was perpendicular to the release direction.

2.2.6 *Weather Measurements*

Ambient conditions were measured using two systems: a Skye SKH-2053 temperature and humidity probe mounted alongside a WindSonic ultrasonic anemometer on a 3 m high stand on the downwind edge of the concrete pad approximately 20 m from the release point; and a PCE-FWS-20 weather station was positioned locally to the release station at 1.5 m height.

2.2.7 *Cameras*

A subsection of the following cameras were used to capture the events in each trial: three Sony FDR-AX53 handy cams recording at 50 fps provided standard footage with three views; a high speed Phantom Mira LC320 recording at 3600 fps captured detailed footage of the blast; and a FLIR X8400sc thermal camera indicated the flame front.

2.3 Measurement errors

The accuracy of the sensors used in the experiment are summarised below in Table 1. The information is taken from the respective manuals for the equipment. The inherent

variability in conducting experiments outdoors needs to be taken into consideration when interpreting the results.

Table 1: Sensor accuracies.

Sensor	Manufacturer	Model	Range	Accuracy
Blast pressure	Kulite	HKL-375 (M)	2 bara 5 bara	±0.5% of Full Scale
Noise	Bruel and Kjaer	2238 Mediator	80-140 dB	±1.5 dB
Heat flux	Medtherm	-	0-113.6 kW/m^2	Indicator
Pipework thermocouples	TC Direct	1.5 mm Type T Mineral insulated	–200 to 350°C	±1.5% of Reading
Pressure	Wika	IS-3	0-10 barg	±0.5% of Full Scale
Tank Pressure	N/A	Dial gauge	0-15 barg	Visual
Mass flow	Emerson	Micro Motion Coriolis meter	0-7.5 kg/s	±3% of Reading*
Near-field weather station	PCE Instruments	PCE-FWS-20	0-240 km/h 10-90 % humidity	Indicator
Far-field wind sensor	Gill Instruments	Windsonic	0-60 m/s 0-359°	±3% of Reading ±2°
Far-field humidity sensor	Skye Instruments	SKH 2053	0-100 % -20 to 70°C	±2% ±0.05°

2.4 Test programme

Table 2 shows the planned test programme. As well as the conditions shown below, the initial tanker pressure was also changed with trials being conducted at 1 bar and 5 bar. The experiments are displayed in the test programme as approximately least to highest risk and were therefore conducted in that order. Test no. 5.5.5 reached noise limits at the control room so no further tests were conducted. As such, tests 5.5.6 to 5.5.10 have a grey background in table 2.

Table 2: Test plan

Work Package	Experimental Subtask	Test No.	Pool/jet	Orifice size (mm)	Blockage ratio	Confinement
5	5.5	5.5.1	Jet	6	Low	Open
5	5.5	5.5.2	Jet	12	Low	Open
5	5.5	5.5.3	Jet	25.4	Low	Open
5	5.5	5.5.4	Jet	6	High	Open
5	5.5	5.5.5	Jet	12	High	Open
5	5.5	5.5.6	Jet	25.4	High	Open
5	5.5	5.5.7	Pool	25.4	Low	Open
5	5.5	5.5.8	Pool	25.4	High	Open
5	5.5	5.5.9	Jet	6	Low	2 sides closed
5	5.5	5.5.10	Jet	6	Low	2 sides closed

2.5 Procedure

Over time the temperature of the LH2 in the tank increases, resulting in an ullage pressure above ambient and increasing the likelihood of flashing in the pipework. For consistency, prior to each day of testing, the temperature of the bulk LH2 was reduced to close to the normal boiling point by venting some ullage gas and lowering the pressure – cooling the liquid. The pressure in the ullage could be raised above the vapour pressure of the liquid by allowing LH_2 from the bottom of the tank into a heat exchanger and feeding the gas back into the top of the tank.

Air in the pipework with LH_2 poses significant hazards, as there is the potential to form both blockages and flammable mixtures. As such, immediately before each set of releases the pipework was purged; firstly with nitrogen, then with ambient hydrogen gas. Once the purge was complete, LH_2 could be introduced to the pipework. This operation purged the majority of the pipework, but a 1.75 m section of flexible hose located after the main release valve was not purged.

Recording was initiated in the data logging software and the main release valves opened. The initial conditions of the experiments mirrored those in previous work packages so that, in particular, the dispersion would be better understood. The release before ignition was not a set time, but a steady state in the output was required so the congestion rig was saturated by the time of ignition. Care was taken to avoid ignitions if the hydrogen cloud, indicated by the mist, had moved to an undesirable location.

3 Results

A series of 23 ignited congestion trials were conducted as a part of work package 5. Table 3 shows the initial conditions of each trial, the peak measured overpressure (and the location of that pressure transducer), the noise measured outside of the control room and approximate maximum pressures recorded at a range of 6.5 and 11.5 m from the centre of the congestion rig.

Table 3: Experimental series initial conditions and results overview.

Test No.	Orifice Diameter (mm)	Tanker pressure (barg)	Ignition point	Congestion level	P max (bar)	At	Noise (dB)	Pmax 6.5m (mbar)	Pmax 11.5m (mbar)
1	6	1	Front	Low	0.01	K6	*1	2	1
2	12	1	Front	Low	0.52	K7	*1	40	23
3	25.4	1	Front	Low	0.16	K5	*1	5	4
4	12	1	Front	Low	0.03	K5	123	12	7
5	25.4	1	Front	Low	0.02	K5	117	11	5
6	12	1	Front	Low	0.04	K5	125	12	7
7	25.4	1	Front	Low	0.38	K5	114	7	4
8	12	1	Rear	Low	0.07	K6	*2	14	8
9	12	1	Rear	Low	0.04	K6	123	10	5
10	25.4	1	Rear	Low	0.01	K6	108	4	2
11	6	5	Front	Low	0.14	K5	122	13	7
12	12	5	Rear	Low	0.39	K5	132	40	25
13	12	5	Front	Low	0.13	K5	131	50	30
14	12	5	Rear	Low	0.53	K5	127	20	12
15	12	5	Front	Low	0.10	K5	132	40	20
16	12	5	Rear	Low	0.55	K6	134	40	20
17	12	5	Front	Low	0.67	K5	129	30	15
18	25.4	5	Front	Low	0.04	K5	120	15	7
19	25.4	5	Rear	Low	0.15	K5	137	70	40
20	6	1	Front	High	0.01	K6	*2	3	2
21	12	1	Front	High	0.15	K5	134	40	25
22	12	1	Front	High	0.13	K5	132	65	40
23	12	1	Front	High	1.28	K5	145	470	205

**1 Noise measurements not made.*

**2 Noise too low to discern from local ambient noise.*

3.1 Weather conditions

The wind conditions during the releases had an impact on the outcome by acting on the cloud. Appendix B contains images of each trial immediately prior to ignition and illustrates this effect. The wind speed was measured at two locations for the experimental campaign and table 4 shows the output. The 5 minute average wind speed and direction measured at the release point, and the average wind speed and direction measured in the far field averaged for 30 seconds prior to ignition.

Table 4: Wind conditions for each trial.

Trial No.	Local 5 min average wind speed (m/s)	Local 5 min average wind direction	Far-field wind speed (m/s)	Far-field wind direction (°)
1	1.0	W	2.03	172
2	3.4	S	2.00	136
3	2.0	SW	0.52	224
4	2.7	SE	1.09	123
5	2.4	W	1.38	189
6	0.7	SE	1.44	107
7	1.7	SSE	1.62	112
8	2.0	W	2.58	266
9	2.0	W	3.74	243
10	2.0	N	2.62	250
11	1.0	NE	1.01	127
12	0.7	SE	1.44	45
13	1.0	NW	1.01	139
14	1.0	NE	2.48	79
15	2.4	NE	2.14	42
16	2.7	N	1.24	299
17	0.7	N	0.69	312
18	0.7	SE	0.60	70
19	0.7	E	1.21	179
20	2.0	E	1.37	94
21	1.4	SE	2.70	85
22	2.4	E	2.14	50
23	2.0	E	3.22	71

3.2 Overpressure

The overpressure was measured at eight points in and around the congestion frame. Graphs showing the responses from all pressure transducers for each trial are held in Appendix C.

3.2.1 *Trials 1, 11, and 20*

Trials 1, 11 and 20 were carried out through the 6 mm nozzle and showed consistently low overpressures and noise. A qualitative review of the footage shows a much smaller visible mist when compared to the other nozzle sizes, indicating a much lower hydrogen inventory in these trials. The congestion did not appear to have a significant impact on the measured overpressures as both trial 1 and 20 show similar behaviour. The higher tanker pressure resulted in a larger hydrogen inventory and therefore overpressures.

3.2.2 *Trial 2*

Trial 2 was unique as it is the only trial in which the peak overpressure was measured at K7, which is off the centreline of the release. This suggests that the cloud was off centre, corroborated by both table 3 and the footage, with a still shown in figure 9.

Fig. 9: Image of trial 2 immediately prior to ignition.

3.2.3 *Trials 3 to 7*

Trials 3 to 7 were conducted with the low level of congestion, 1 barg tanker pressure and a front ignition. The nozzle was alternated between a 12 mm and 25.4 mm orifice. Peak overpressures were consistently measured at K5 and those from the larger nozzle were typically higher, due to the larger hydrogen inventory. However, trial 5 showed particularly low measured overpressures. A qualitative review of the footage shows a swirling wind on the pad, which could have diluted the cloud in this case.

3.2.4 *Trials 8 to 10*

Trials 8 to 10 were conducted with the low level of congestion, 1 barg tanker pressure and a rear ignition. Both 12 mm and 25.4 mm orifices were used. Peak overpressures were

consistently measured at K6 however the release through the 25.4 mm nozzle was lower than those through the 12 mm nozzle for these tests.

3.2.5 *Trials 12 to 17*

Trials 12 to 17 were tests involving the same initial conditions of 5 barg tanker pressure releases through the 12 mm nozzle and the low level of congestion, but with alternating ignition locations. When grouped by ignition location, the average measured peak overpressure is 0.3 bar for front ignitions and 0.49 for rear ignitions, although there is much higher variation in the front ignitions. Figures 10 and 11 show the measured peak overpressures at the centreline pressure transducers for trials 12 to 17, grouped by ignition location and averaged against the distance of the pressure transducer from the ignition point. The highlighted region shows where congestion is present. As displayed in table 3, for all trails other than trial 16 the maximum overpressure was measured at K5. For comparison, figure 12 shows the peak pressure measured on the centreline pressure transducers against the distance from the ignition point for trial 16.

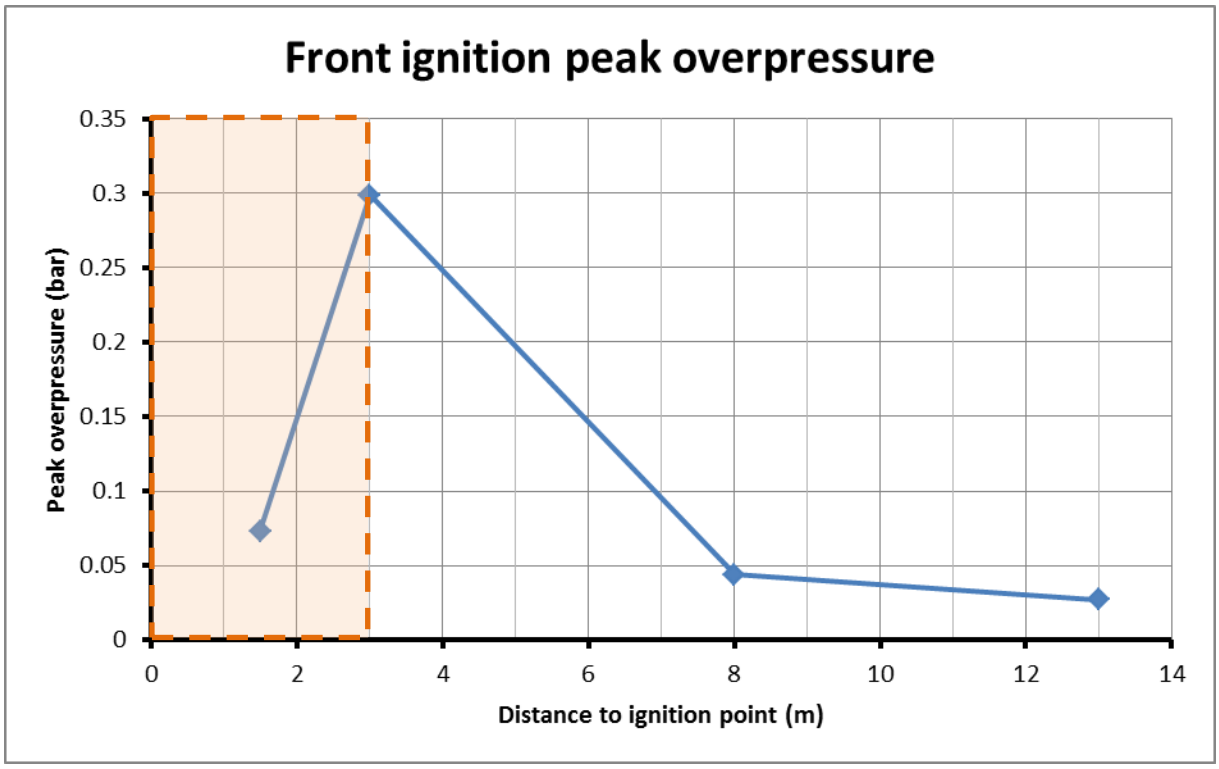

Fig. 10: Average peak measured overpressures against distance for front ignitions.

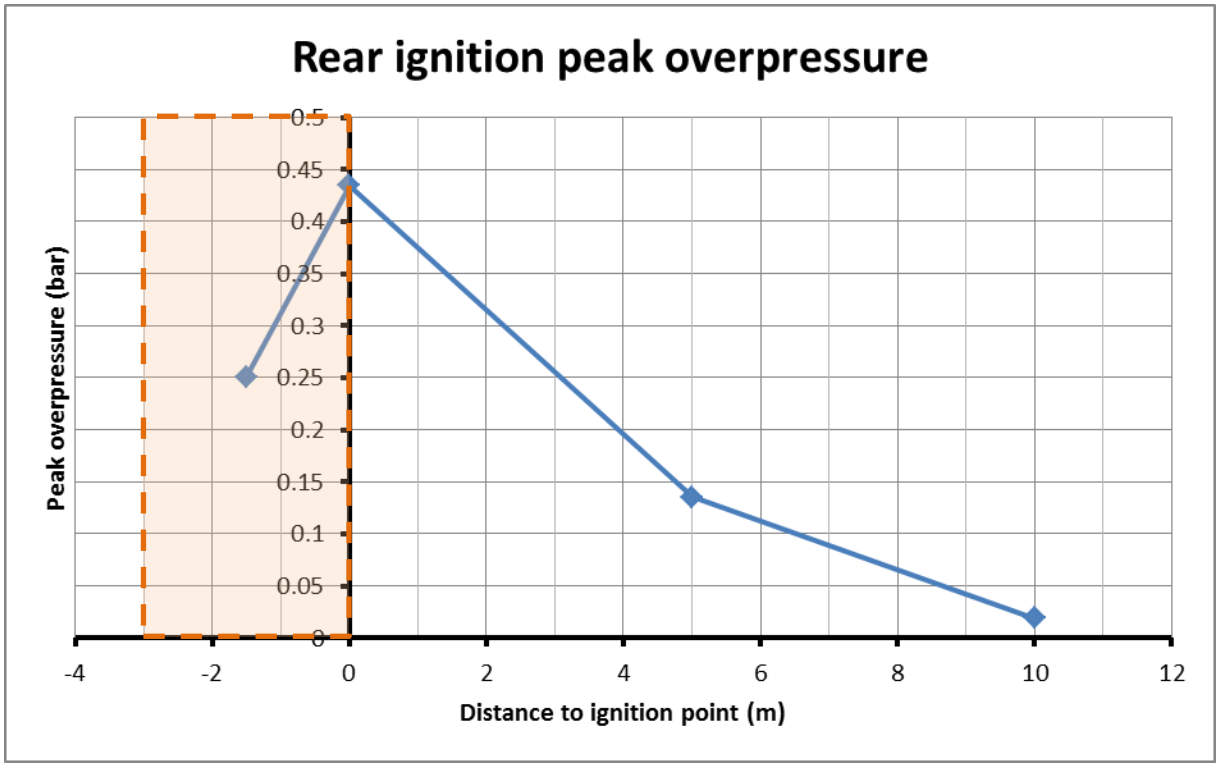

Fig. 11: Average peak measured overpressures against distance for rear ignitions.

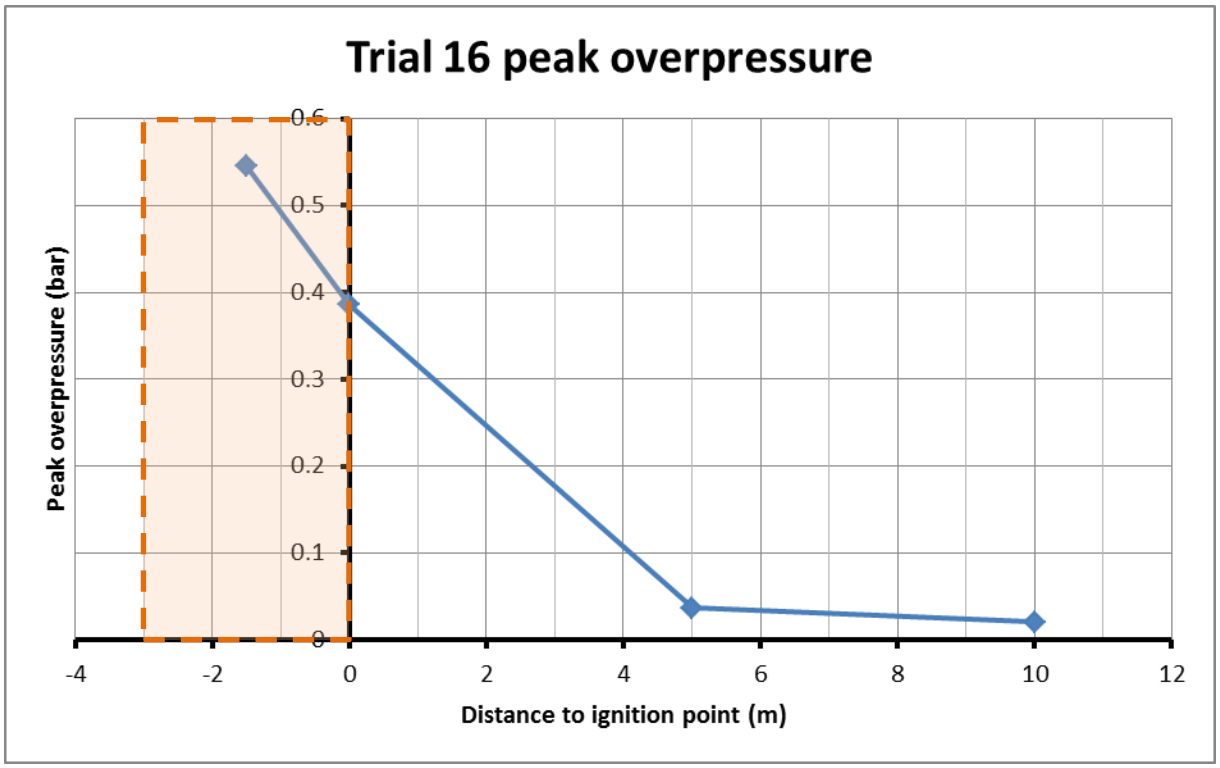

Fig. 12: Peak measured overpressures against distance for trial 16.

3.2.6 *Trials 18 and 19*

Trials 18 and 19 were conducted with similar initial conditions to trials 12 to 17, but with the 25.4 mm nozzle. The peak overpressure was higher for the rear ignition, although the average was lower than the measured overpressures for the similar 12 mm nozzle releases. For trial 19, however, this shows a significant discrepancy between the noise at 200 m and the measured overpressure.

3.2.7 *Trials 21 to 23*

Trials 21 to 23 were repeat tests with initial conditions of 1 barg tanker pressure, 12 mm nozzle and front ignitions using the high level of congestion. All three tests were carried out in sequence over a period of about 40 minutes in very similar average weather conditions. Trials 21 and 22 showed consistent behaviour, but 23 showed almost a tenfold increase in overpressure. This is shown in figure 13, which has the overpressure output from K1 and K2 for each of these trials. These pressure transducers were approximately 8 m and 13 m from the front ignition point respectively, along the centre line of the release on the far side of the congestion.

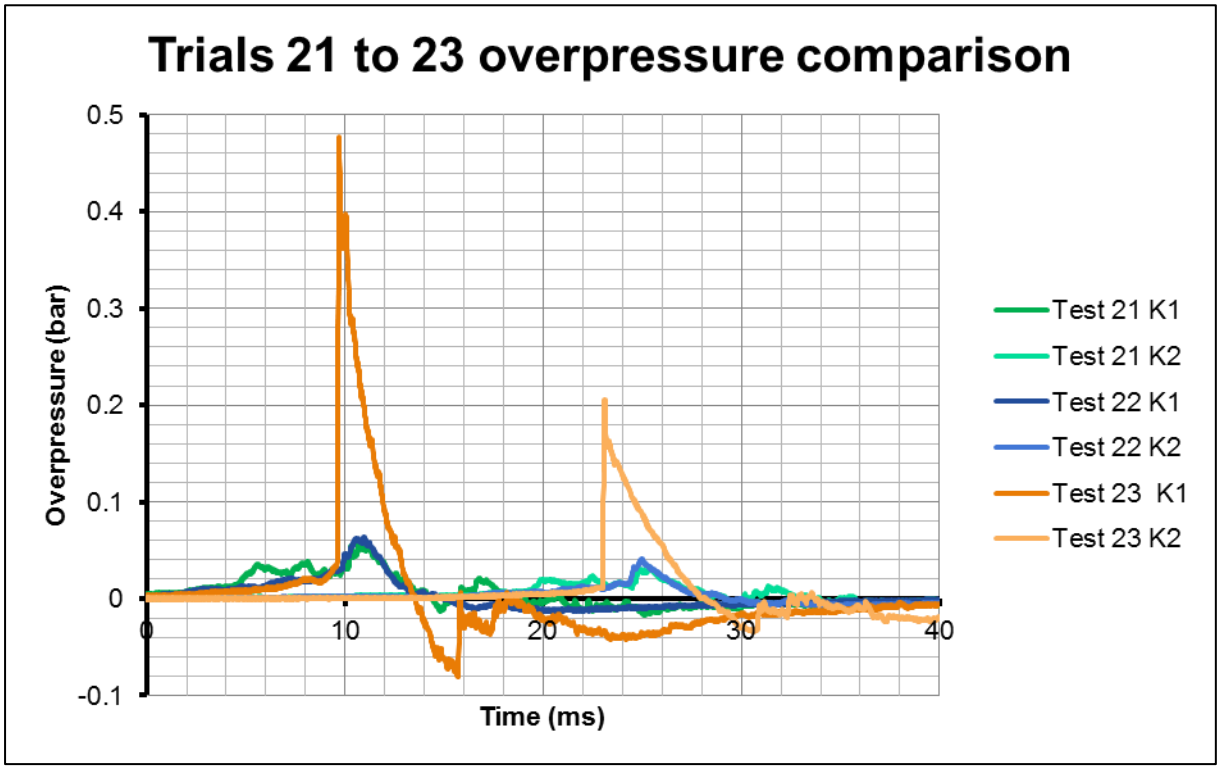

Fig. 13: Overpressure comparison for the repeated trials 21 to 23.

3.3 Heat flux

Three radiometers were used at varying distances in an attempt to measure the heat flux of the combusting cloud. Unfortunately, between the narrow field of view of the sensors, the obstruction caused by the congestion frame and the uncertain nature of the events, only one sensor consistently provided reportable measurements. These measurements, however, did identify both the initial blast and jet fire phases. Figure 14 shows the measured heat flux from trials 21 to 23.

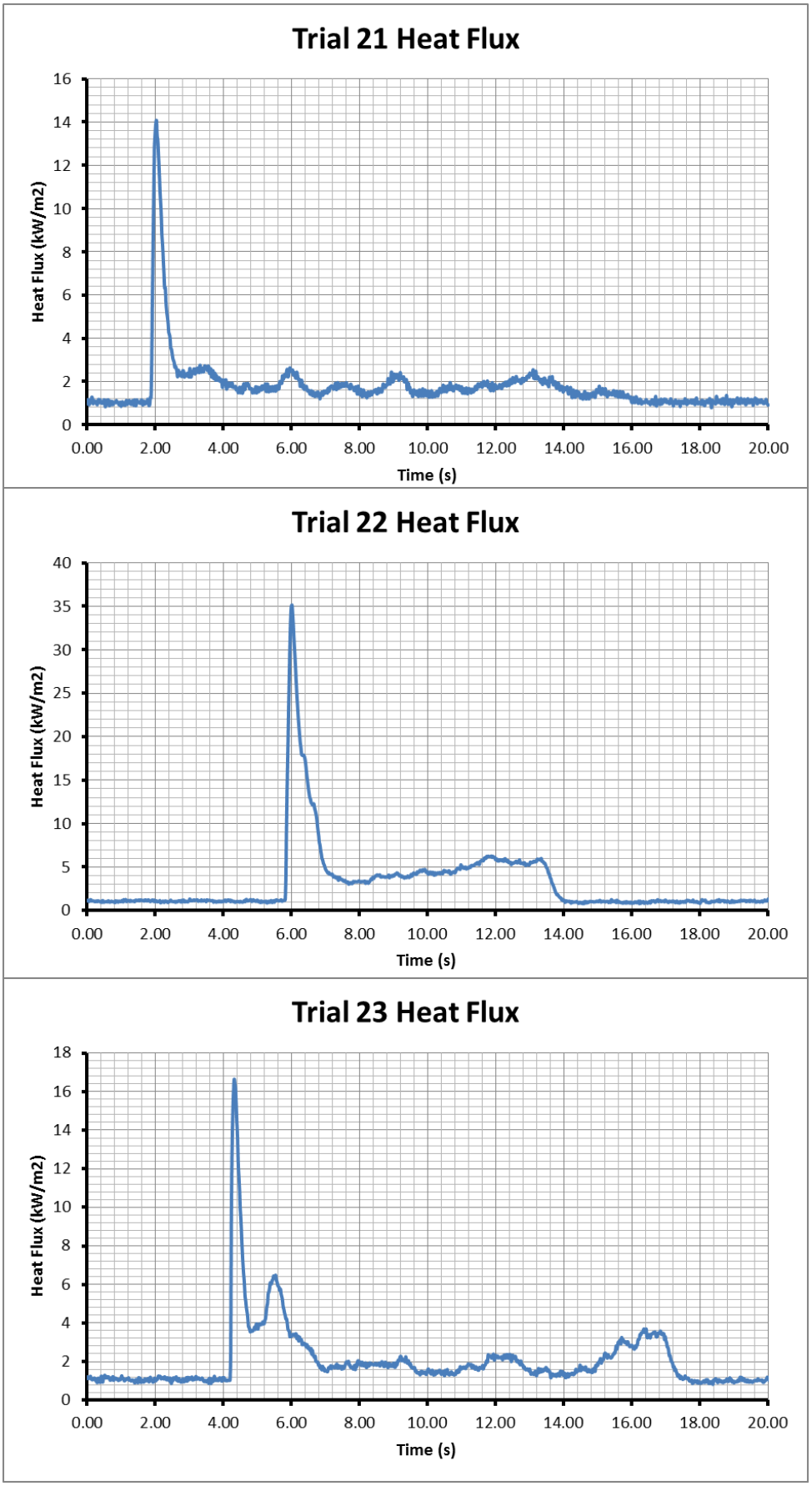

Fig. 14: Heat flux outputs from trials 21 to 23.

4 Discussion and analysis

4.1 Noise levels

As the series of experiments were conducted, it became apparent that the noise levels being achieved at the control room were higher than predicted. As such, the planned experiments after 5.5.5 were not conducted due to the noise threshold being reached by the low-pressure experiments conducted with high levels of congestion. Unfortunately, this means that the effects of neither partial confinement nor congested pools were studied. To compensate for this, multiple repetitions were carried out to give a higher degree of reliability with the results.

4.2 Mass flow rate

Two initial conditions had an effect on the hydrogen inventory within the congestion rig: tanker pressure and release nozzle size. Since the pipework was the same as used in the WP 3 trials, table 5 from D3.6 shows the predicted mass flow rates for each initial condition should be consistent with the releases in this work package.

Table 5: Mass flow rates for each initial condition.

Pressure	Nozzle diameter	Mass flow
5 bar	6mm (¼ ”)	90-100 g/s
5 bar	12mm (½”)	265 g/s
5 bar	1” (open pipe)	298 g/s
1 bar	6mm (¼ ”)	Unknown
1 bar	12mm (½”)	104-107 g/s
1 bar	1” (open pipe)	135-144 g/s

A general pattern that was observed was that the increased tanker pressure reliably increases the noise and overpressure levels. This is due to higher mass flow rates and flow speeds; resulting in a greater mass of hydrogen being combusted and higher initial turbulence levels. However, the nozzle size shows different behaviour, the 6 mm and 24.5 mm nozzle typically show lower noise levels than the 12 mm nozzle. While it is likely that the low mass flow rates of the 6 mm nozzle result in a much lower hydrogen inventory inside the congestion rig, it is postulated that the results from the 25.4 mm nozzle are primarily an effect of mixing, with the releases through the 25.4 mm nozzle being too rich within the congested array to efficiently combust the hydrogen.

4.3 Ignition point

In practice, when measured at a long distance, there is little correlation in the effect of ignition position on the noise measured. This can be clearly seen with the repeated tests through the 12 mm nozzle with a 5 bar tanker pressure. The average peak noise level at the control room was 131 dB for rear ignitions and 130.67 dB for front ignitions.

When analysing the peak overpressures however, a trend does become apparent. The general trend that was identified when changing the ignition points from front to rear was that the overpressure tended to increase for the front ignitions as the flame accelerated through the congestion rig, whereas the overpressures tended to reduce through the congestion rig with rear ignitions. This led to the peak overpressure being consistently measured at K5, which corresponds to 3 m from the ignition point for front ignitions, and 0 m from the ignition point for rear ignitions.

There were exceptions to this trend. Trial 16 showed unusual behaviour in that the peak overpressure measured at K6 was higher than K5, indicating that either the flame accelerated downstream at a faster rate than the other rear ignitions, or the cloud had developed in an unusual manner.

4.4 High congestion tests

The three final tests (Nos 21-23) were carried out with the higher level of congestion. The nozzle size was 12 mm and driving pressure 1 bar. Test 23 was a severe explosion that caused damage to the building housing the video and IR cameras. High noise levels at the exclusion zone threshold meant that the programme could not be extended to higher outlet pressures and larger nozzle sizes.

Test 23 showed a qualitatively different behaviour to other the two preceding tests – even though these were carried out immediately before, in similar conditions[1]. High overpressures and the shape of the pressure peaks, with a large discontinuous increase in pressure following the passage of a shock, suggest a high order deflagration or detonation (Level 8-10 in the TNO Multi Energy Method).

4.4.1 *Positive Pressure Pulses*

Figures 15 to 16 show that Friedlander curves fit well to the positive pressure pulse. This type of fit allows the maximum pressure to be estimated more reliably than simply reading the maximum values –which can be affected by noise and very high frequency structural responses to shock in the sensors.

Friedlander curve $P = P_{max} e^{-\frac{t}{t^*}} \left(1 - \frac{t}{t^*}\right)$ t* is the duration of the positive pulse

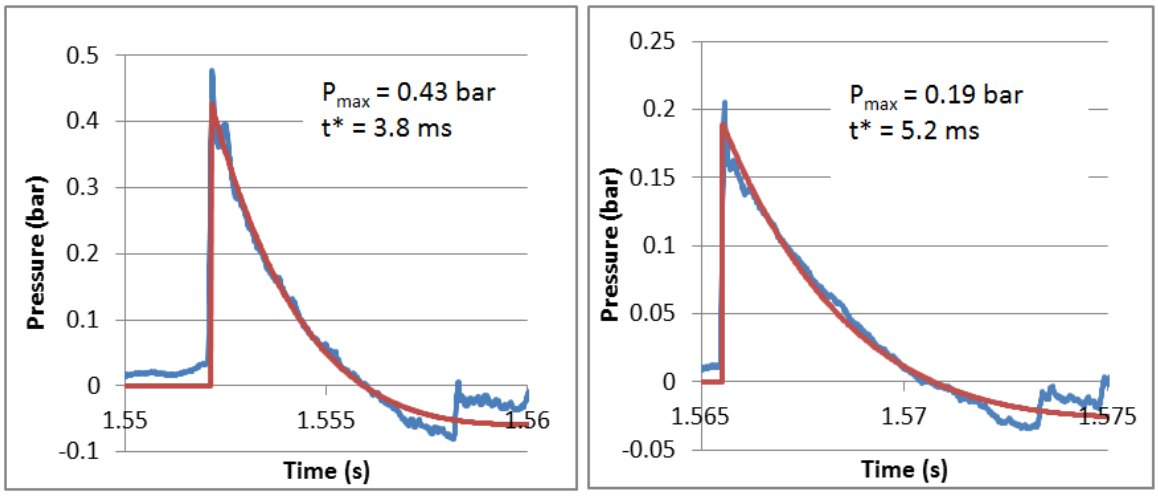

Fig. 15: Test 23 - Pressure gauges K1 (6.5m) and K2 (11.5 m) – distance from centre along jet axis

[1] Tests 21, 22 and 23 were carried out over period of around 40 minutes

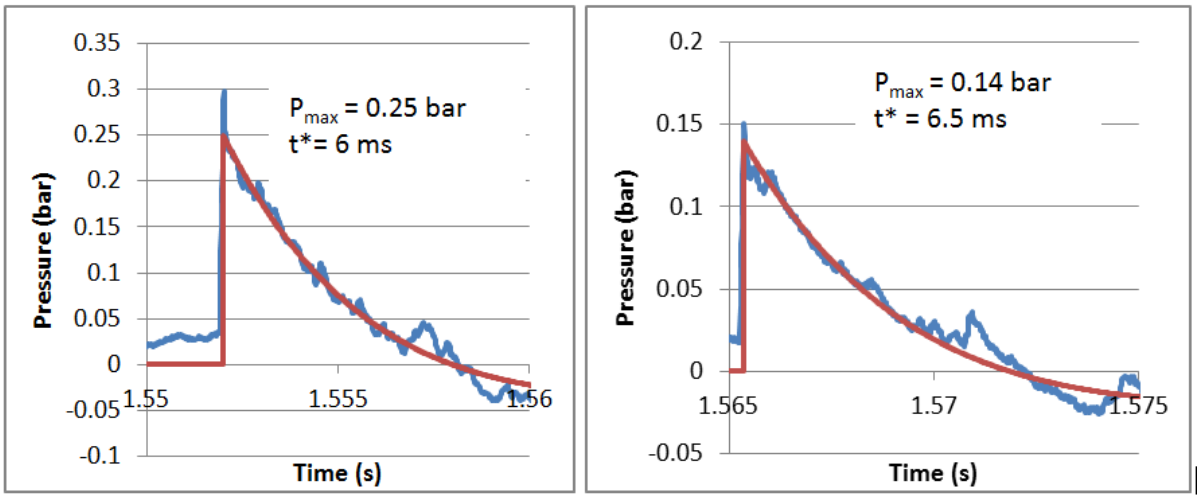

Fig. 16: Test 23 - Pressure gauges K3 (6.5m) and K4 (11.5 m) – distance perpendicular to jet axis

The time of passage between K1-K2 and K3-K4 was in the range 13.35 -13.41 ms. This gives an average shock velocity of 372 - 374 m/s. This is the shock speed associated with an overpressure of around 0.24 bar [4] which is reasonably consistent with the pressure measurements.

The measured overpressures are higher at K1 and K2 than K3 and K4. There are a number of potential explanations for this:

1. Residual asymmetry in the pressure field with higher overpressures in the direction of propagation of the (high order) explosion: This is difficult to discount completely but it was not observed in the Buncefield detonation trials [5]. By the time pressures had declined to a few hundred millibars the asymmetry in pressure signature had disappeared.

2. Variation in the location of the exploding gas cloud: This seems more likely. High speed video shows rapid combustion of the parts of the cloud along the line to K1/K2 both in and just outside the congestion rig. In contrast there is residual slower combustion of parts of the cloud outside the congestion rig on the line towards K3/K4. It is possible that sensors K3/K4 are simply further away from the area where the intense combustion occurred.

4.4.2 *TNT equivalence*

The issue of specifying the location of the effective centre of the explosion relative to the pressure measurement points means there is significant uncertainty about the amount of hydrogen that was involved, or the TNT equivalence of the explosion.

The sensors at 11.5 m from the congestion centre are most useful as the distance is (proportionally) known with more accuracy.

If it is assumed that the explosion centre is coincident with the congestion rig centre then the observed pressures at K2 and K4 correspond to 1.5 kg and 2.5 kg TNT respectively[2]. The positive pulse durations for these TNT explosions would be 5.5 - 6.2 ms respectively

[2] Hemispherical charges at ground level.

which is roughly similar to the measured values. If the explosive energy release for TNT is assumed to be 4.533 MJ/kg, the energy associated with TNT charges to match the pressure at this range would have to have been 6.8 to 11.3 MJ. The use of a single equivalent amount of TNT to describe the effects of a gas explosion is problematic because the amount of TNT required varies with distance. This is discussed further below.

4.4.3 *Energy release by comparison with a well-mixed detonation test*

The overpressure curves are very similar in form to those observed in the large detonation tests described in the SCI Report on Buncefield JIP trials (Figure 17). In this case, a detonation (initiated with explosives) progressed through the length of a well-mixed near stoichiometric propane cloud with dimensions 30 x 10 x 3 m. Pressures were measured at different distances from the edge of the cloud.

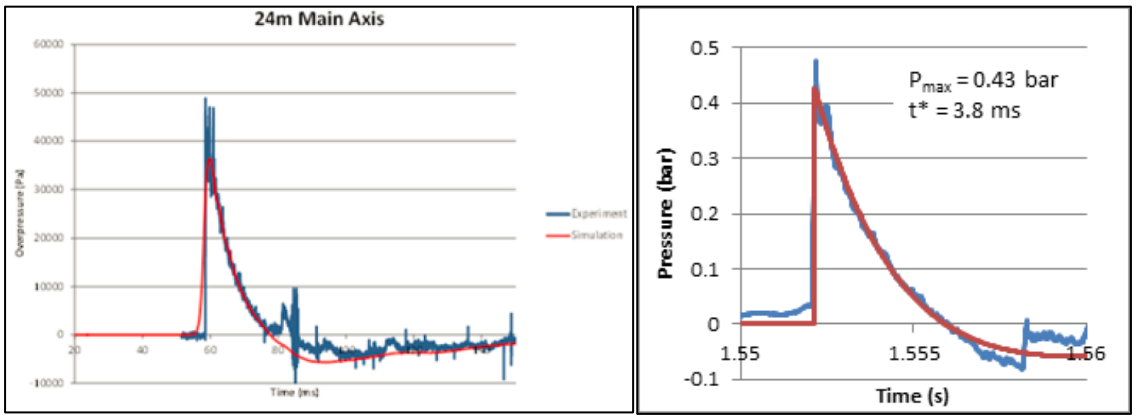

Fig. 17: (Left) propane detonation 30 x 10 x 3 m, (Right) PRESLHY test K1 (6.5m)

The overpressures in these two cases are similar but the distance scale for the PRESLHY test is about 5 times less than the large explosion[3]. The timescale of the pressure pulse is also about 5 times less.

One could expect the length scale and duration of the pulse to vary as $(E/P_0)^{1/3}$ which suggests the energy release in the PRESLHY test was approximately $(5)^3 = 125$ times less than the larger test.

The energy release in the large test was around 2800 MJ leading to an estimate for the PRESLHY Test 23 of 2800 / 125 = 22 MJ.

4.4.4 *TNO Multi-Energy Method*

Another method of estimating energy release is to use the blast curves from the TNO Multi-Energy Method (MEM) - Figure 18.

[3] It is possible to see the location of the edge of the combustion zone on video of the tests and to determine the distance to the pressure transducer with more confidence than the distance to the explosion centre.

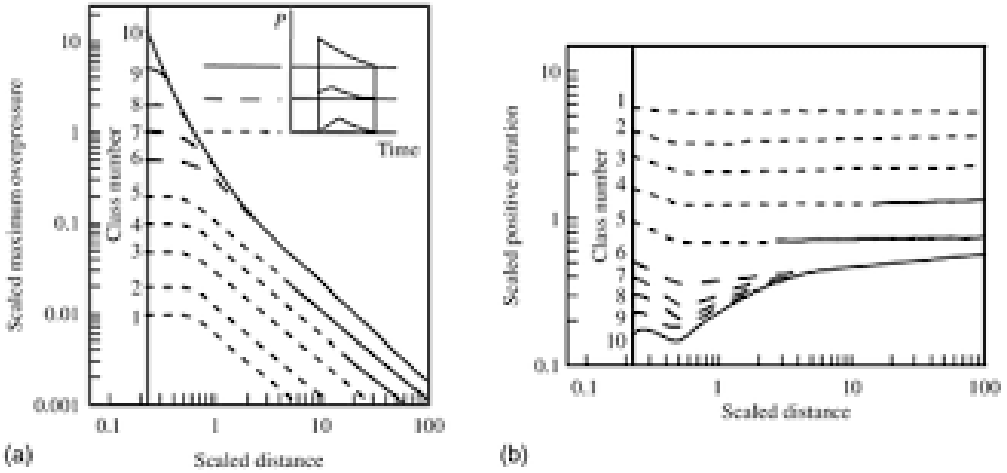

Fig. 18: Scaled overpressure and duration data from the TNO MEM.

For a high order explosion in the relevant range of scaled distances R' the scale overpressure is [6]

$P/P_0 = 0.467\ R'^{-1.58}$

Where R' is the scaled distance $R' = R/(E/P_0)^{1/3}$

The measured values of pressure ratio P/P_0 at a range of 11.5 m from the rig centre range was between 0.14 (K4) and 0.19 (K2). According to the MEM fit above this corresponds to a range of reduced distances of R'= 1.76 to 2.1.

We have no reliable way to accurately determine R – the actual distance to the explosion centre but it must be roughly 11.5 m. With this assumption the results imply a range of energies between 16 and 27 MJ. If, as seems likely, the K2 gauge is somewhat closer to the centre of the explosion then the upper limit would be reduced. If the effective distance were 10.5 m, the upper limit on the energy estimate would be 21 MJ.

These figures are broadly consistent with the estimate of energy release based on comparison with the larger scale detonation test.

4.4.5 *Comparison between MEM and TNT equivalence methods*

It is straightforward to show that the idea of a single equivalent quantity of TNT is inconsistent with the TNO MEM blast curves. Table 6 shows the how the energy of a gas explosion (from MEM) compares with the mass of TNT required to produce a given pressure. The ratio of the two is not generally 4.533 MJ/kg – the explosive energy release of TNT. At close range (pressures over 100 mbar) the energy in a gas explosion must be twice the explosive energy of a TNT charge to generates the same overpressures.

Table 6: Comparison between MEM and TNT blast curves

$R' = R/(E/P_o)^{1/3}$ P_o(Pa), E(J), R(m)	$\Delta P/P_o$ (MEM Levels 8-10)	$Z = R/W^{1/3}$ W(kg), R(m)	E (TNT) (MJ/kg)
1	0.467	4.7	10.3
3	0.0919	14.1	10.4
10	0.0236	39	5.9
50	0.0038	142	2.3

This difference appears in the previous analysis of PRELHY measurements in the range 100-500 mbar. The energy of the gas explosion required is of order 20 MJ, whereas the mass of the TNT charge that would produce the same effect at this range is only around 2 kg – which would have an explosive energy release of about 9 MJ.

4.4.6 *Previous work*

Groethe et al [7] carried out a 300 m^3 hemispherical stoichiometric hydrogen detonation (E= 864 MJ). This was analysed by Mélani et al. [8] and shown to fit the TNO blast prediction for a high level explosion. For example: at 22 m from centre the value of $R' = R/(E/P_0)^{1/3} = 1.07$. Predicted and measured pressures at this location were around 500 mbar. A 190 kg TNT charge would have an explosive energy of 864 MJ. This would produce substantially higher pressures than those which were measured.

Wakabayashi et al [9] carried out hydrogen detonations in a cylindrical tent with height and diameter 3.4 m. Test concentrations (v/v) were 21%, 28.7% and 52%. At 21% the measured overpressures (in the 100-500 mbar range) were substantially less than those for a TNT explosion with a similar explosive energy release - calculated on the basis of 4.533 MJ/kg. These results were in line with Groethe's results and the MEM.

However, at 28.7% the pressures measured by Wakabayashi were close to the level expected for a TNT charge with a similar explosive energy. The gas cloud was significantly different in shape to that used by Groethe and assumed in the MEM, but the discrepancy remains to be explained.

Wakabayashi et al also found that the very rich cloud 52% caused pressures equal to those for the stoichiometric case (in the range of pressures <1000 mbar). The impulse was much larger for the rich cloud. This shows that the entrainment and combustion of additional oxygen occurs so quickly and efficiently that it contributes to the blast energy.

4.4.7 *Measurements of gas concentration*

Figure 19 shows average concentrations at approximately the height of the jet half way through the congestion array (1.5m from source) and at the downstream edge of the congestion array (2.9m from source).

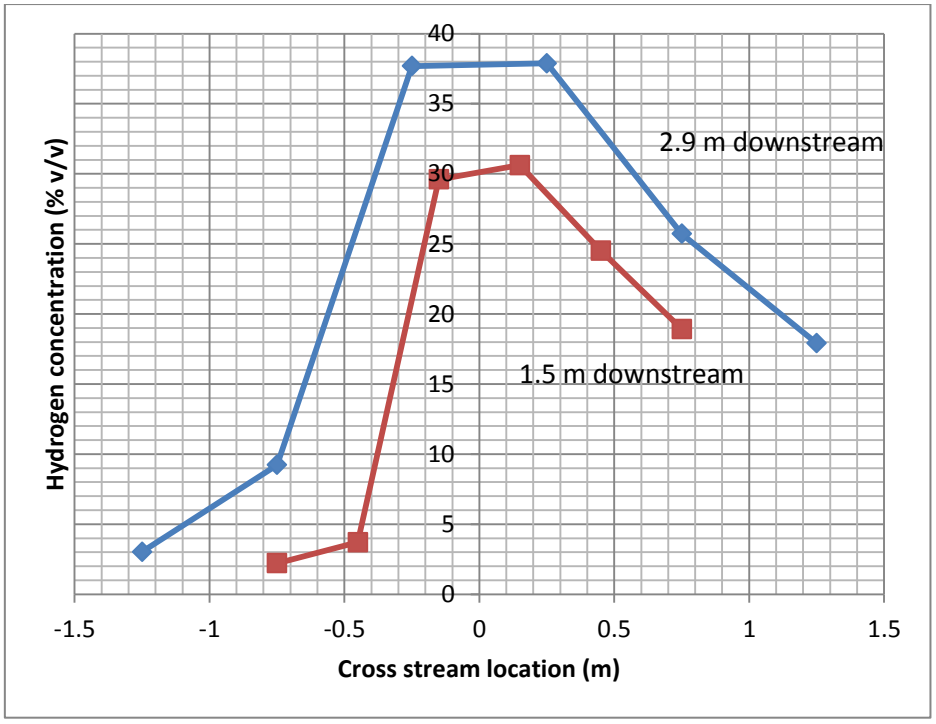

Fig. 19: Concentrations profiles at 1.5 and 2.9 m from the source

The concentrations are higher at the downstream edge of the congestion array – further form the source - which is odd. Probably a slight deflection of the jet by the opposing wind or outlet nozzle misalignment meant that the highest concentrations were not registered by the closer array.

The measurements close to the downstream edge show that almost all of the width of the rig was exposed to gas in the flammable range and about two-thirds of the width saw gas in the detonable range. Measurements 750 mm above and below the axis of the jet at a distance of 1.5 m from the source also showed some concentrations above stoichiometric.

Because the opposing wind blew gas in the jet back into the congestion array there was insufficient instrumentation to be able to fully characterise the jet/cloud prior to ignition. The estimate of burned hydrogen inventory from blast analysis was approximately 20 MJ which corresponds to a mass of hydrogen of around 160 g or a volume (at stoichiometric concentration) of about 6.6 m^3. The total volume of the rig is 18 m^3 and the estimate of burned inventory seems plausible given the available concentration measurements – especially if excess gas in volumes over the stoichiometric level can mix quickly enough to contribute to blast energy, as was observed by Wakabayashi et al.

4.4.8 *Comparison between Test 21 and 23*

Tests 21 to 23 were repeats carried out over a relatively short period of time in similar conditions. Figure 20 compares the concentration profiles close to the downstream edge of the congestion array in Tests 21 and 23, immediately prior to ignition. The differences in concentration are relatively small. The average hydrogen concentration over all of the measurements points was around 2% v/v higher for Test 23. One would expect such differences to make only a marginal difference to the observed flame speed and associated overpressure.

However, the outcome of the two tests was remarkably different. Typical overpressures are compared in Figure 21. Overpressures in Test 23 exceed those in Test 21 by a factor

7-8. Assuming, for illustrative purposes, that the flame speed was the same in the two tests then the energy release in Test 23 would have had to be approximately $4.4^3 = 85$ times that in Test 21 – Figure 22.

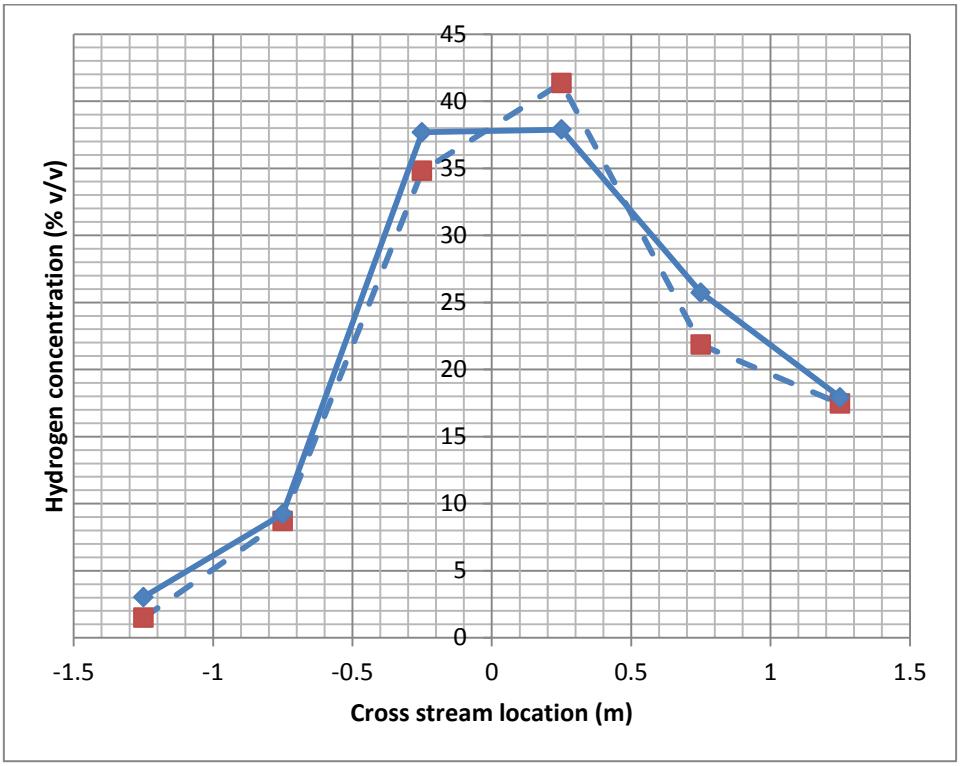

Fig. 20: Comparison of the concentration profiles 2.9 m downstream in Tests 21 and 23

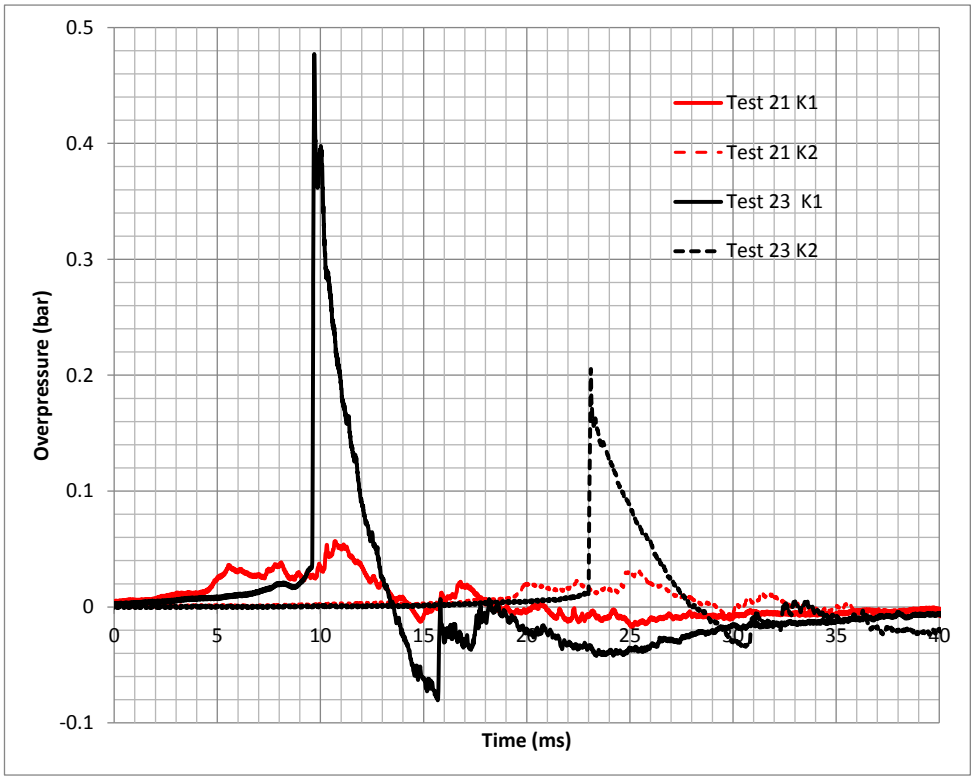

Fig. 21: Comparison of overpressure measurements for Test 21 and 23

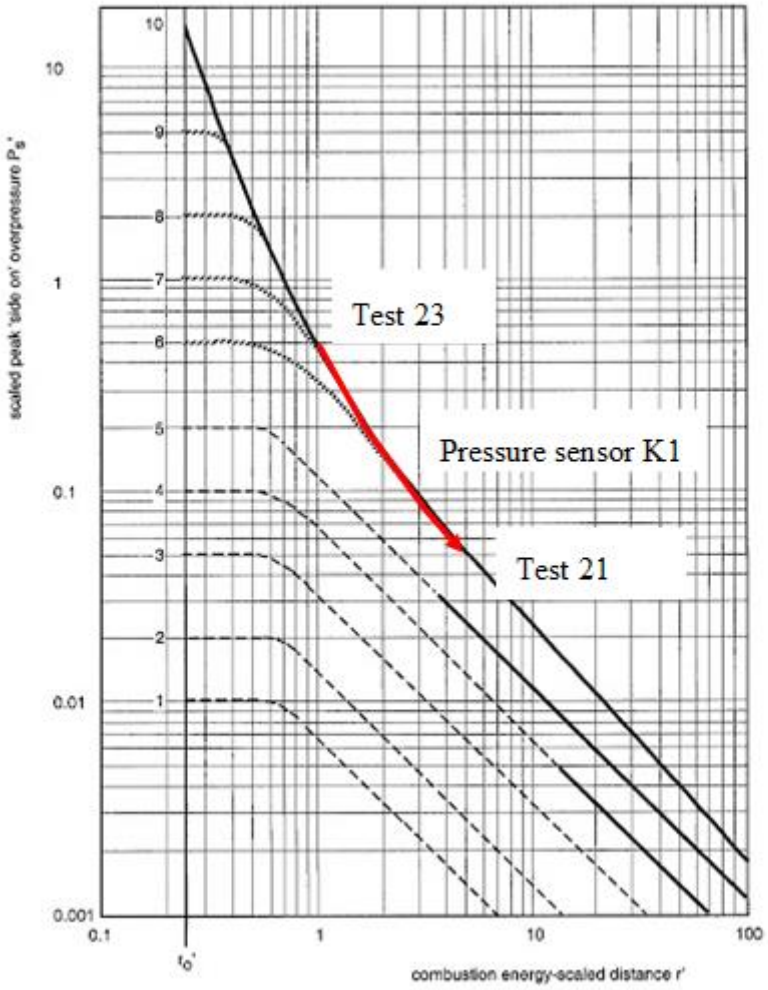

Fig. 22: Change in combustion scaled distance between Test 23 and 21 – this is on the (incorrect) assumption that the flame speeds are similar in the two tests. Note $E \propto r'^{-3}$

In reality the concentrations were similar in the two tests and the total amount of gas burned and energy released would have been similar. The difference in overpressures was caused by a difference in the speed of explosion propagation and the consequent efficiency of conversion of energy into blast. This is illustrated in Figure 23 which shows the change in blast overpressure as the speed of explosion or TNO explosion category changes. The observed changes in overpressure roughly correspond to the difference between a high order explosion and a TNO Level 4 explosion.

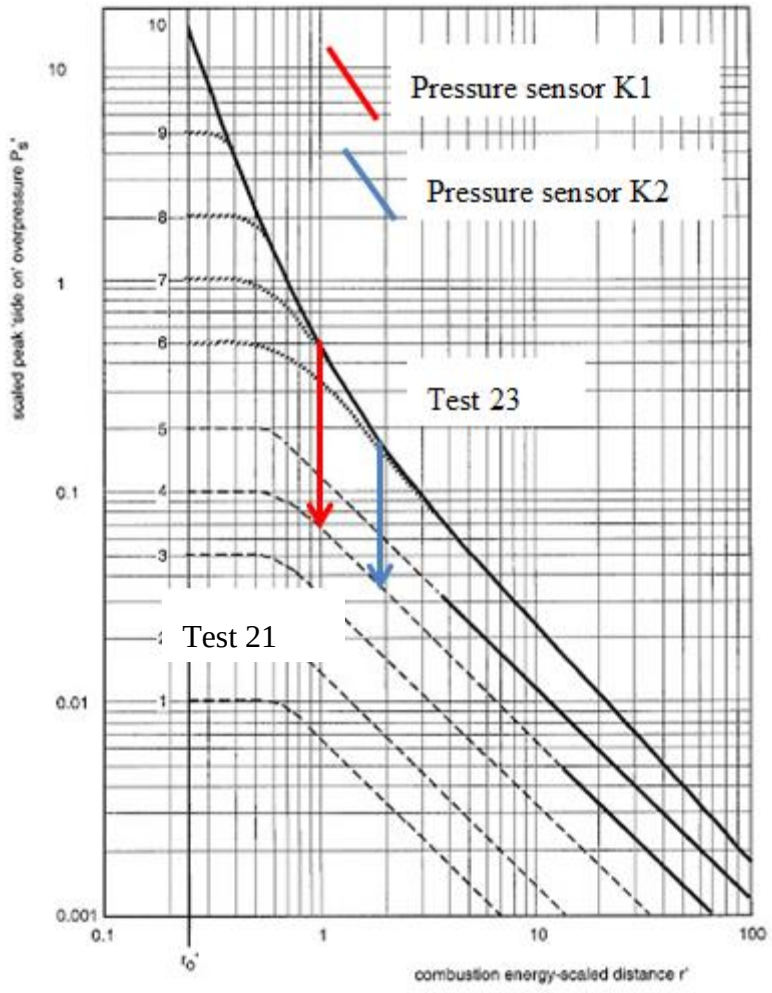

Fig. 23: Change in flame speed (TNO Explosion Level) between Test 23 and 21

These results illustrate the difficulty in assessing flame speed in congested arrays. Very small changes in congestion or cloud structure may push the combustion over the boundary between a relatively stable explosion and one that self-accelerates to very high speed or DDT. If this occurs the character of the explosion changes completely.

4.5 Lower congestion level tests

Figure 24 shows the pressure signals recorded at locations K1- K4 during Test 2. This test involved the same jet (nozzle size and pressure) as Test 23 but with the low level of congestion. The maximum pressures are 37–40 mbar at 6.5 m and 22-25 mbar at 11.5 m.

Figure 25 compares the concentration profiles 2.9 m from the nozzle in the two tests. The jet is shifted towards the direction of K3/4 by the wind but the concentrations are fairly similar.

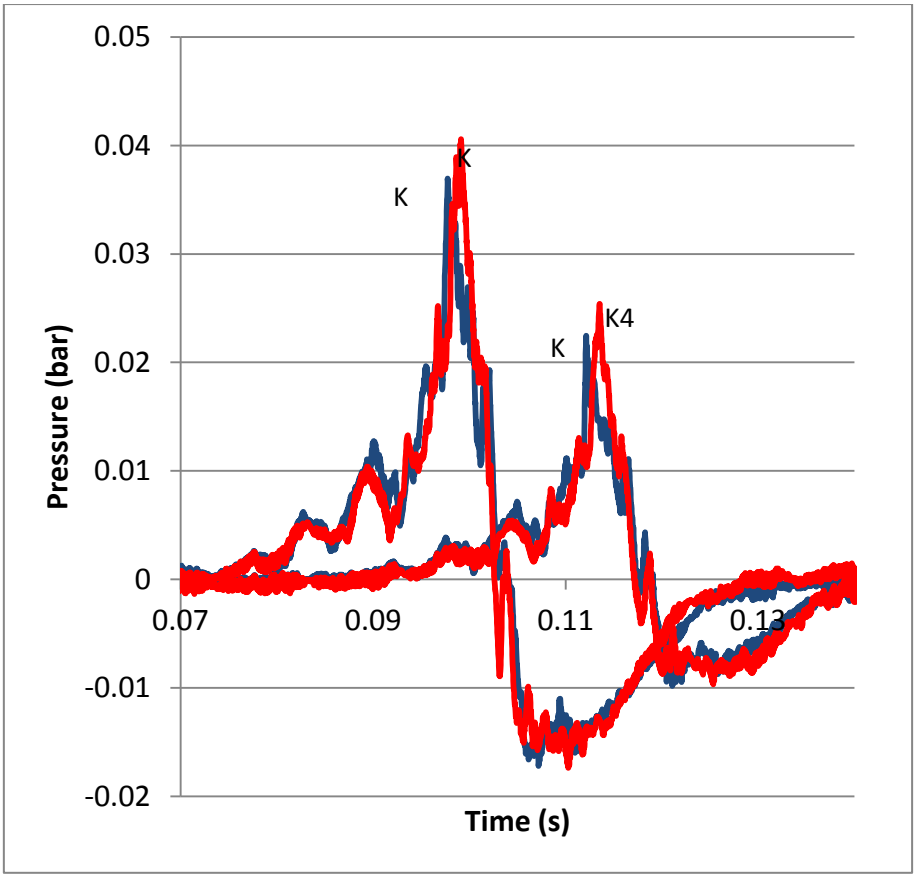

Fig. 24: Pressure signals recorded at 6.5 and 11.5 m from rig centre in Test 2

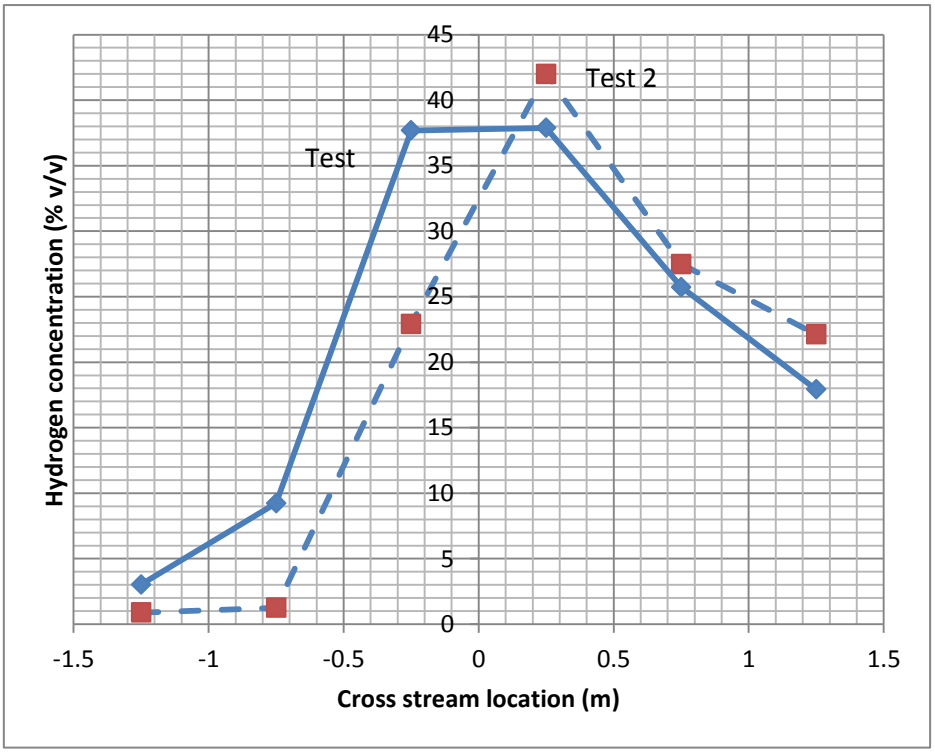

Fig. 25: Comparison of concentration profiles 2.9 m from nozzle in Tests 2 and 23

It seems reasonable to assume that the total energy release in the two cases would be similar – approximately 20 MJ. In this case the values of R' can be estimated. Values of R' and measured overpressure are plotted in Figure 26. The severity level is between 3 and 4.

All other tests with a 12 mm nozzle, low congestion and 1 bar pressure (Tests 4, 6, 8 and 9) gave explosion strength of around 3.

The explosion strengths in all of the low congestion tests are summarised in Table 7. The total energy release has been assumed to be proportional to the flow rates. The assessment of explosion strength is not particularly sensitive to this assumption because the value of the reduced distance varies as the third power of energy release.

Table 7: Summary of approximate TNO explosion strength class for low congestion tests

	12 mm nozzle	25.4 mm nozzle
1 bar	Class 3-4	Class 3
5 bar	Class 4	Class 4

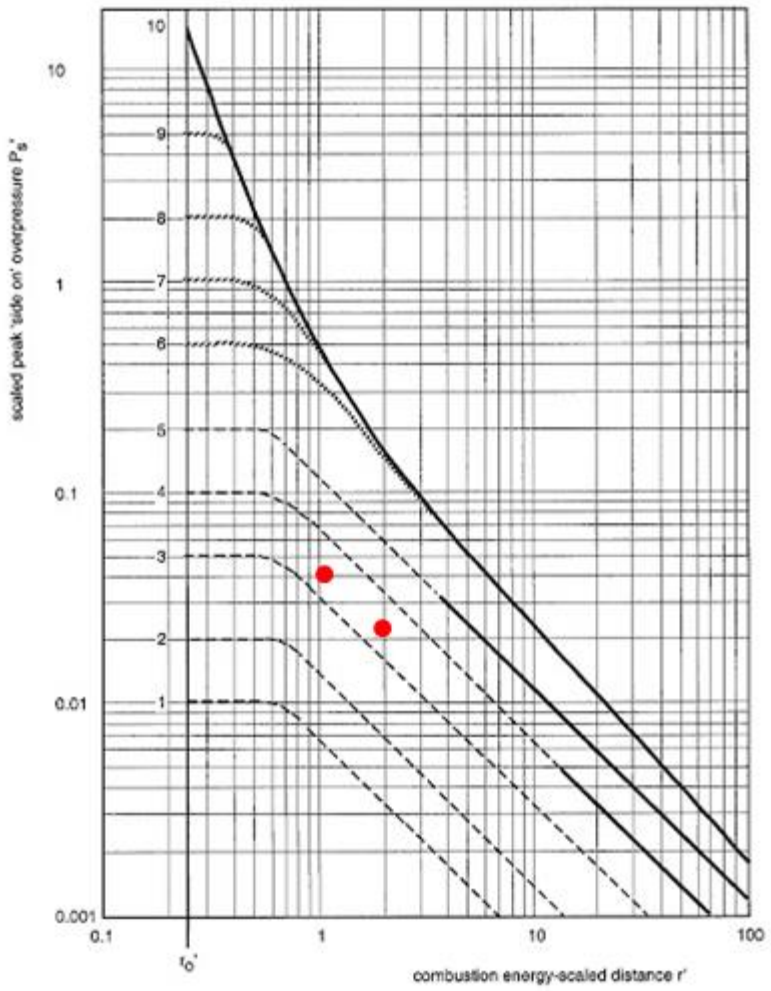

Fig. 26: Explosion severity plot for pressure measurements in Test 2.

4.6 Implications for explosion assessment

It is not clear whether or not there was DDT in Test 23; none of the transducers adjacent to or within the congestion array recorded close to the C-J pressure but they may not have been in the region that detonated. Pressures were in excess of 1200 mbar suggesting that the explosion was at TNO MEM Level 8-10. It is likely that a hydrogen flame that accelerates to this extent could undergo DDT with a minor change in cloud structure or congestion level.

Overall, the results suggest that for the low level of congestion (Volume blockage ratio ~1.5%, Area blockage ~1 m^2/m^3, Congestion length scale 26 mm) there is little risk of uncontrolled flame acceleration. An assumption of TNO Level 5 would be appropriately conservative; to be applied only to the portion of the cloud within the congested area.

Where there is a densely congested area (Volume blockage ratio >4 %, Congestion length scale 25-50 mm) with a volume of more than about 15 m^3 then it would be appropriate to assume that a high level explosion or DDT could occur. It would be reasonable to assume that such an explosion could involve all of the cloud.

4.7 Weather effects

As discussed above, Test 23 showed much more severe consequences that either Test 21 or 22, in spite of similar source conditions. The effect of wind conditions is illustrated in Figure 27 below, which shows the effect on cloud shape of a sudden strengthening of the opposing wind immediately prior to ignition in Test 23.

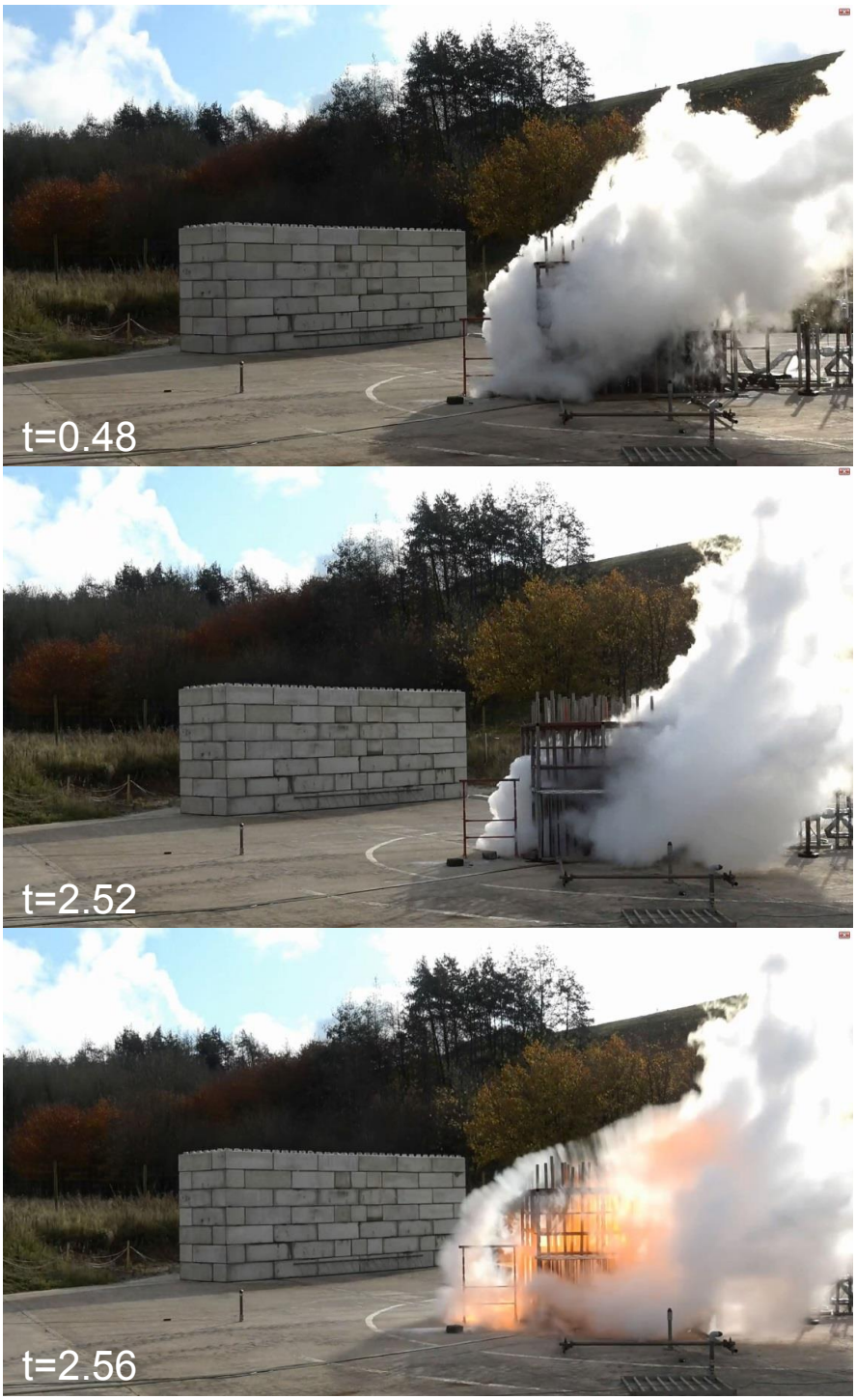

Fig. 27: Series of stills showing sudden gust immediately prior to ignition.

Trial 2 was the only case in which the peak measured overpressure was at pressure transducer K7. This is due to the dominant wind and can be seen clearly in appendix B with the cloud developing towards the near side. Table 4 showing the weather conditions

also shows that this trial had the highest local wind speed in the 5 minutes proceeding ignition. This moved the epicentre of the event closer to K7.

While the dominant wind moved the epicentre of the event towards the sensors in trial 2, trial 19 showed the opposite behaviour. The image shows a dominant far side wind, moving the epicentre of the event away from the pressure sensors. This resulted in the event with the second highest noise at 215 m (137 dB) showing a peak overpressure of only 0.15 bar. A similar effect occurred in trial 16, with a far side dominant wind moving the epicentre of the event from the typical K5 to K6.

With the wind impacting the measurements in the tests, the outcome of the tests, and being impractical to measure to the extent that would be required, a quantification not only of the effect of the wind, but other parameters including congestion becomes difficult.

4.8 Heat flux measurements

When comparing the results from the present experimental series to those from the previous ignited LH_2 work, it is clear that the measured values are considerably lower than a flame in the open space and contain much more variability.

This is likely due to a combination of the positioning of the sensor and obstruction from the congestion frame. Since the effect of the congestion frame would not be uniform across the rig, the heat flux could have been different if measured from a different location.

However, while this does mean that a safety distance based on radiative heat cannot be determined, the experiments do show similar regimes to the previous work – both the blast and jet fire phase were witnessed. In some cases, a small fire persisted at the nozzle after the release had been stopped due to the remaining hydrogen in pipework expanding and sustaining the flame.

5 Conclusion

The objective of this experimental campaign was to determine the effect of different levels of congestion upon the ignition behaviour of a cryogenic hydrogen plume. To this end, 23 ignited trials were carried out at the HSE Science and Research Centre whereby cryogenic hydrogen was released into a steel congestion frame. As well as two levels of congestion, the initial conditions of the release were altered with similar conditions to the other experiments carried out as part of this project, within Work Packages 3 and 4.

By comparing the results with those from a previous set of experiments in which LH2 was released and ignited in the free field, it is clear that higher levels of volumetric congestion increases the measured overpressures in releases with the same initial conditions. The results also show that an increasing hydrogen inventory, either through an increased release pressure or larger nozzle, can result in a larger event upon ignition. However, the mixing of the jet also plays a part; some releases through the largest release orifice diameter showed lower overpressures potentially due to the hydrogen cloud being too rich.

A severe deflagration or detonation was observed in the final trial, although trials with similar initial conditions did not show the same behaviour. This has been attributed to wind conditions causing recirculation and encouraging a slightly higher hydrogen volume within the congestion frame at ignition. While some consistency was observed between tests with similar initial conditions, a qualitative review of the footage shows that the wind played a dominant role in the dispersion and development of the hydrogen cloud from a release of LH2. This includes transient and localised gusts that are difficult to measure and predict.

Notwithstanding the variability introduced by the wind our results suggest the following as a reasonable basis for risk assessment for some releases during tanker operations:

Location with a low level of congestion

For the low level of congestion (Volume blockage ratio <1.5%, Area blockage <1 m^2/m^3, Congestion length scale 25-50 mm) there is little risk of uncontrolled flame acceleration. An assumption of TNO Level 5 would be appropriately conservative; to be applied only to the portion of the cloud within the congested area. As a rule of thumb, if all of the cloud could be in the congested area, the explosive energy release for 1 bar tanker pressures would be approximately 20 MJ and for 5 bar pressure 50 MJ.

Location with a high level of congestion

Where there is a densely congested area (Volume blockage ratio >4 %, Congestion length scale 25-50 mm) with a volume of more than about 15 m^3 then it would be appropriate to assume that a high level explosion or DDT could occur. It would be reasonable to assume that such an explosion could involve all of the cloud.

Since the definitive boundary of congestion level beyond which severe explosions have a higher propensity to occur was not found, depending on the sensitivity of potential targets it might be appropriate to assume that a severe explosion could occur for congested volumes of limited size or of intermediate levels of congestion.

6 References

[1] Hall, J. (2014), Ignited releases of liquid hydrogen, HSE Research Report RR987.
[2] Atkinson, G. (2020), Experiments and analyses on condensed phases (E4.5), D4.8, Pre-normative REsearch for Safe use of Liquid Hydrogen (PRESLHY).
[3] Lyons, K.; Coldrick, S.; Atkinson, G. (2020), Summary of experiment series E3.5 (Rainout) results, D3.6, Pre-normative REsearch for Safe use of Liquid Hydrogen (PRESLHY).
[4] Kingery-Bulmash Blast Parameter calculator, accessed 19/02/21, https://www.un.org/disarmament/un-saferguard/kingery-bulmash/
[5] SCI (2014) Dispersion and Explosion Characteristics of Large Vapor Clouds Volume 1 –Summary Report, Steel Construction Institute, SCI Document ED023
[6] Alonso, F.; Ferradás, E.; Sanchez, J.F.; Aznar, A.; Ruiz Gimeno, J.; Alonso, J., Characteristic overpressure-impulse-distance curves for vapour cloud explosions using the TNO Multi-energy method, Journal of Hazardous Materials (2006), Vol. 137, pages 734-741.
[7] Groethe, M.; Merilo, E.; Colton, J.; Sato, Y. and Iwabuchi, H. (2007) Large scale hydrogen deflagrations and detonations, International Journal of Hydrogen Energy, Vol. 32, pages 2125-2133.
[8] Melani, L.; Sochet, I.; Rocourt, X. and Jallais, S. (2009) Review of methods for estimating the positive overpressures and positive impulses resulting from hydrogen-air explosions. ICHS conference paper, accessed 19/02/21, https://h2tools.org/bibliography/review-methods-estimating-overpressure-and-impulse-resulting-hydrogen-explosion
[9] Wakabashi, K.; Mogi, T.; Kim, D.; Ishikawa, K.; Kuroda, E.; Matsumura, T.; Nakayama, Y.; Horguchi, S.; Oya, M. and Fujiwara, S. (2019) A Field Explosion Test of Hydrogen –Air Mixtures. ICHS conference paper, accessed 19/02/21, https://h2tools.org/bibliography/field-explosion-test-hydrogen-air-mixtures

7 Appendix A – Data sheet

A series of 23 ignited liquid hydrogen (LH_2) trials were conducted to investigate the effect of different levels of congestion when a plume of LH_2 is ignited. This was done by releasing and igniting LH_2 in a steel frame. Instrumentation measuring the outflow properties, dispersion within the steel congestion frame and ambient conditions, such as humidity, enable a more thorough analysis of the plume measurement results. Pressure transducers, noise meters and radiometers were used to quantify the ignition characteristics. Cameras, including high speed and thermal imaging provide context and additional information to the results. Details of the experimental setup, instrumentation, data acquisition and results formats are described with the aim of providing the necessary context to fully interpret the results.

7.1 Experimental Set-Up

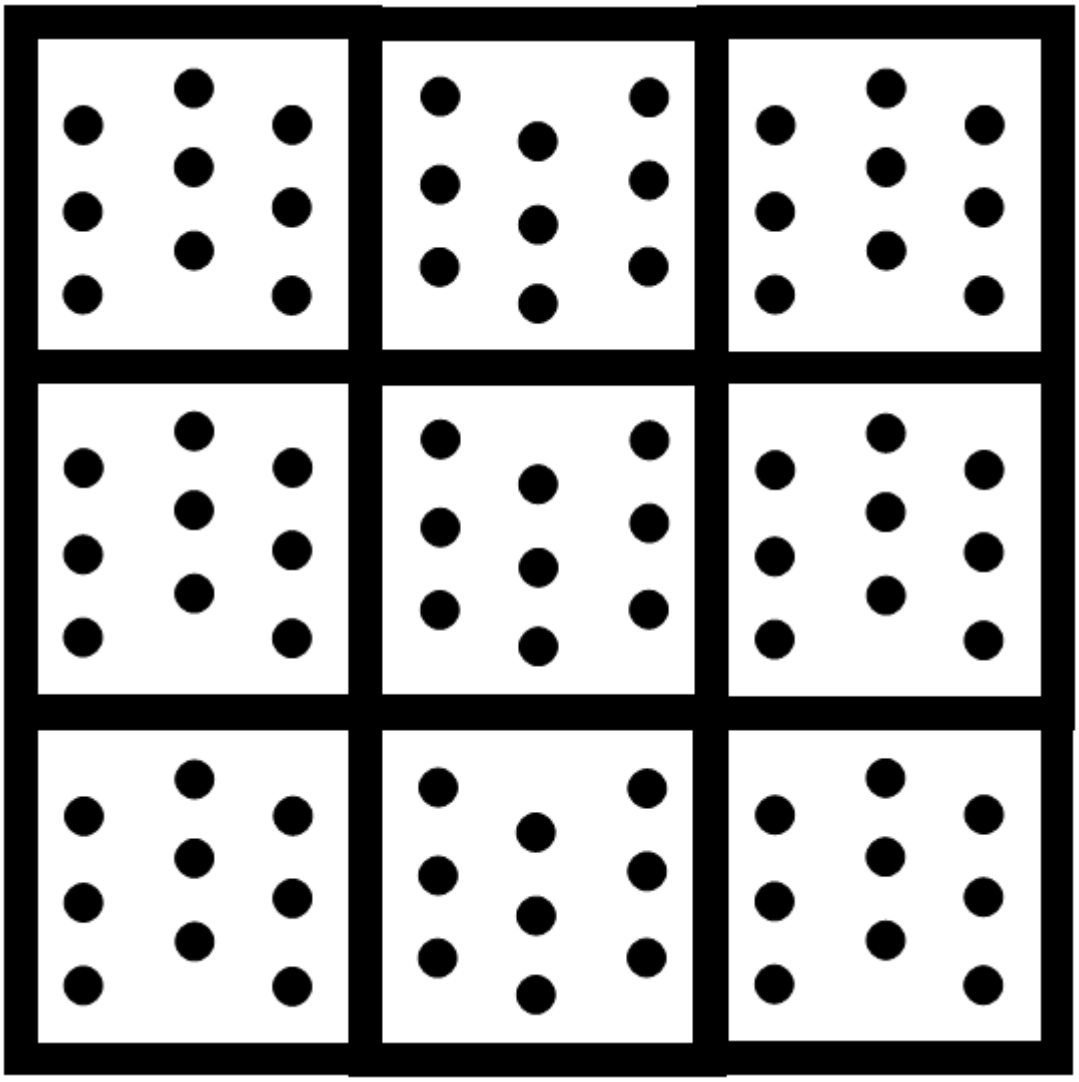

Fig. A1: Sketch of congestion pole placement.

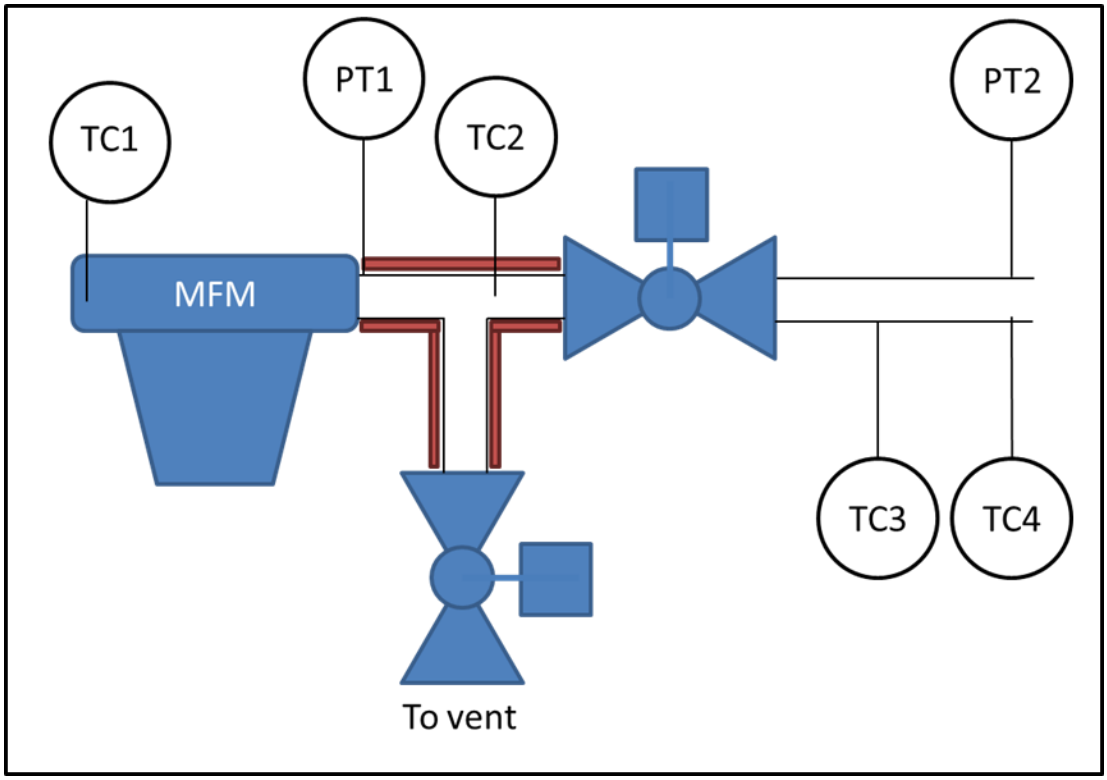

Figure A1: Sketch of the LH_2 release facility with instrumentation.

Table A1: Sensor positions on the release pipework.

Name	Description	Distance to release point (m)
TC1	In-flow thermocouple	3.25
WS	Weather station	2.75
MFM	Mass flow meter	2.55
TC2	In-flow thermocouple	2.35
PT1	Pipework pressure transducer	2.35
PT2	Pipework pressure transducer	0.08
TC3	In-flow thermocouple	0.08
TC4	Pipework wall thermocouple	0.02

Table A2: Dimensions of 25.4 mm nominal bore pipe sections.

Description	Length (m)	Thermal conductivity (W/m.K)*
Vacuum insulated hose	20	2.5 W/m
Electrically isolated pipe	0.5	0.021
Mass flow meter	0.4	n/a
Valve section	0.6	13-17
Flexible hose	1.75	0.034

**Typical values for the insulation materials are given, taken from the datasheets of the manufacturers. The vacuum insulated hose had units of W/m.*

Table A3: Locations of weather stations.

Weather station	Model	Distance (m)	Height (m)	Angle from release point	Angle from North
Local	PCE	2.75	1.5	180°	255°
Far-field	Windsonic & Skye	20	3	-15°	60°

Note the release pointed at approximately 75° from North.

Table A4: Hydrogen sensor and thermocouple locations.

Serial No	ID	X (m)	Y (m)	Z (m)	TC ID
10DC96	M1S1	1.50	0.75	0.75	TC2318
10DC95	M1S2	1.50	0.45	0.75	TC2319
04DC52	M1S3	1.50	0.15	0.75	TC2320
04DC53	M1S4	1.50	-0.15	0.75	TC2321
04DC54	M1S5	1.50	-0.45	0.75	TC2328
04DC58	M1S6	1.50	-0.75	0.75	TC2329
04DC59	M1S7	2.90	1.25	0.75	TC2330
04DC60	M1S8	2.90	0.75	0.75	TC2336
02EC42	M2S1	2.90	0.25	0.75	TC2322
02EC43	M2S2	2.90	-0.25	0.75	TC2323
02EC44	M2S3	2.90	-0.75	0.75	TC2331
02EC45	M2S4	2.90	-1.25	0.75	TC2337
02EC46	M2S5	2.00	0.75	1.50	TC2324
10DC100	M2S6	2.00	0.00	1.50	TC2332
10DC101	M2S7	2.00	-0.75	1.50	TC2333
04DC51	M2S8	3.00	0.00	1.50	TC2338

7.2 Data Acquisition Systems

Table A5: Primary data acquisition system components.

Chassis	Logging card	Sensors
NI cDAQ-9181	NI 9215	Wind and weather sensors.
NI cDAQ-9185	NI-9203	4 Kulite pressure transdusers.
	NI-9203	4 Kulite pressure transdusers.
NI cDAQ-9188XT	NI 9215	2 Pressure transducers, mass flow meter
	NI 9215	3 Radiometers
	NI 9219	Spare
	NI 9472	Valve control.
	NI 9421	Spare
NI cDAQ-9188	NI 9213	16 Type T mineral insualted thermocouples.
	NI 9213	13 Type T mineral insualted thermocouples.

Table A6: Channel settings for the acquisitions system

Instrument	Column header	Units	Description
Cold junction thermocouple	Cold_junction	°C	Cold junction temperature
Cold junction thermocouple	Cold_junction_error	µV	Cold junction thermovoltage
Isolated pipe current	EV1_Streaming_current	nA	Current
Congestion thermocouple	MXSY_TCSSSS	µV	Thermovoltage from thermocouple SSSS colocated with senor MXSY
Congestion thermocouple	MXSY_TCSSSSC	°C	Thermovoltage from thermocouple SSSS colocated with senor MXSY
Flow meter	MFM1_Mass_Flow_Rate	g/s	Mass flow through meter
Flow meter	MFM2_Drive_Gain	%	Flow meter drive gain
Pressure transducer	KX	barg	Pressure transduvers for blast overpressure measurement
Pressure transducer	PT1_Pipe_Pressure	barg	Pressure at outlet nozzle
Pressure transducer	PT2_Nozzle_Pressure	barg	Pressure downstream from flowmeter
Heat flux sensor	RADX_Radiometer_SSSSS	kW/m^2	Heat flux sensor X serial number SSSSS
Weather station	Relative_Humidity	%	Weather station at pad edge
Pipework thermocouples	TCX_abcd	µV	Thermovoltage from pipework thermocouple X
Pipework thermocouples	TCX_abcdC	°C	Temperature from pipework thermocouple X
Weather station	Wind_Direction	°	Wind direction from N
Weather station	Wind_Speed	m/s	Wind speed at 3 m

8 Appendix B – Images prior to ignition

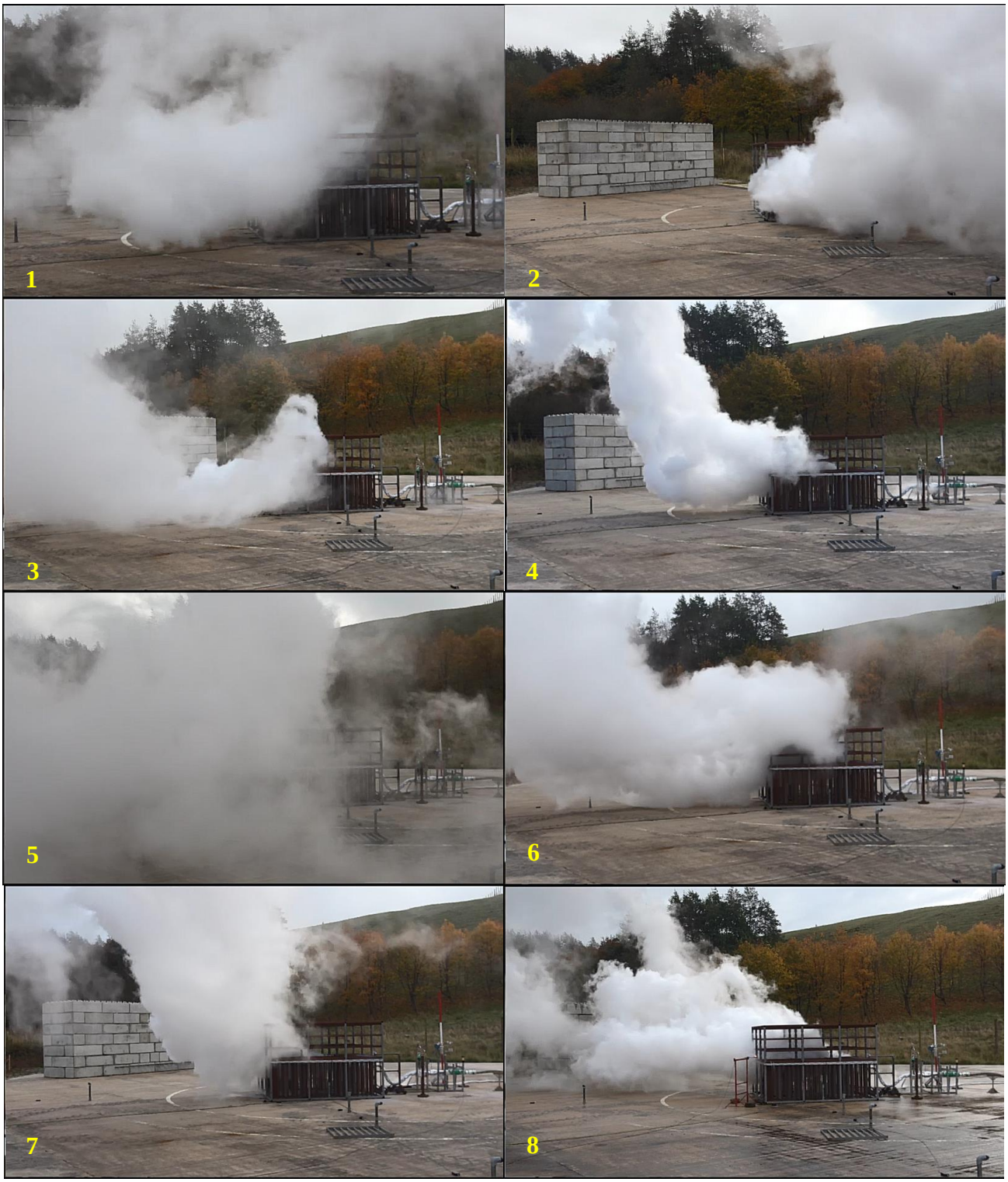

Fig. B1: Trials 1 to 8 images immediately prior to ignition.

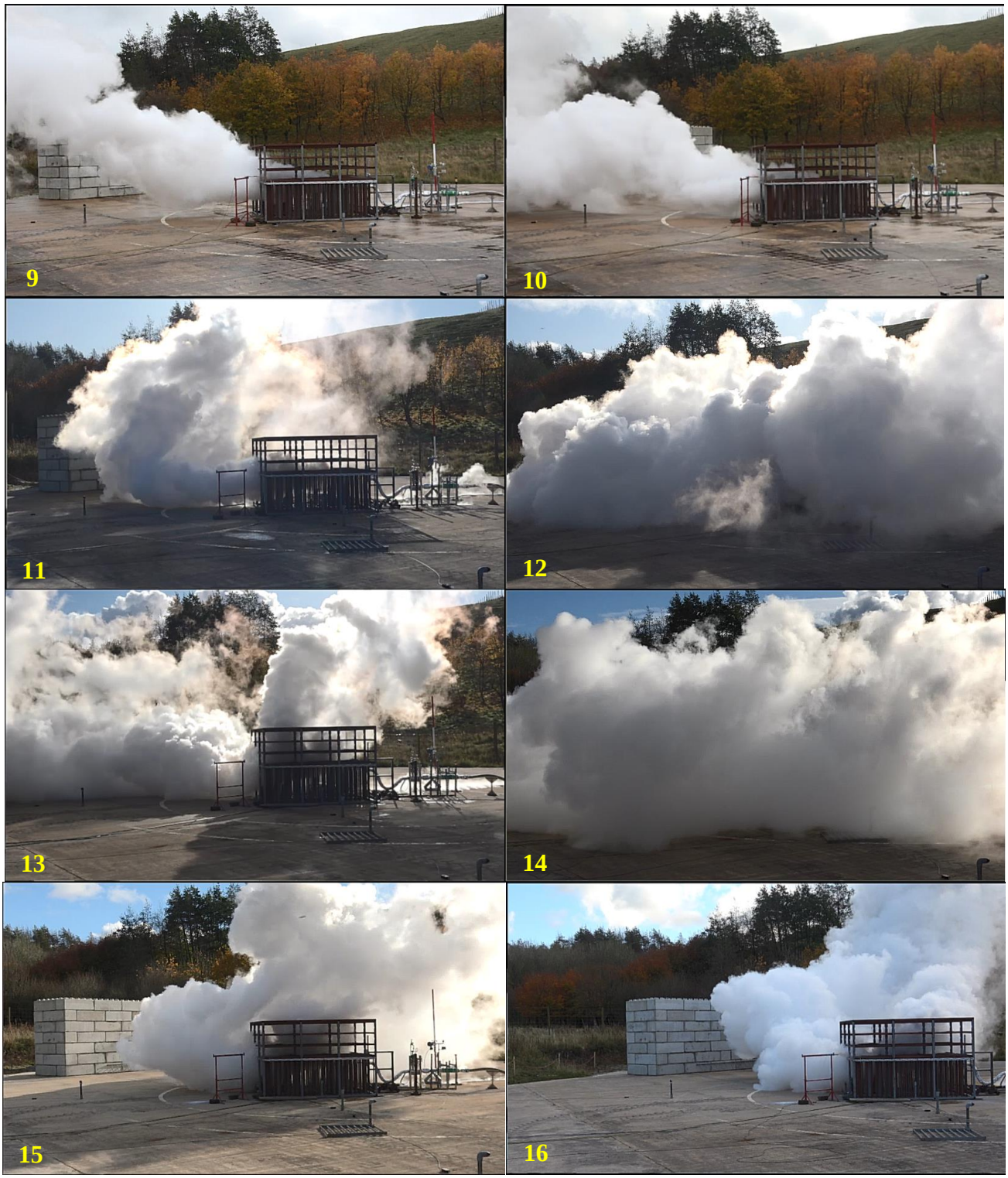

Fig. B2: Trials 9 to 16 images immediately prior to ignition.

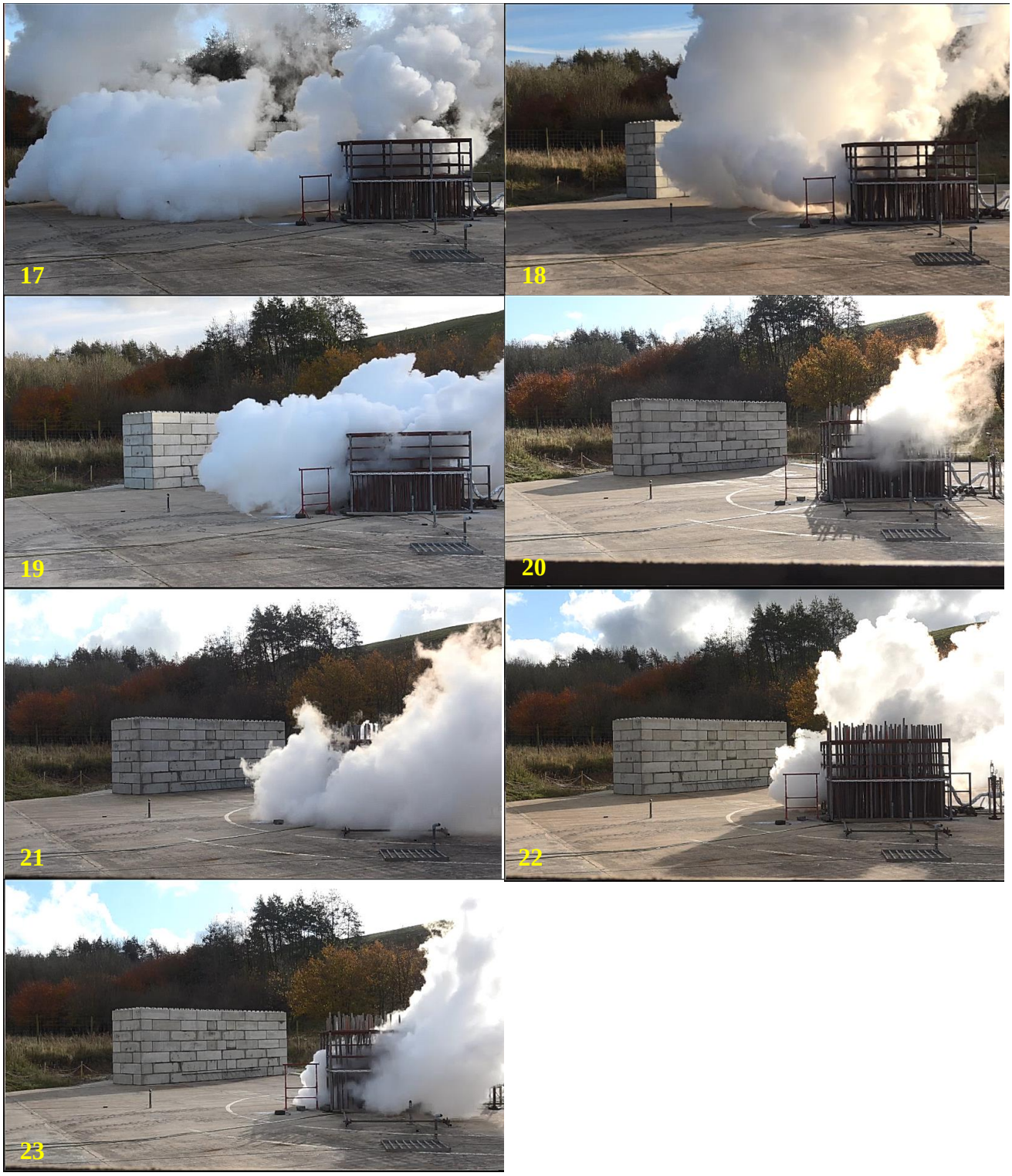

Fig. B3: Trials 17 to 23 images immediately prior to ignition.

9 Appendix C – Overpressure graphs

This section contains the overpressure graphs from each of the 23 trials. The time is in milliseconds and has an arbitrary start time, based on when the plots began to show response. The time of ignition is shown in the table below to allow for the cross reference with the other data.

With the fast logging rate, signal noise is present on the overpressure plots and is particularly noticeable on the plots with a small measured peak. To compensate for this, a 10 point moving average was used, which reduced the noise magnitude from a width of approximately 0.04 bar to approximately 0.004 bar. This makes the behaviour of the graphs clearer but does reduce the peak measured overpressure. In this report, the averaged data is used exclusively to avoid confusion, but both the raw and averaged data is provided in the supplemental data sheets.

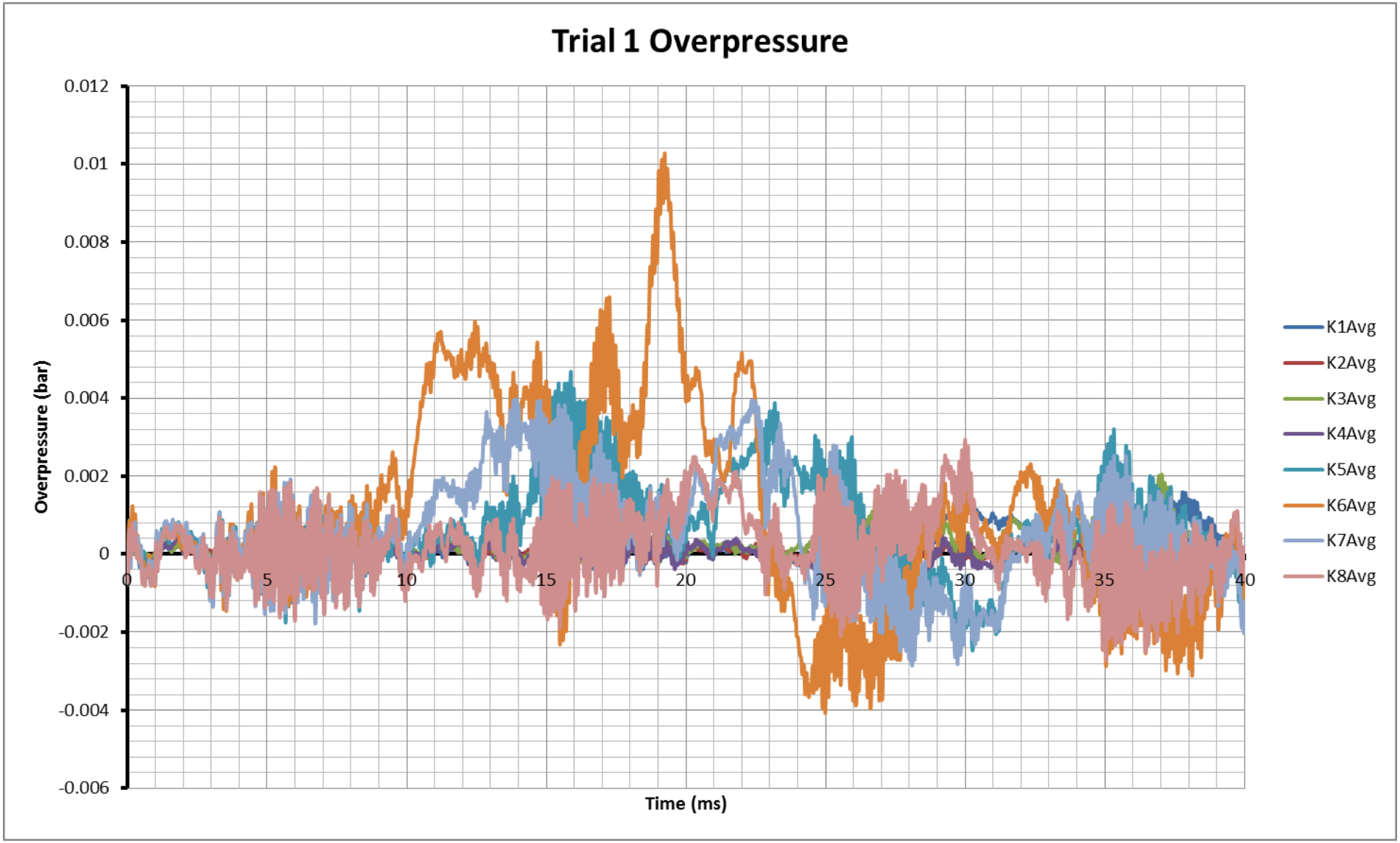
Trial 1 Overpressure
Overpressure (bar)
0.012
0.01
0.008
0.006
0.004
0.002
0
-0.002
-0.004
-0.006
0
5
10
15
20
25
30
35
40
Time (ms)
K1Avg
K2Avg
K3Avg
K4Avg
K5Avg
K6Avg
K7Avg
K8Avg

Fig. C1

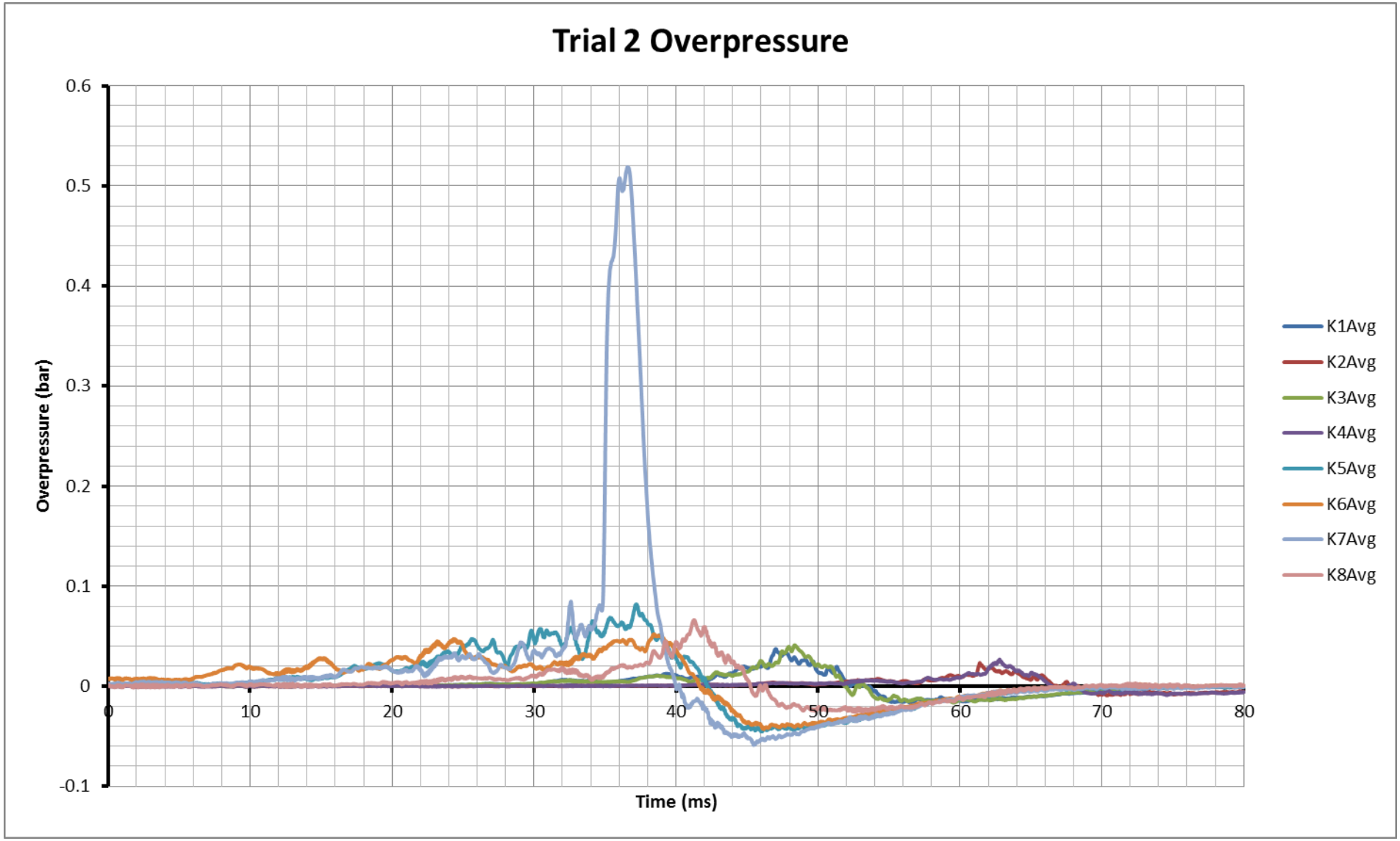
Trial 2 Overpressure
Overpressure (bar)
0.6
0.5
0.4
0.3
0.2
0.1
0
-0.1
0
10
20
30
40
50
60
70
80
Time (ms)
K1Avg
K2Avg
K3Avg
K4Avg
K5Avg
K6Avg
K7Avg
K8Avg

Fig. C2

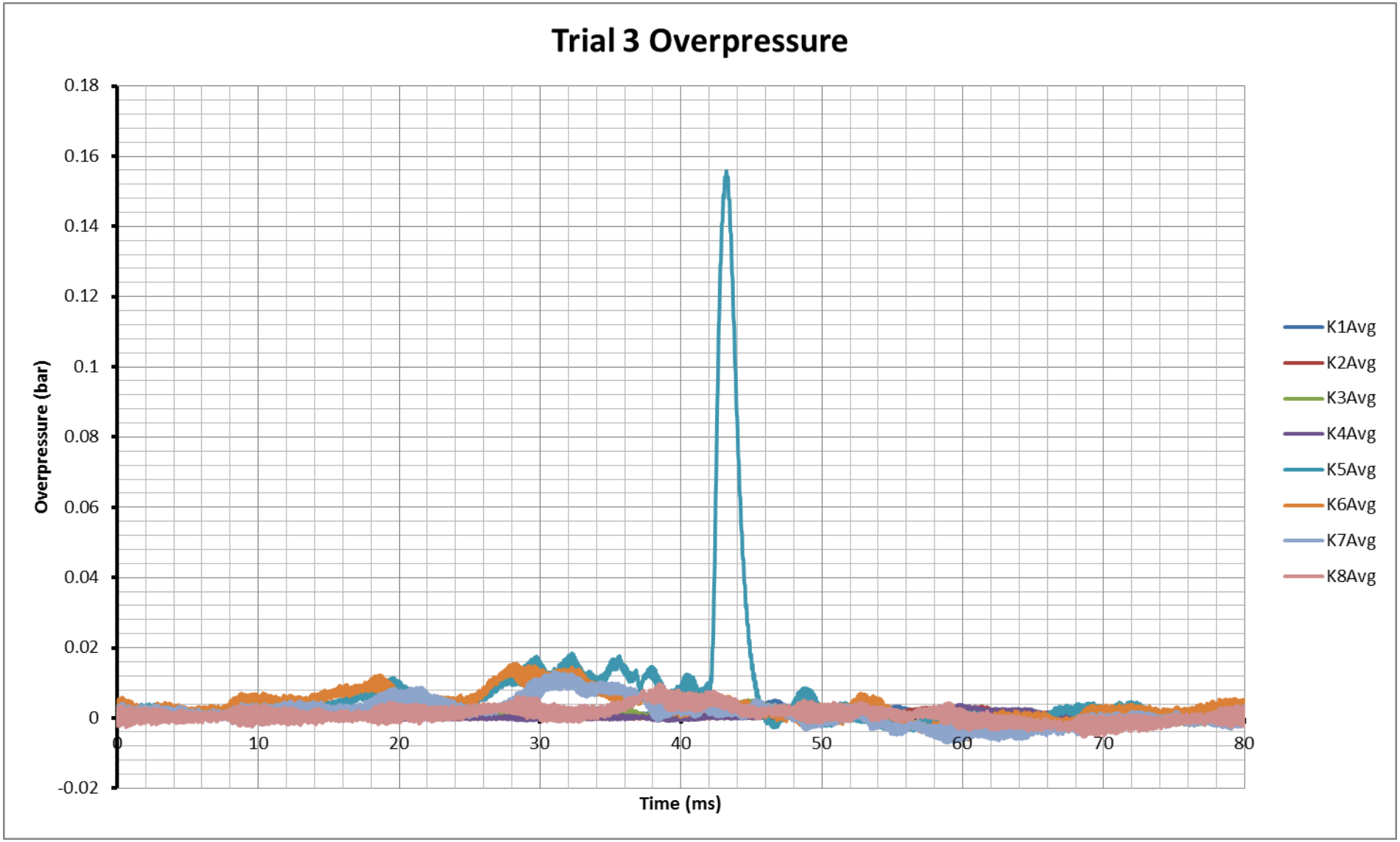
Trial 3 Overpressure
Overpressure (bar)
0.18
0.16
0.14
0.12
0.1
0.08
0.06
0.04
0.02
0
-0.02
0
10
20
30
40
50
60
70
80
Time (ms)
K1Avg
K2Avg
K3Avg
K4Avg
K5Avg
K6Avg
K7Avg
K8Avg

Fig. C3

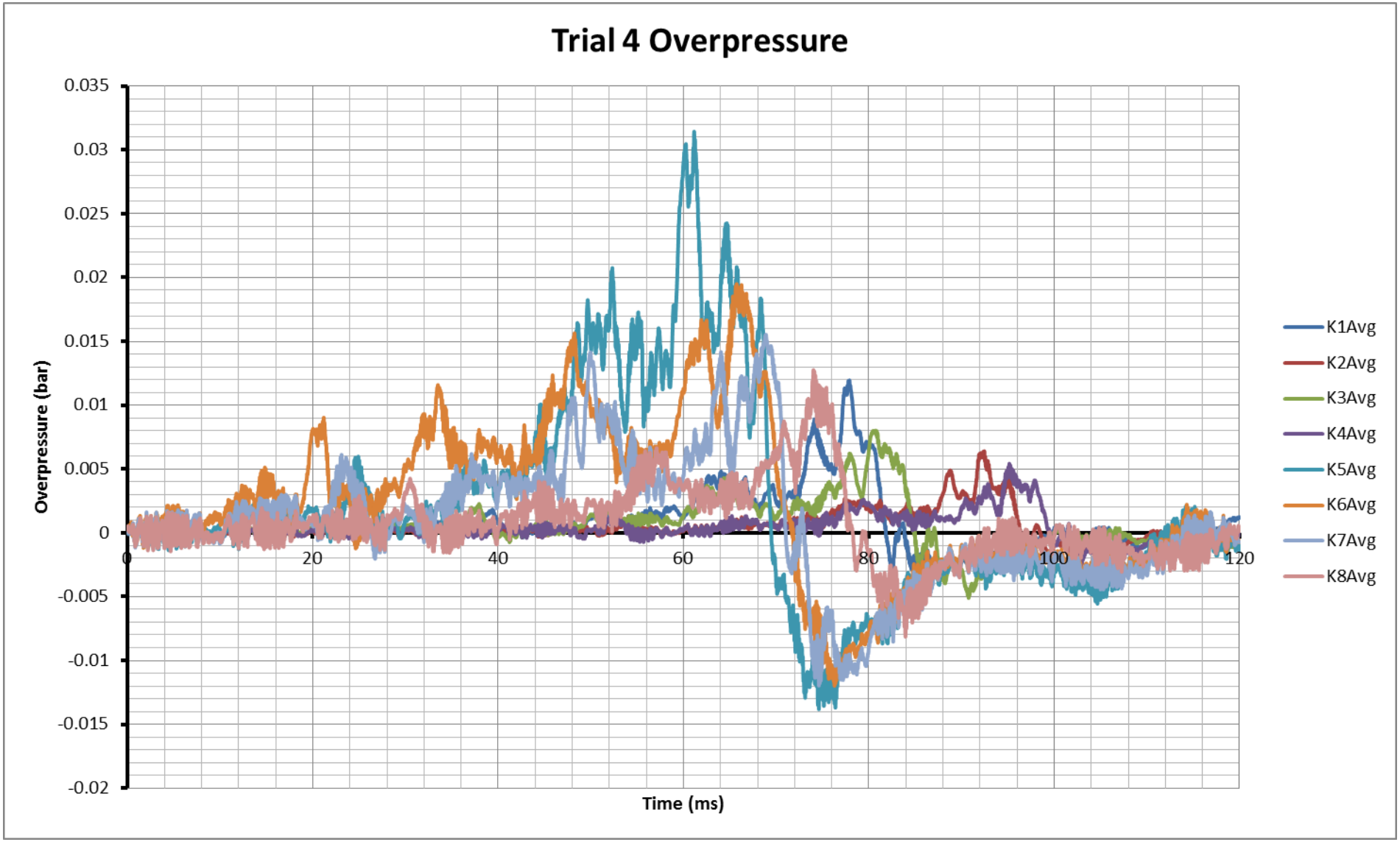
Trial 4 Overpressure
Overpressure (bar)
0.035
0.03
0.025
0.02
0.015
0.01
0.005
0
-0.005
-0.01
-0.015
-0.02
0
20
40
60
80
100
120
Time (ms)
K1Avg
K2Avg
K3Avg
K4Avg
K5Avg
K6Avg
K7Avg
K8Avg

Fig. C4

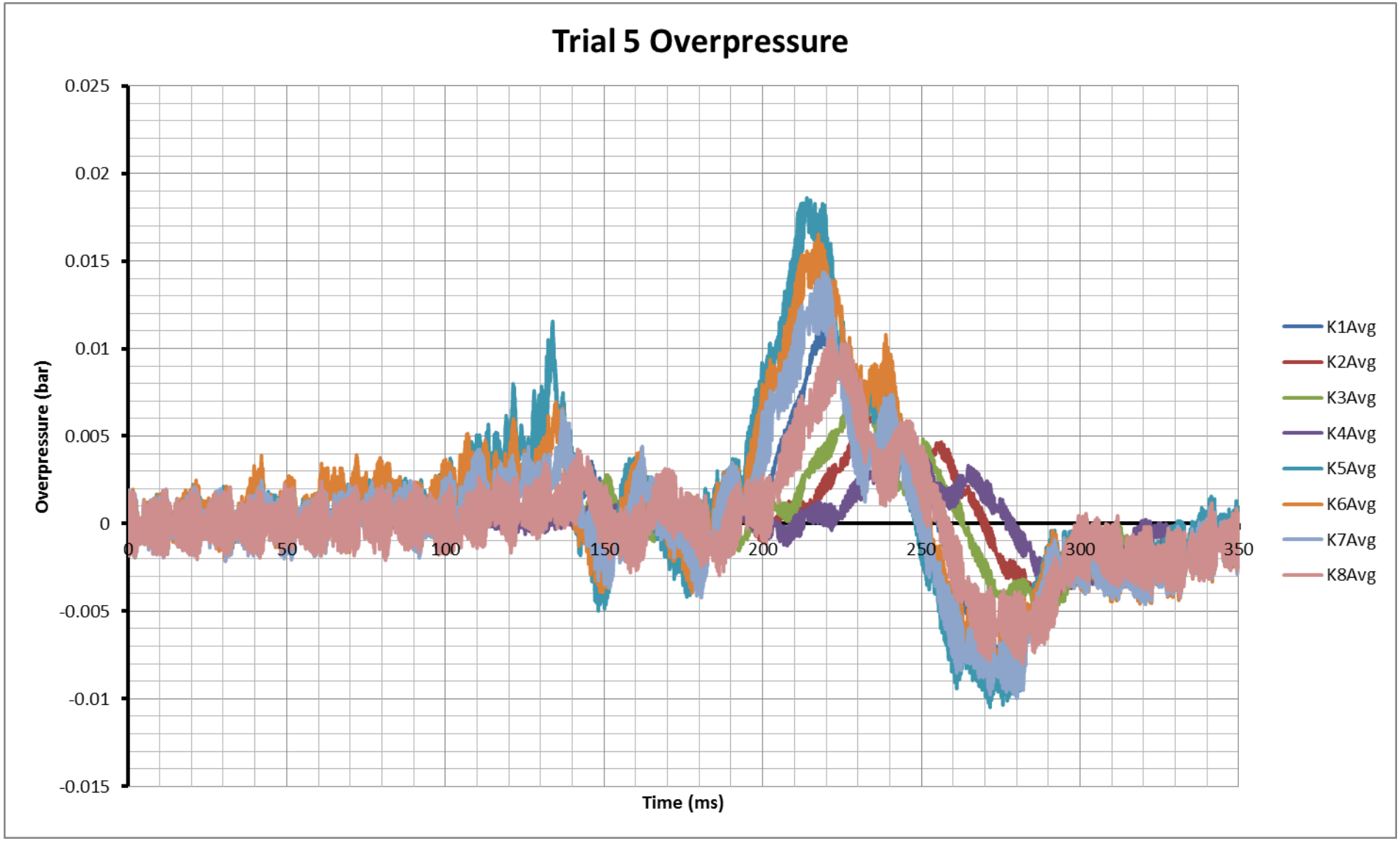
Trial 5 Overpressure
Overpressure (bar)
0.025
0.02
0.015
0.01
0.005
0
-0.005
-0.01
-0.015
0
50
100
150
200
250
300
350
Time (ms)
K1Avg
K2Avg
K3Avg
K4Avg
K5Avg
K6Avg
K7Avg
K8Avg

Fig. C5

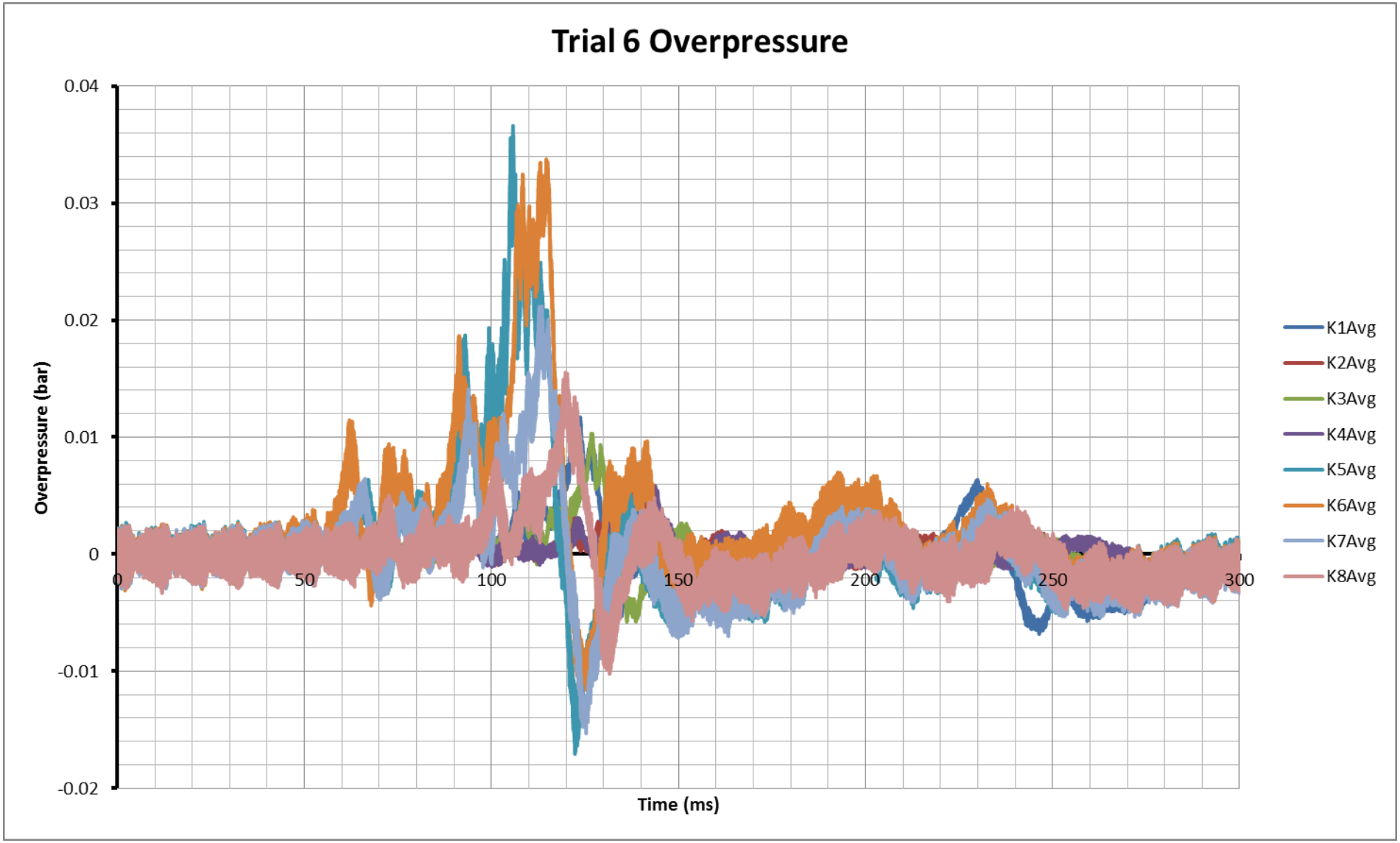
Trial 6 Overpressure
Overpressure (bar)
0.04
0.03
0.02
0.01
0
-0.01
-0.02
0
50
100
150
200
250
300
Time (ms)
K1Avg
K2Avg
K3Avg
K4Avg
K5Avg
K6Avg
K7Avg
K8Avg

Fig. C6

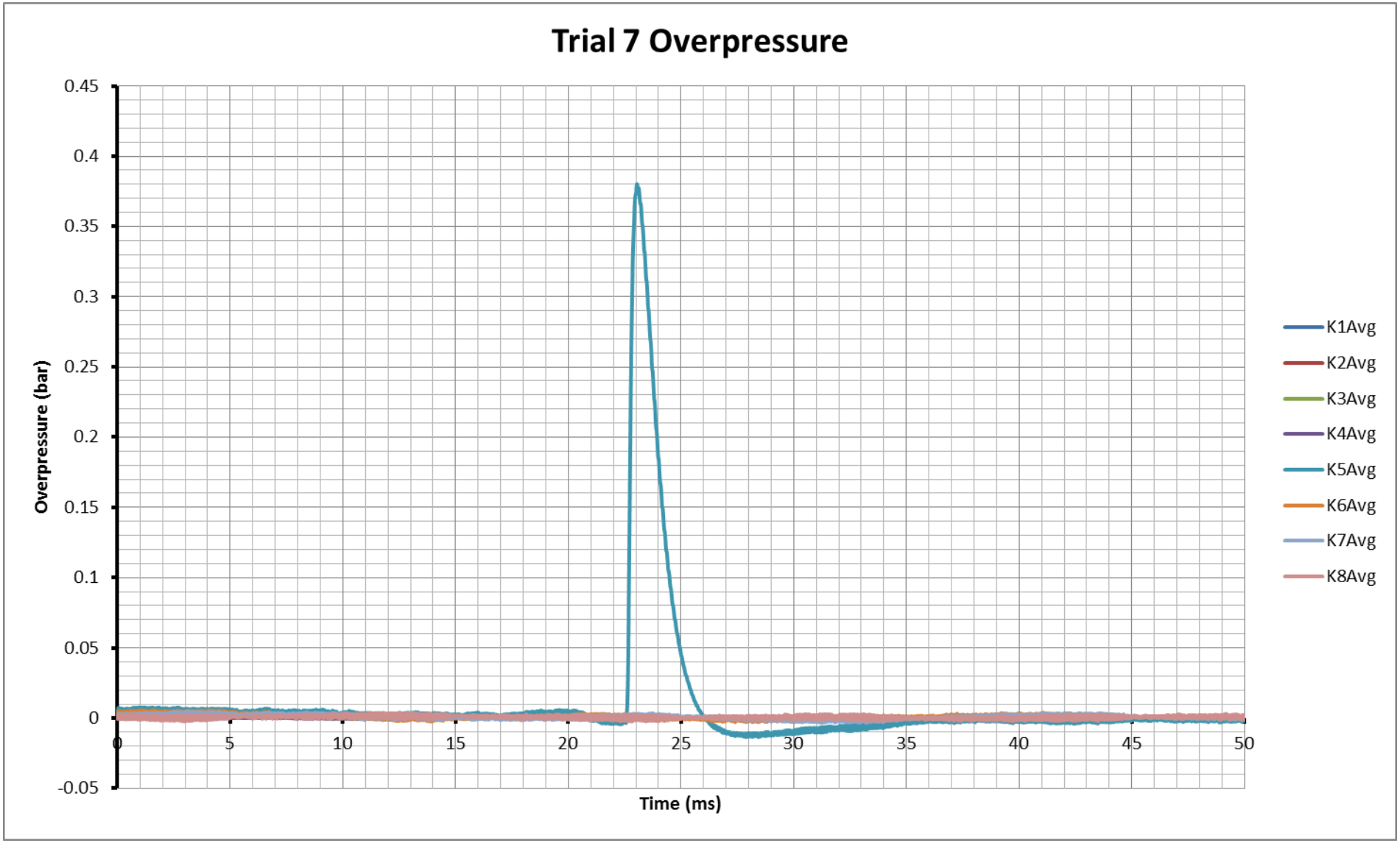
Trial 7 Overpressure
Overpressure (bar)
0.45
0.4
0.35
0.3
0.25
0.2
0.15
0.1
0.05
0
-0.05
0
5
10
15
20
25
30
35
40
45
50
Time (ms)
K1Avg
K2Avg
K3Avg
K4Avg
K5Avg
K6Avg
K7Avg
K8Avg

Fig. C7

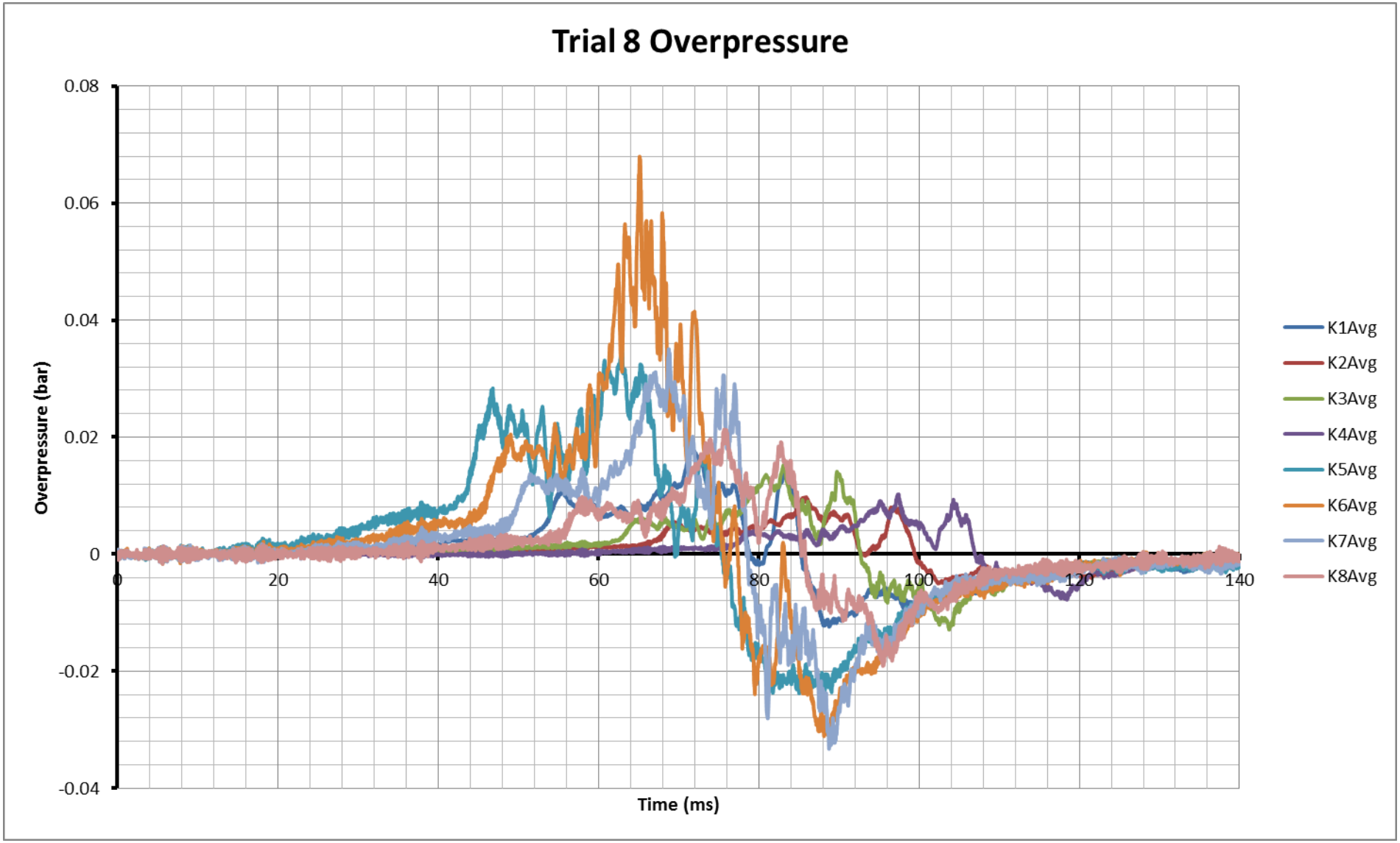
Trial 8 Overpressure
Overpressure (bar)
0.08
0.06
0.04
0.02
0
-0.02
-0.04
0
20
40
60
80
100
120
140
Time (ms)
K1Avg
K2Avg
K3Avg
K4Avg
K5Avg
K6Avg
K7Avg
K8Avg

Fig. C8

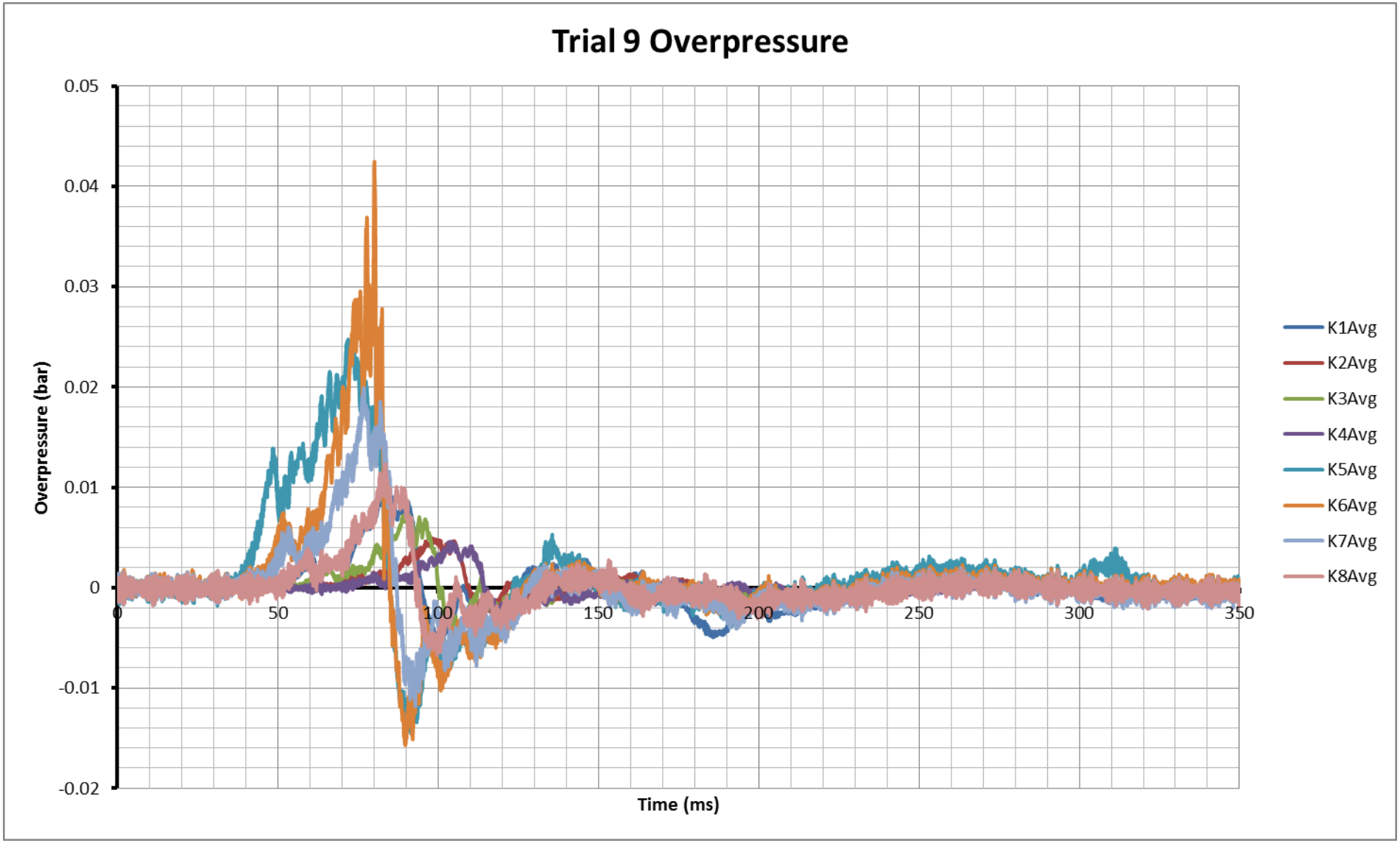
Trial 9 Overpressure
Overpressure (bar)
0.05
0.04
0.03
0.02
0.01
0
-0.01
-0.02
0
50
100
150
200
250
300
350
Time (ms)
K1Avg
K2Avg
K3Avg
K4Avg
K5Avg
K6Avg
K7Avg
K8Avg

Fig. C9

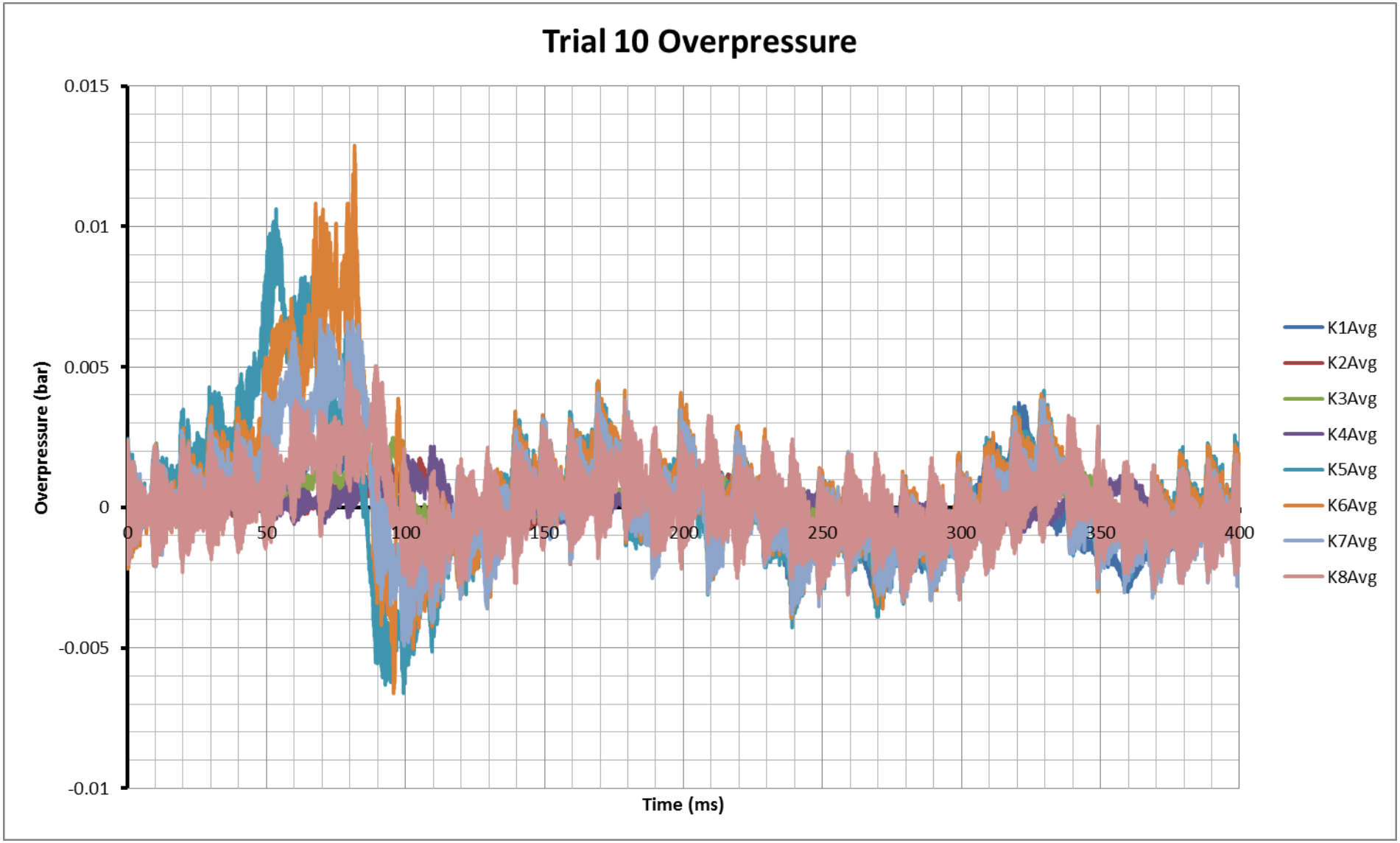
Trial 10 Overpressure
0.015
0.01
0.005
0
-0.005
-0.01
Overpressure (bar)
0
50
100
150
200
250
300
350
400
Time (ms)
K1Avg
K2Avg
K3Avg
K4Avg
K5Avg
K6Avg
K7Avg
K8Avg

Fig. C10

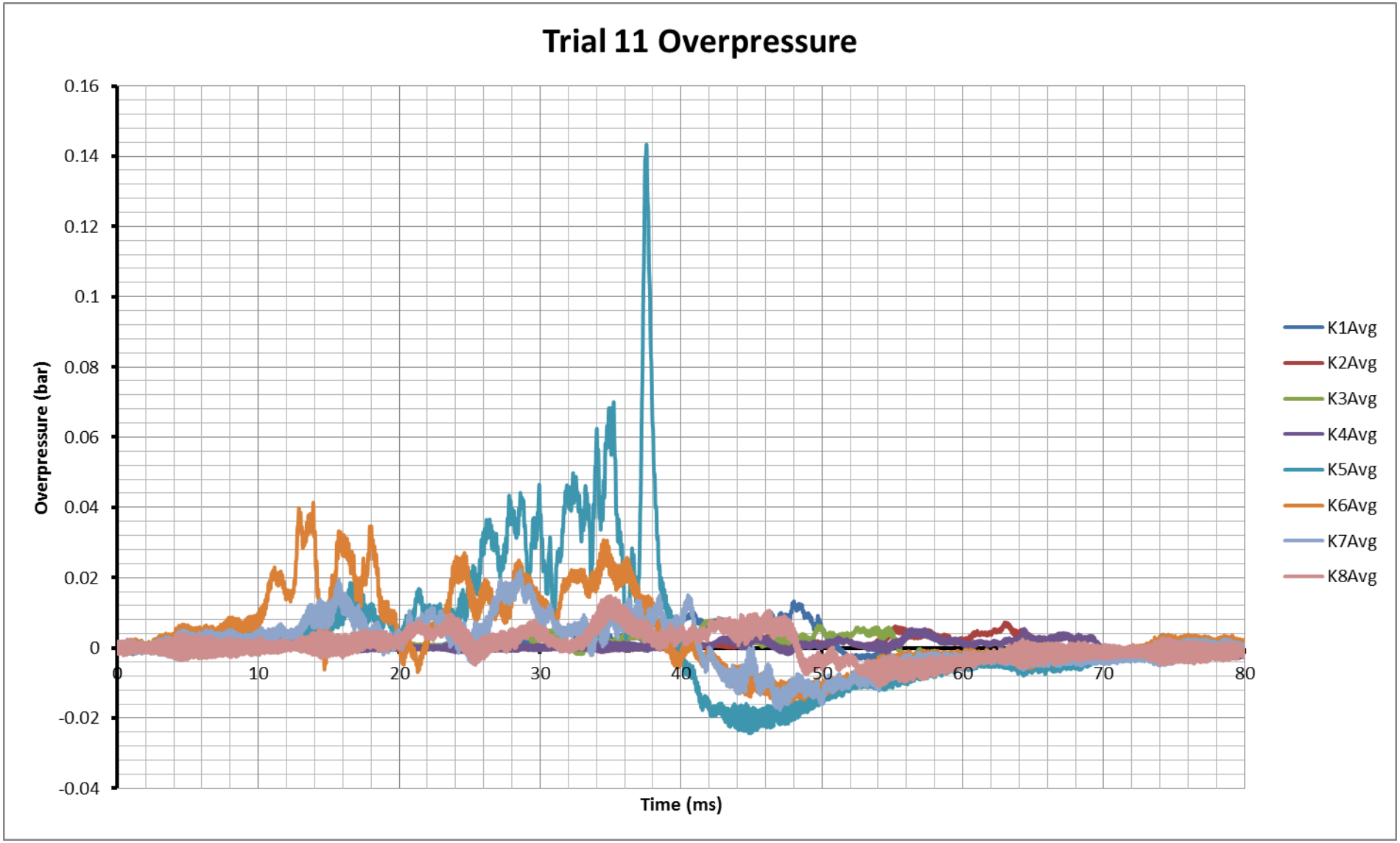
Trial 11 Overpressure
Overpressure (bar)
0.16
0.14
0.12
0.1
0.08
0.06
0.04
0.02
0
-0.02
-0.04
0
10
20
30
40
50
60
70
80
Time (ms)
K1Avg
K2Avg
K3Avg
K4Avg
K5Avg
K6Avg
K7Avg
K8Avg

Fig. C11

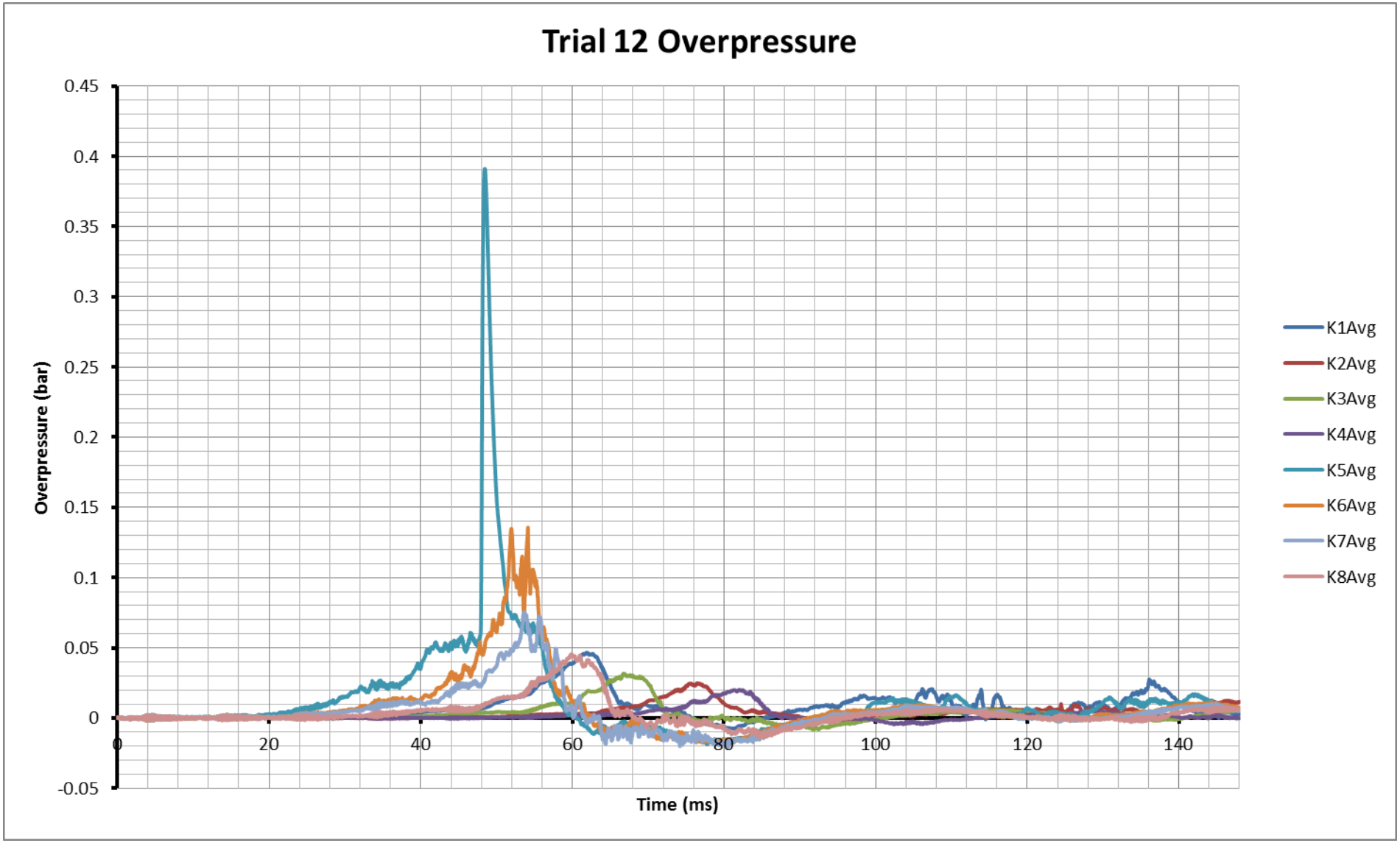
Trial 12 Overpressure
Overpressure (bar)
0.45
0.4
0.35
0.3
0.25
0.2
0.15
0.1
0.05
0
-0.05
0
20
40
60
80
100
120
140
Time (ms)
K1Avg
K2Avg
K3Avg
K4Avg
K5Avg
K6Avg
K7Avg
K8Avg

Fig. C12

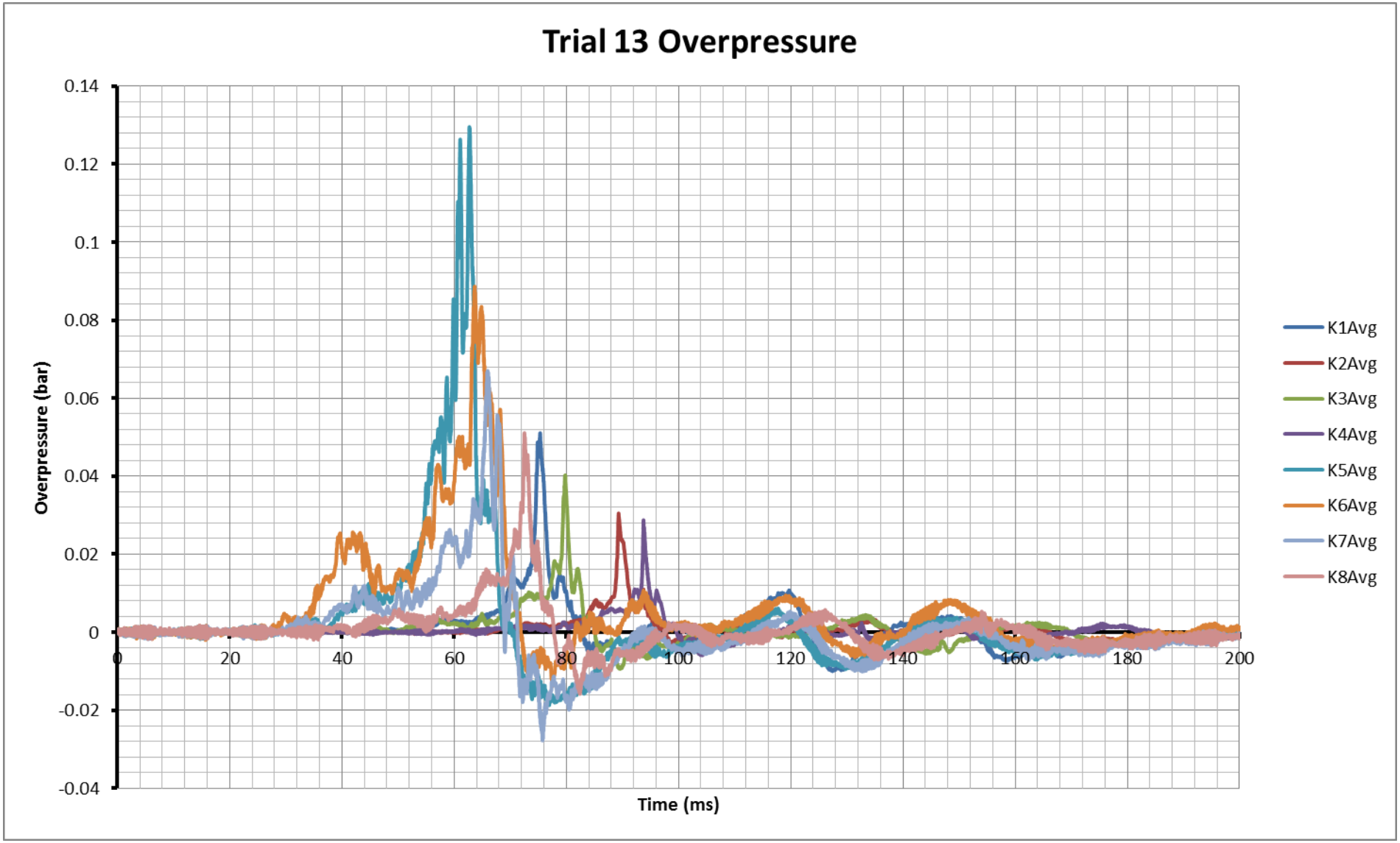
Trial 13 Overpressure
Overpressure (bar)
0.14
0.12
0.1
0.08
0.06
0.04
0.02
0
-0.02
-0.04
0
20
40
60
80
100
120
140
160
180
200
Time (ms)
K1Avg
K2Avg
K3Avg
K4Avg
K5Avg
K6Avg
K7Avg
K8Avg

Fig. C13

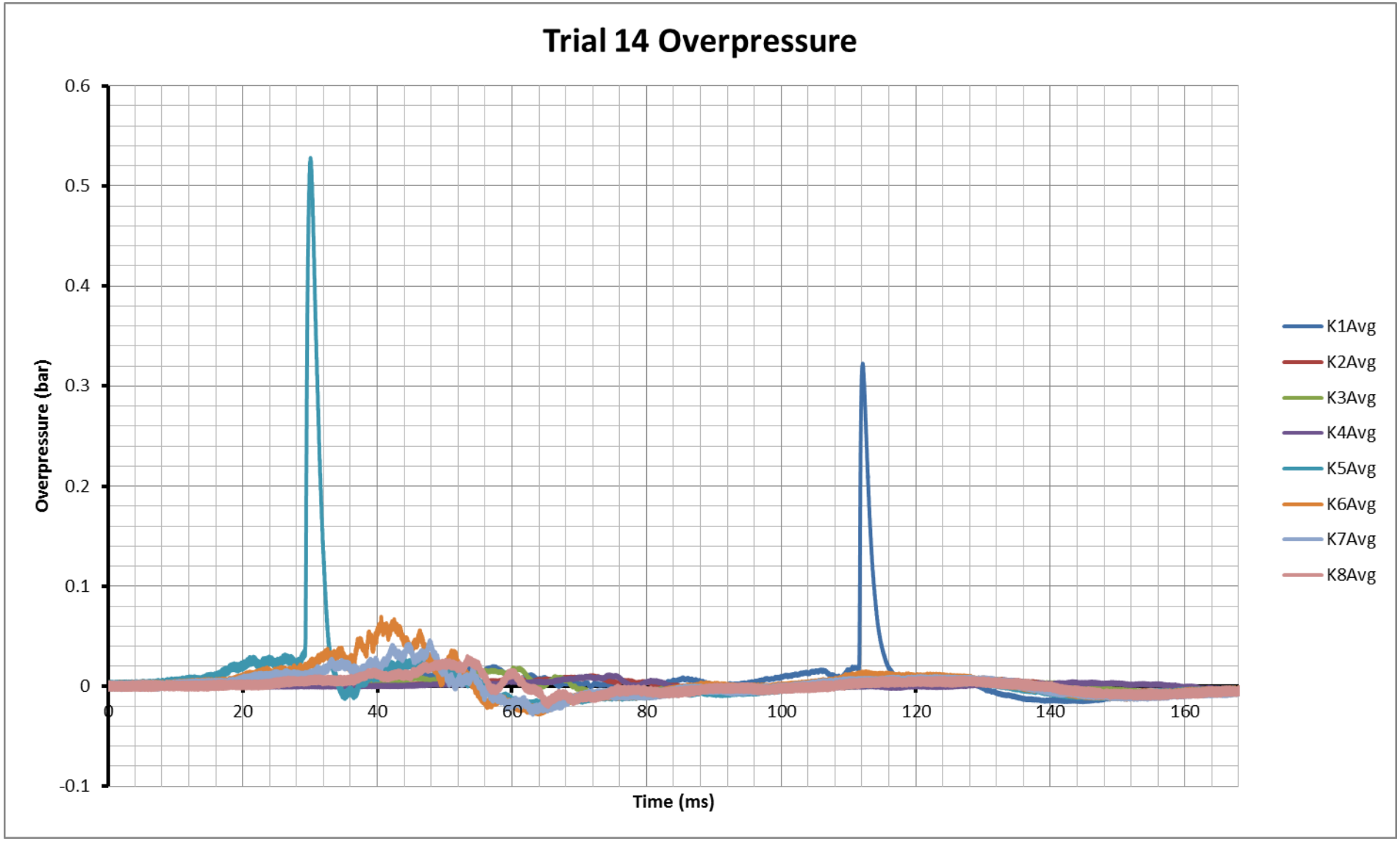
Trial 14 Overpressure
Overpressure (bar)
0.6
0.5
0.4
0.3
0.2
0.1
0
-0.1
0
20
40
60
80
100
120
140
160
Time (ms)
K1Avg
K2Avg
K3Avg
K4Avg
K5Avg
K6Avg
K7Avg
K8Avg

Fig. C14

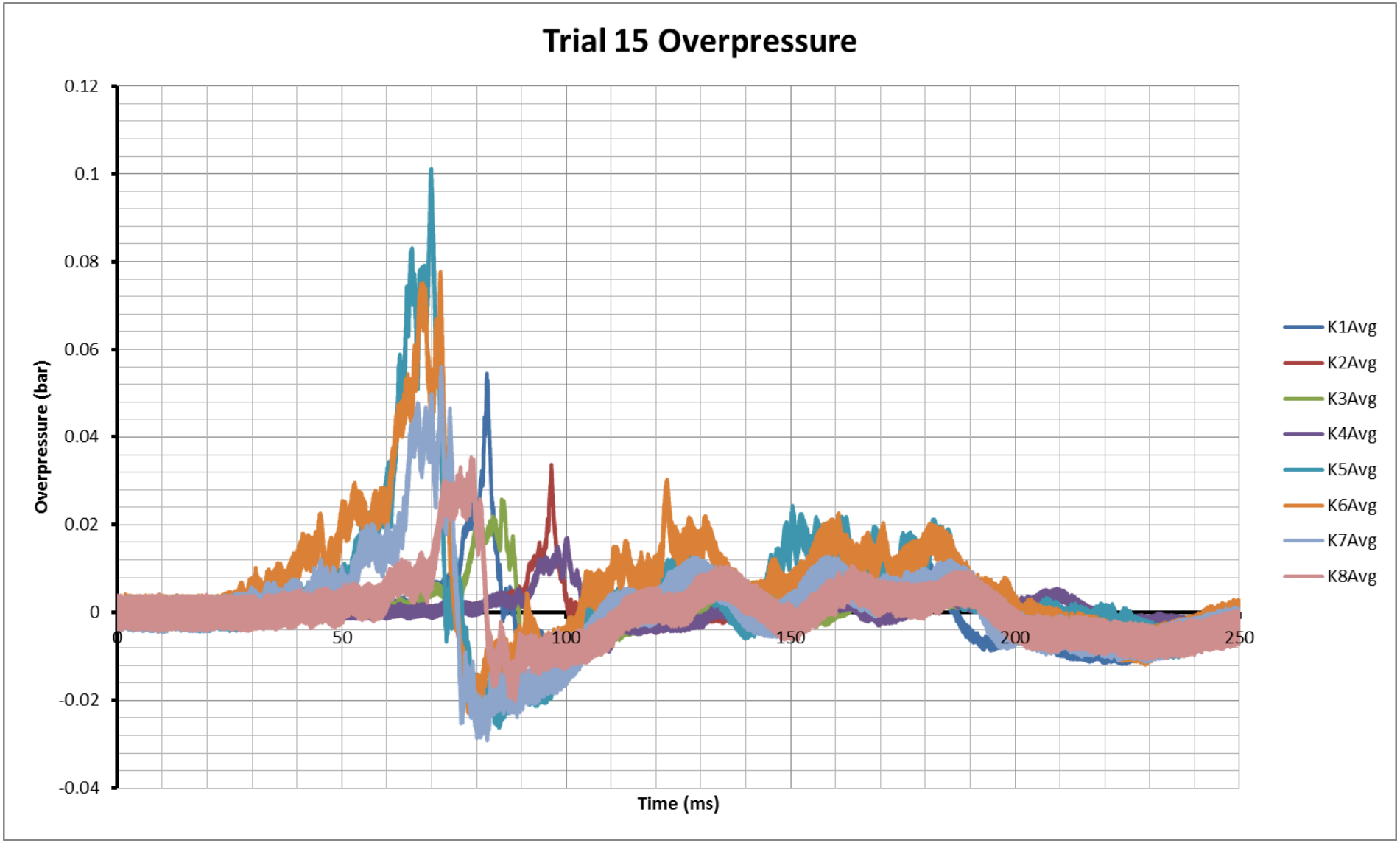
Trial 15 Overpressure
Overpressure (bar)
0.12
0.1
0.08
0.06
0.04
0.02
0
-0.02
-0.04
0
50
100
150
200
250
Time (ms)
K1Avg
K2Avg
K3Avg
K4Avg
K5Avg
K6Avg
K7Avg
K8Avg

Fig. C15

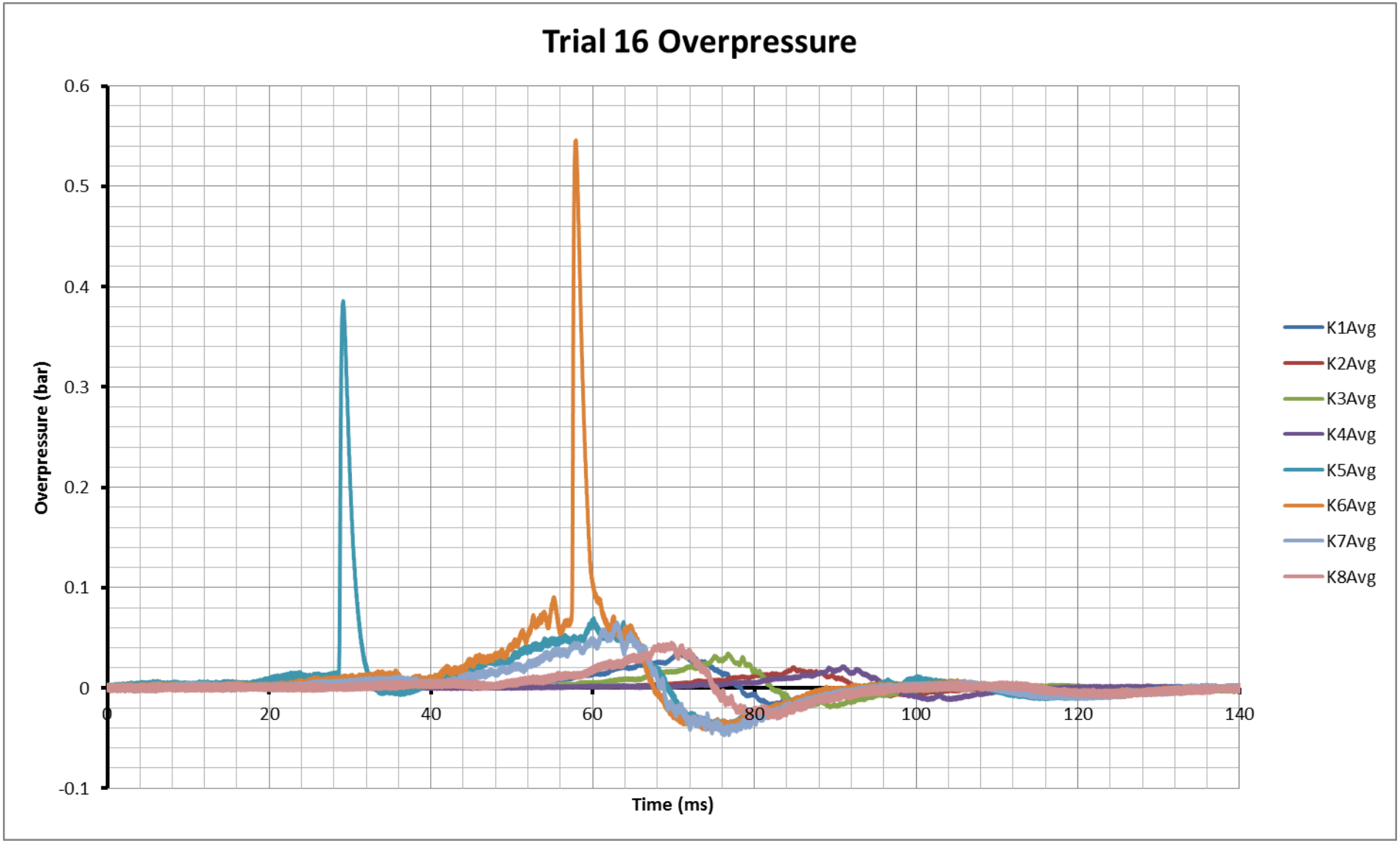
Trial 16 Overpressure
Overpressure (bar)
0.6
0.5
0.4
0.3
0.2
0.1
0
-0.1
0
20
40
60
80
100
120
140
Time (ms)
K1Avg
K2Avg
K3Avg
K4Avg
K5Avg
K6Avg
K7Avg
K8Avg

Fig. C16

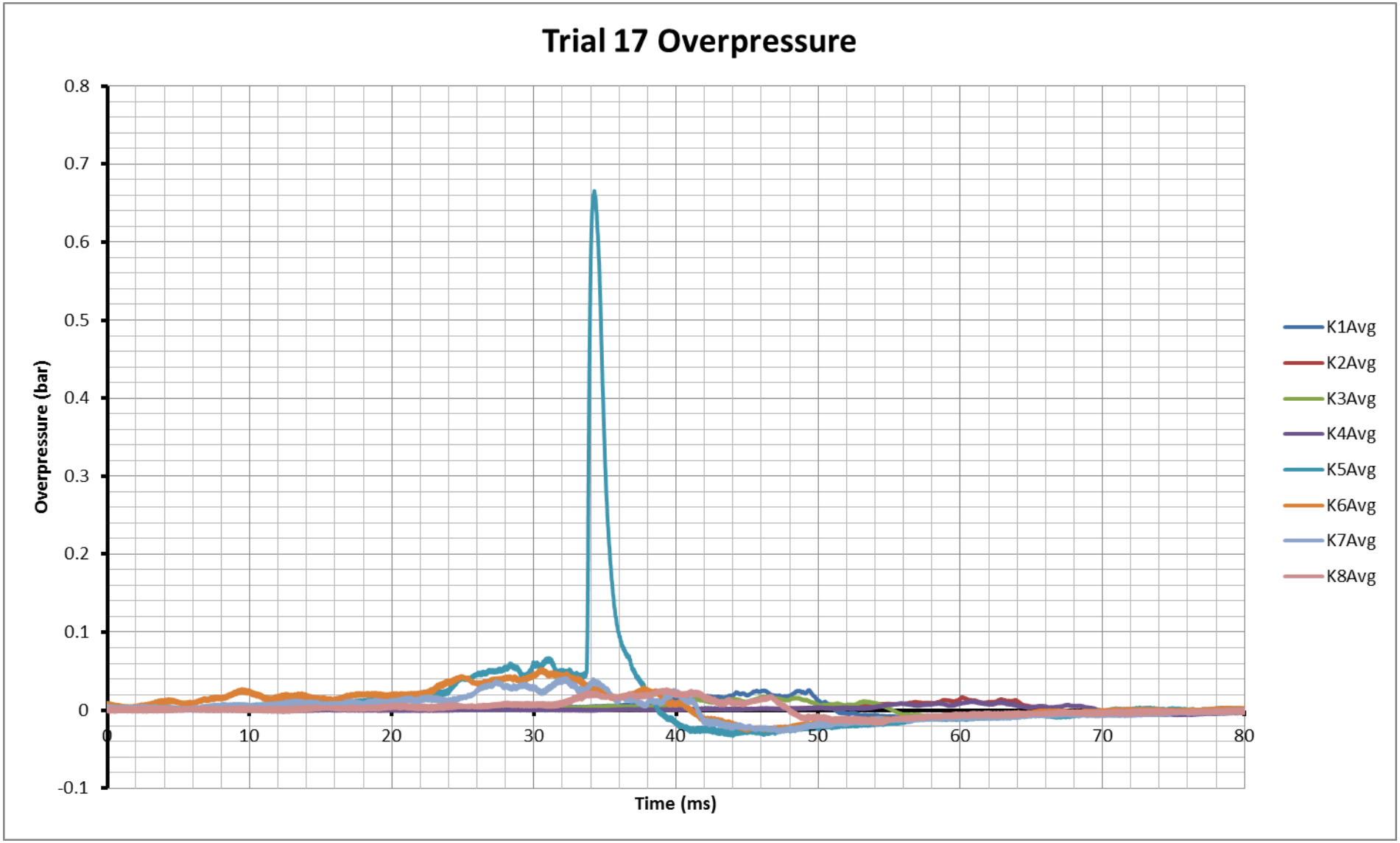
Trial 17 Overpressure
Overpressure (bar)
0.8
0.7
0.6
0.5
0.4
0.3
0.2
0.1
0
-0.1
0
10
20
30
40
50
60
70
80
Time (ms)
K1Avg
K2Avg
K3Avg
K4Avg
K5Avg
K6Avg
K7Avg
K8Avg

Fig. C17

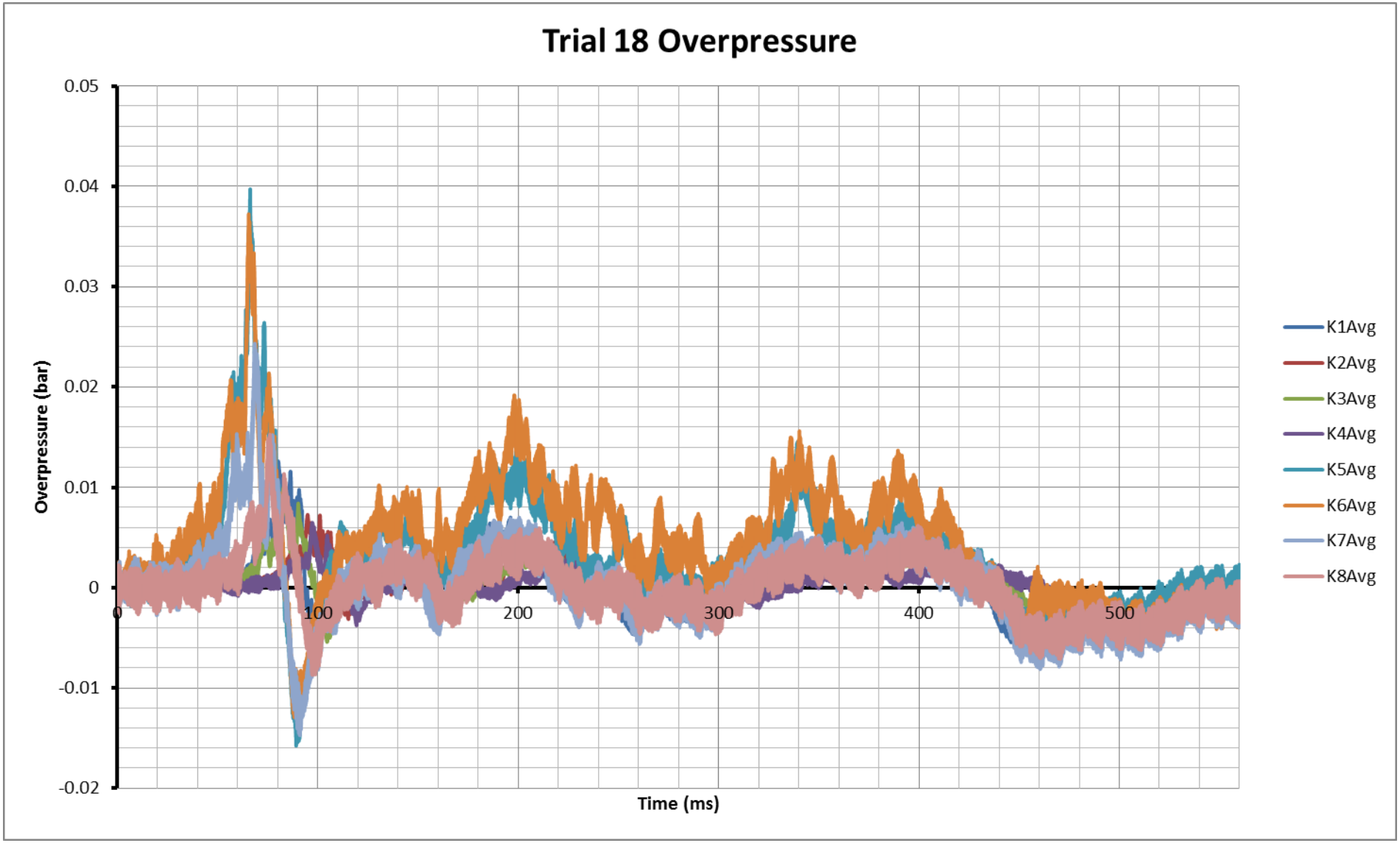
Trial 18 Overpressure
Overpressure (bar)
0.05
0.04
0.03
0.02
0.01
0
-0.01
-0.02
0
100
200
300
400
500
Time (ms)
K1Avg
K2Avg
K3Avg
K4Avg
K5Avg
K6Avg
K7Avg
K8Avg

Fig. C18

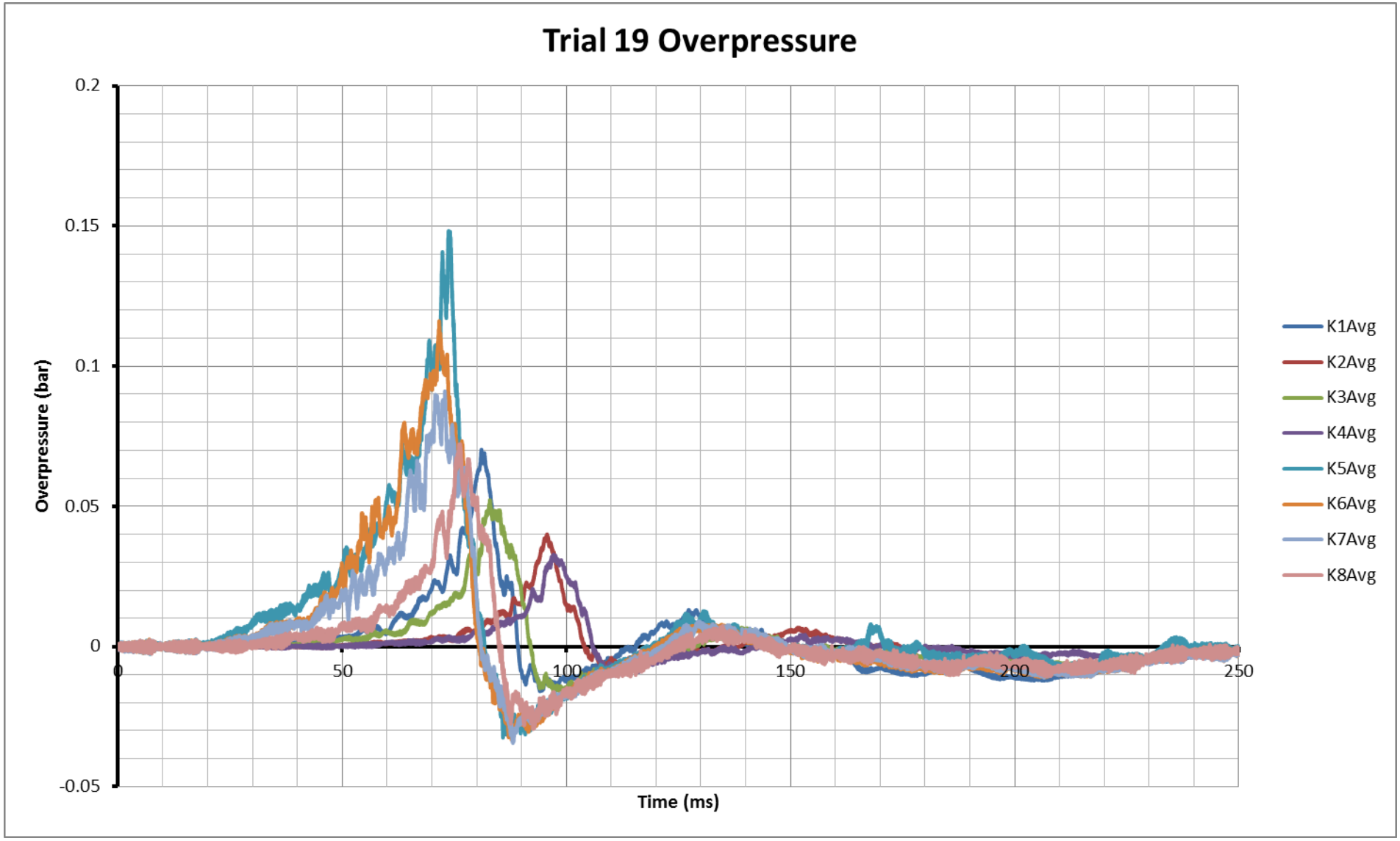
Trial 19 Overpressure
Overpressure (bar)
0.2
0.15
0.1
0.05
0
-0.05
0
50
100
150
200
250
Time (ms)
K1Avg
K2Avg
K3Avg
K4Avg
K5Avg
K6Avg
K7Avg
K8Avg

Fig. C19

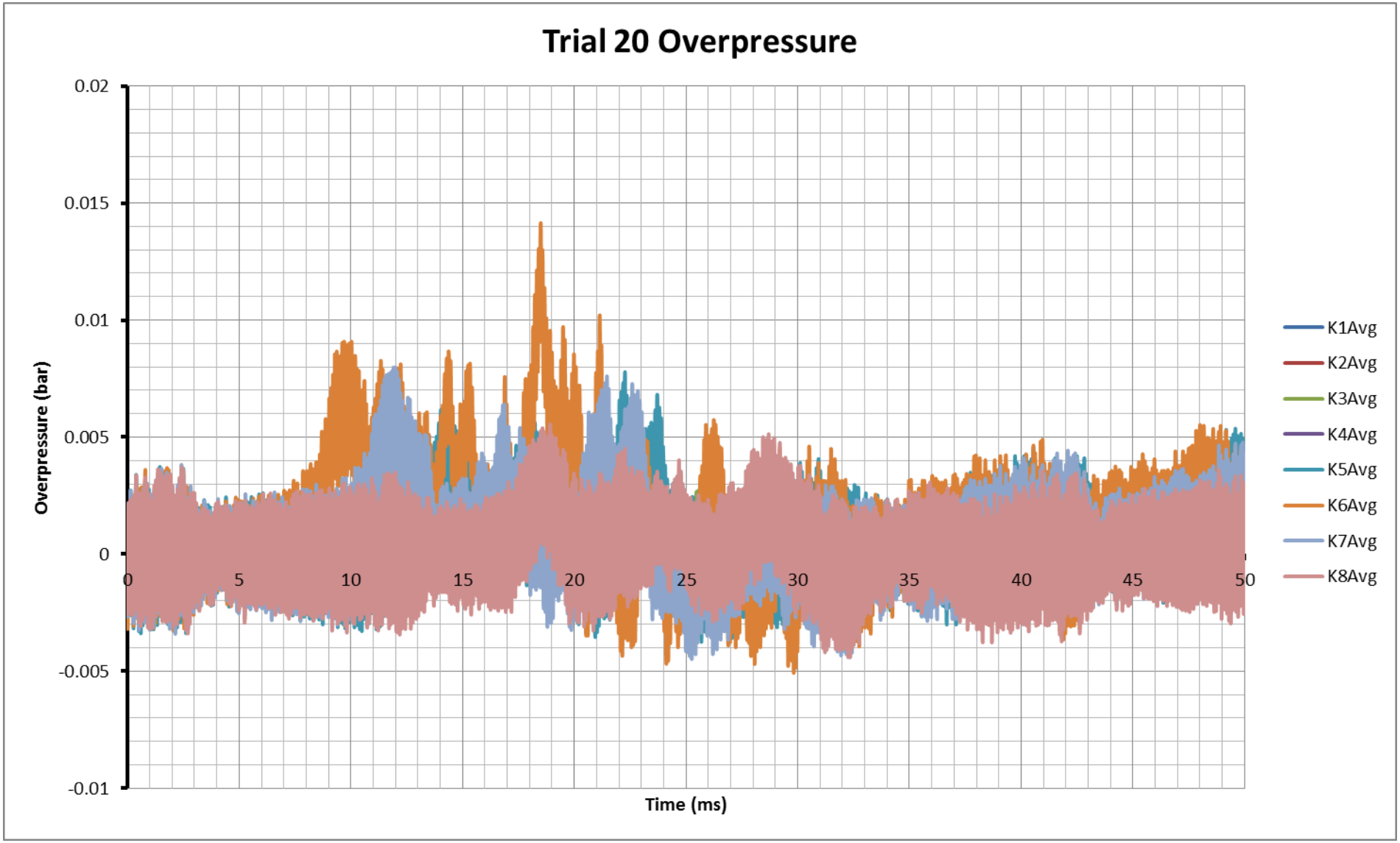
Trial 20 Overpressure
Overpressure (bar)
0.02
0.015
0.01
0.005
0
-0.005
-0.01
0
5
10
15
20
25
30
35
40
45
50
Time (ms)
K1Avg
K2Avg
K3Avg
K4Avg
K5Avg
K6Avg
K7Avg
K8Avg

Fig. C20

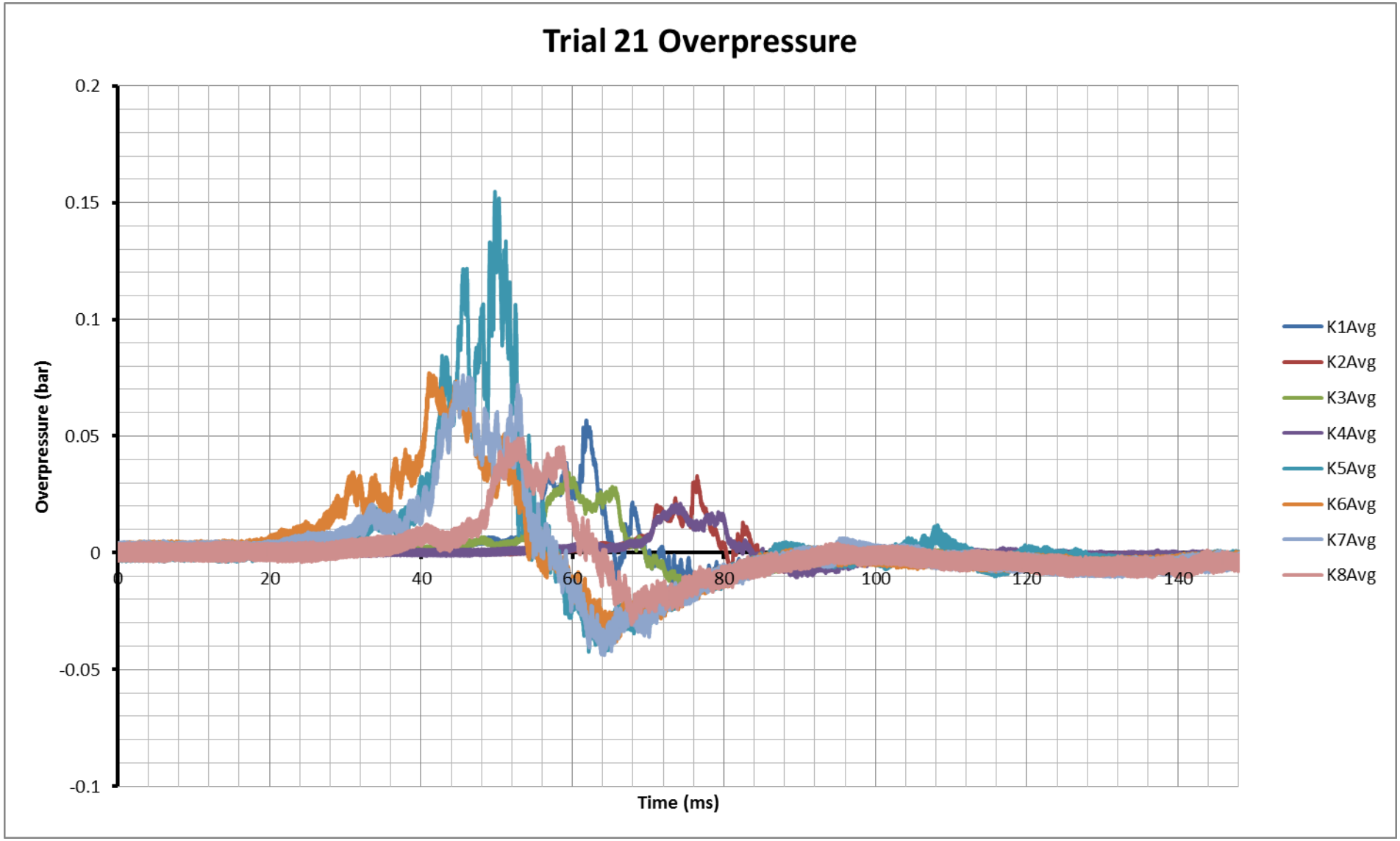
Trial 21 Overpressure
Overpressure (bar)
0.2
0.15
0.1
0.05
0
-0.05
-0.1
0
20
40
60
80
100
120
140
Time (ms)
K1Avg
K2Avg
K3Avg
K4Avg
K5Avg
K6Avg
K7Avg
K8Avg

Fig. C21

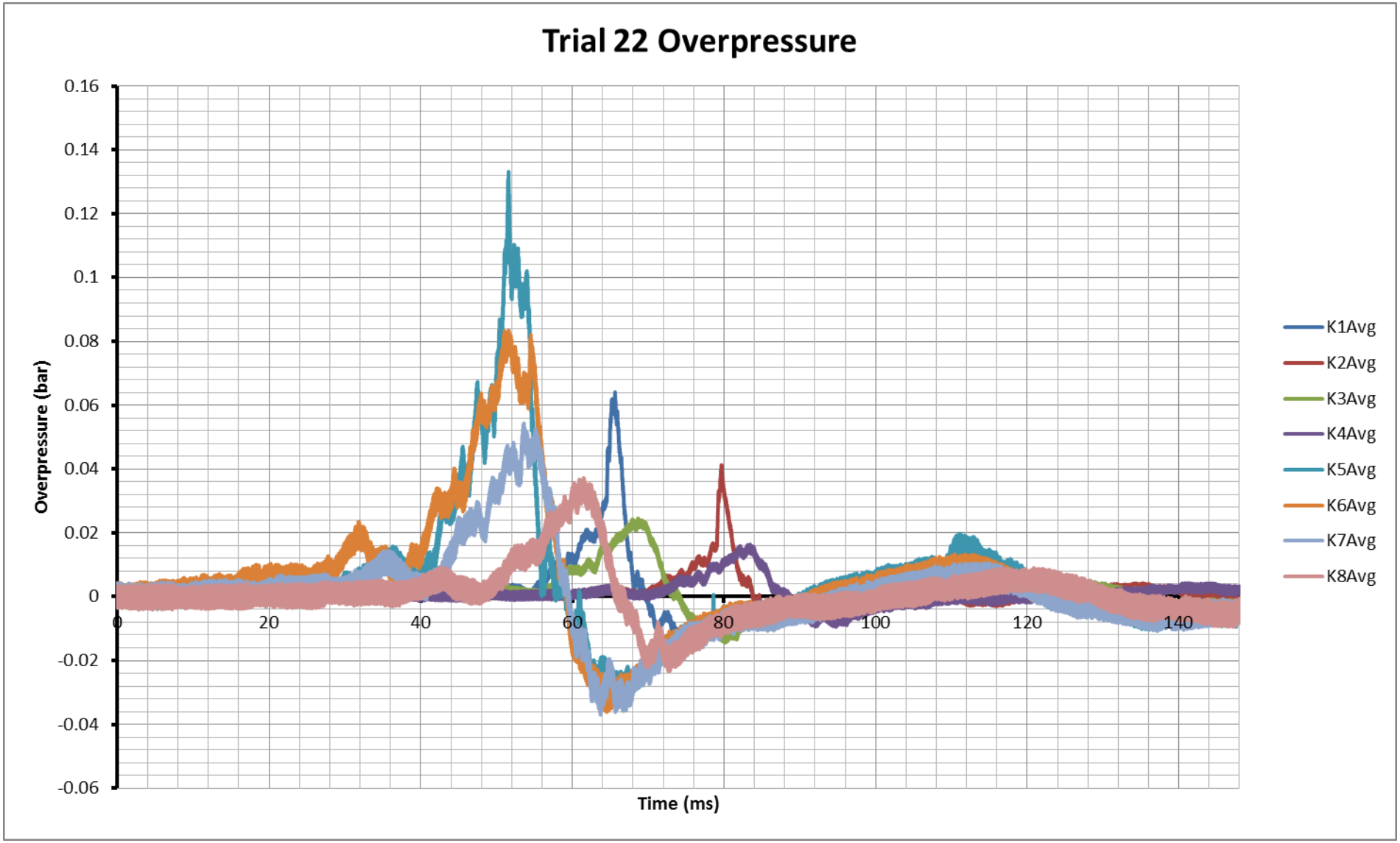
Trial 22 Overpressure
Overpressure (bar)
0.16
0.14
0.12
0.1
0.08
0.06
0.04
0.02
0
-0.02
-0.04
-0.06
0
20
40
60
80
100
120
140
Time (ms)
K1Avg
K2Avg
K3Avg
K4Avg
K5Avg
K6Avg
K7Avg
K8Avg

Fig. C22

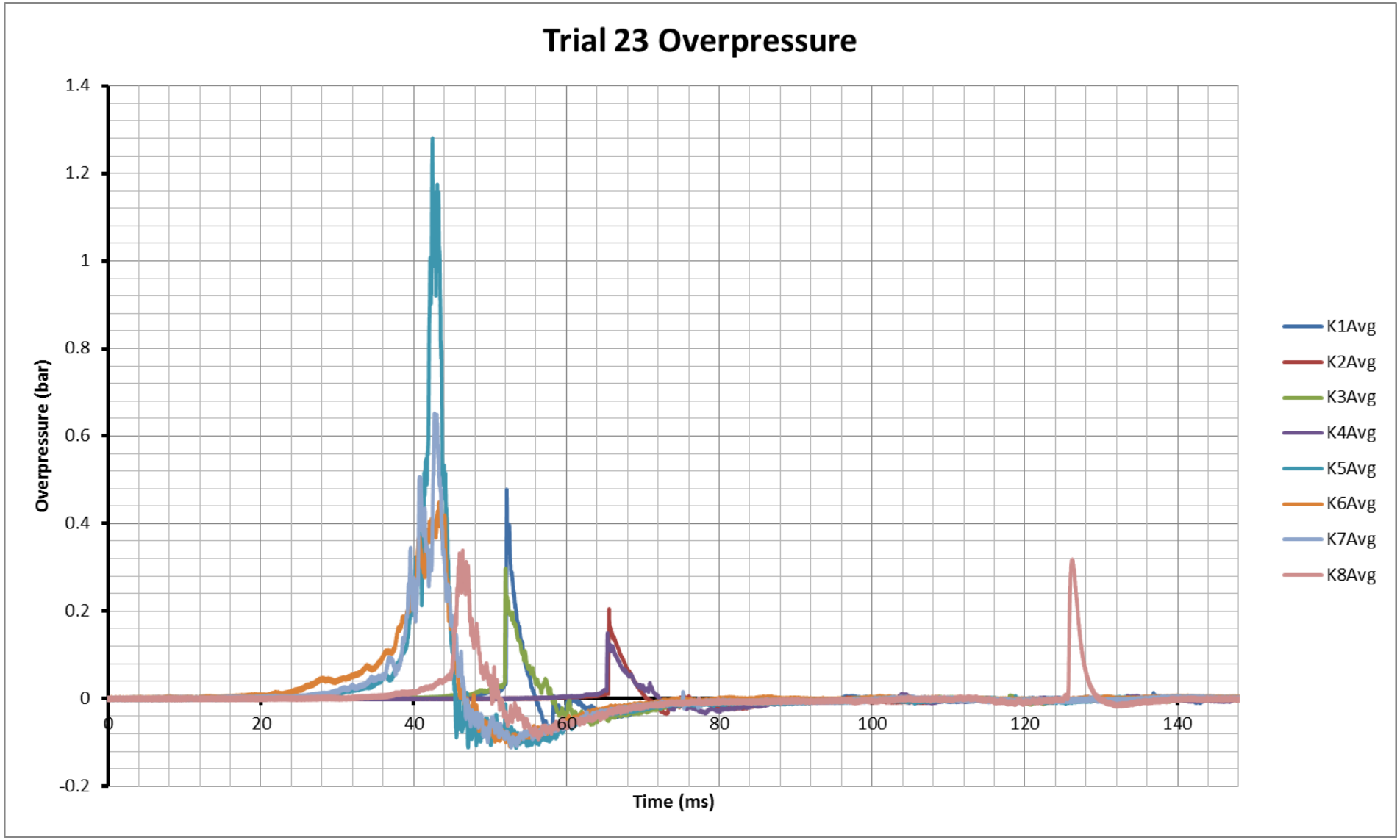
Trial 23 Overpressure
Overpressure (bar)
1.4
1.2
1
0.8
0.6
0.4
0.2
0
-0.2
0
20
40
60
80
100
120
140
Time (ms)
K1Avg
K2Avg
K3Avg
K4Avg
K5Avg
K6Avg
K7Avg
K8Avg

Fig. C23